Detection and Characterization of DNA Damage

Written by: Brian Reguly

Thesis submitted for the Master of Science degree in the Faculty of Science and Environmental Studies

Department of Biology

Lakehead University, Thunder Bay, Ontario, Canada

Declaration:

I hereby declare that, to the best of my knowledge and belief, the research presented in this document is original, except where appropriate acknowledgment has been credited.

Brian Reguly

I. Acknowledgements

I would like to thank and acknowledge Dr. Carney Matheson for taking me on as his student, for all of his help and guidance, and for always treating me like I was not "just" a student. Also, I would like to thank him for involving me on peripheral research projects which have taught me more than a text book ever could.

I would like to acknowledge my graduate committee, Dr. Kam Leung and Dr. Heidi Shraft, and my external reviewer for their time and consideration in reviewing my thesis.

A special thanks to those at Genesis Genomics Inc. for their generosity and support throughout my studies, most notably Jennifer Creed and Kerry Robinson.

I would also like to thank Ain Raitsakas and Allan MacKenzie at the Lakehead University Instrumentation Laboratory, Stephen Fratpietro at Paleo-DNA, and Debbie Leach at Lakehead University Chemistry Stores for their support of instrumentation and reagents.

Finally, I would like to thank John and Alice Reguly for their continual support and enthusiasm in my academic and educational pursuits and for "accepting" my grumpiness after a late night in the lab.

II. Table of Contents

III. List of Figures

IV. List of Tables

V. List of Equations

VI. List of Abbreviations

A	Adenine
aDNA	Ancient DNA
AP	Apurinic/Apyrimidinic
APS	Ammonium persulfate
BER	Base excision repair
bp	Base pair
C	Cytosine
CPD	Cyclobutane pyrimidine dimers
ddNTP	Dideoxyribonucleotide triphosphate
DMSO	Dimethyl sulfoxide
DNA	Deoxyribonucleic acid
dNTP	Deoxribonucleotide triphosphate
dsDNA	Double stranded DNA
G	Guanine
GC-MS	Gas chromatography-Mass spectrometry
HPLC	High performance liquid chromatography
MMR	Mismatch repair
mRNA	Messenger RNA
mtDNA	Mitochondrial DNA
nDNA	Nuclear DNA
NER	Nucleotide excision repair
PCR	Polymerase chain reaction
PK	Proteinase K
Pol	Polymerase
qPCR	Quantitative PCR
ROS	Reactive oxygen species
rRNA	Ribosomal RNA
SIM	Selective Ion Monitoring
ssDNA	Single stranded DNA
T	Thymine
Taq	*Thermus aquaticus*
TMS	Trimethylsilyl
tRNA	Transfer RNA
UVR	Ultraviolet radiation

VII. Abstract

The DNA molecule is constantly subjected to endogenous and exogenous sources of damage which if left unrepaired can lead to genotoxic and cytotoxic outcomes. These lesions have been implicated in the development of numerous diseases, carcinogenesis, and aging. This research focuses on the formation of such lesions, and unlike current research, demonstrates the potential of combining multiple analytical techniques to characterize a potential damage detection system. In this study samples were subjected to numerous damaging agents (hydrogen peroxide, fenton reaction, heat/acid buffer, ultraviolet light, dimethyl sulfoxide, ammonium persulfate, formalin) and in time intervals to induce oxidative, methylation, crosslinking, and apurinic/apyrimidinic lesions. By combining nucleic acid isolation, agarose gel electrophoresis, PCR amplification, GC-MS, and enzymatic reactions, insults to DNA structure were successfully identified. Time interval reactions demonstrated progressive damage pathways which can be utilized in a detection system by characterizing damage severity staging. These results demonstrate the advantages of developing a damage detection system by coupling analytical techniques to identify damage profiles and potential cellular consequences. In addition, a sensitive and specific apurinic/apyrimidinic detection assay to quantify the abundance and type of nucleotide base loss has been developed and demonstrates future potential upon optimization and validation. This research can be utilized to further understand DNA damage pathways, and can also be applied to the development of DNA damage repair assays.

1.0 Introduction

Following the initial identification and structure, deoxyribonucleic acid (DNA) has become one of the most intensely studied molecules. This double stranded helix which contains the genetic blueprint of an organism has contributed to, and has created numerous facets of scientific research and development. The significance of DNA is continuously demonstrated in molecular medicine, forensic science, and ancient DNA analysis. Currently, research involving the study of DNA damage and repair mechanisms has become increasingly extensive due to the association in the development of diseases, cancer, and aging. Despite this volume of research, a clear understanding of the delicate and complex nature of DNA damage and repair is lacking due to the absence of a thorough detection system.

1.1 Structure and Types of DNA

The identification of the structure of DNA is credited to James Watson and Francis Crick (Watson and Crick 1953). The main component of DNA is the nucleotide which consists of one of four nitrogenous bases, the deoxyribose sugar, and a phosphate group. The purine bases consist of adenine (A) and guanine (G), whereas the pyrimidine base group consists of thymine (T) and cytosine (C) (Wyatt 1951). The backbone of the DNA structure is composed of two 5' to 3' antiparallel strands of deoxyribose sugars joined to phosphate groups by a phosphodiester bond at the 3'-hydroxyl (OH) and 5'-OH group of the sugar. The base is attached to the backbone via an N-glycosidic bond at the C^1 position of the sugar moiety. The two separate strands of DNA are held together by hydrophobic interactions and the base pairing of adenine with thymine, and guanine with cytosine by two and three hydrogen bonds, respectively (Watson and Crick 1953). In

eukaryotes, this double stranded DNA is primarily found in the nucleus and the mitochondria organelle.

Nuclear genome

The nuclear genome is a linear genome comprised of 2.91 billion base pairs (bp) (Venter *et al.* 2001) arranged on 22 pairs of autosomal chromosomes and the X and Y sex chromosomes (Makalowski 2001). To package this large genome the DNA is folded by wrapping 146bp around an octamer of histone molecules forming a nucleosome (Goodfellow *et al.* 1994). The DNA is classified into intergenic regions, introns, and exons contributing to approximately 74, 24, and 1.1 percent, respectively, of the bases (Makalowski 2001). It is the exons that exist between the introns (Schmidtke and Epplen 1980) which code for the 26,000-38,000 predicted nuclear genes (Venter *et al.* 2001).

Mitochondrial genome

The mitochondrial genome is a 16.6kb circular double stranded DNA molecule which contains two ribosomal RNAs (rRNAs), 22 tRNAs (tRNAs), 13 polypeptides, and a non-coding D-loop region (Anderson *et al.* 1981). The mitochondrial DNA is present in high copy number per cell which is dependent on cell type and function (Robin and Wong 1988). Further properties of the mitochondrial genome which makes it unique from nuclear DNA include maternal inheritance, high mutation rate, lack of recombination, and altered genetic code (Fernandez-Silva *et al.* 2003). In gene processing the heavy and light strand components are symmetrically transcribed as polycistronic primary RNAs (Taanman 1999), followed by endonucleolytic cleavage at tRNA sequence punctuations and polyadenylation of mRNAs (Fernandez-Silva *et al.* 2003).

1.2 DNA Damage

The genomic contents of a cell are constantly subjected, and vulnerable to, various sources of endogenous and exogenous damage inducing agents. Despite cellular defense mechanisms and repair capabilities, persisting damage may alter such functions as replication, transcription and translation leading to aging, disease, carcinogenesis, and other deleterious mutagenic and genotoxic effects (Altieri *et al.* 2008). Endogenous damage is primarily the result of metabolic processes leading to oxidation, alkylation, hydrolysis, and deamination reactions (Hakem 2008). Exogenous damage agents are those which exist in the environment, such as ionizing radiation (IR) and ultraviolet radiation (UVR), and chemical agents which can be incorporated into the cell and involved in endogenous reactions (Hakem 2008).

Oxidative damage is a significant contributor to mutagenesis, carcinogenesis, and cell death due to the numerous forms in which it exists within the cell. Damage induced by oxidative stress includes modified bases and sugar moieties, double stranded breaks (DSBs), and single stranded breaks (SSBs) (Epe 1996). The reactive oxygen species (ROS) of hydrogen peroxide (H_2O_2), superoxide anion ($O_2^{\cdot-}$), singlet oxygen ($^1O_2$), and the hydroxyl radical ($OH^{\cdot}$) are generated from cellular metabolism and processes (De Bont and van Larebeke 2004). In addition, the oxidizing reactive nitrogen species (RNS) of nitric oxide ($NO^{\cdot}$) and peroxynitrite (ONO_2^-) are formed upon reaction of nitric oxide and the superoxide anion. These species are typically found in monocytes, neutrophils, and macrophages as immune defense mechanisms (Kelly *et al.* 1998). Peroxynitrite is a very reactive oxidant which can react with DNA directly, producing many of the same products as $^{\cdot}OH$, however it has the ability to diffuse throughout the cell (Marnett 2000).

The most common endogenous form of these oxidizing agents is the hydroxyl radical ($OH^{\cdot}$). In Complex I and III of the electron transport chain superoxide is produced during the reduction of oxygen to water and transformed to H_2O_2 by the enzyme superoxide dismutase (SOD). Following the Haber-Weiss reaction (Equation 1), superoxide is reacted with the previously generated H_2O_2 to produce the hydroxyl radical upon catalysis by a transition metal ion (Kehrer 2000).

Equation 1. The Haber-Weiss Reaction

$$O_2^{\cdot-} + H_2O_2 \rightarrow O_2 + OH^- + OH^{\bullet}$$

The major contributing metal to this reaction is ferric iron (Fe^{3+}) which is reduced to ferrous iron (Fe^{2+}) by superoxide (Equation 2), then proceeds to react with H_2O_2 in a Fenton reaction (Equation 3)(Kehrer 2000).

Equation 2. The reduction of ferric iron by superoxide

$$Fe^{3+} + O_2^{\bullet-} \rightarrow Fe^{2+} + O_2$$

Equation 3. The Fenton Reaction

$$Fe^{2+} + H_2O_2 \rightarrow Fe^{3+} + OH^- + OH^{\bullet}$$

The rate of these mutations in the mitochondrial genome is approximately ten times greater than those observed in the nuclear genome (Linnane *et al.* 1989) due to the proximity of the mtDNA to the origin of the damage and the lack of protection from histone proteins (Mecocci *et al.* 1993). In addition, $^{\bullet}OH$ reacts almost immediately with another cellular species upon formation, indicating that the generated radical must be transferred to the nucleus in the form of the diffusible hydrogen peroxide (Marnett 2000).

The $^{\bullet}OH$ radical adds to the double bonds of purines and pyrimidines, targeting the site of highest electron density due to the electrophilic properties of the radical group (Evans *et al.* 2004). The hydroxyl radical adds to the $C^5=C^6$ double bond of cytosine and

thymine to yield C^5 and C^6 adduct radicals. In thymine, an H can also be abstracted from the 5-methyl group resulting in an allyl radical. These radicals can be further reduced or oxidized depending on redox properties and environmental conditions such as the presence of oxygen (Cooke *et al.* 2003). Cytosine products can be further modified by deamination and/or dehydration (Cooke *et al.* 2003). The addition to purines occurs at the C^4, C^5, and C^8 positions resulting in OH adduct radicals. The C^4-$^{\bullet}$OH radical tends to be oxidizing and the C^5-$^{\bullet}$OH radical is typically reducing, however, these radicals may be present in different mesomeric forms resulting in "redox ambivalence" (Evans *et al.* 2004). The C^8-$^{\bullet}$OH adduct radicals, however, are primarily reducing. In adenine and guanine the C^8-$^{\bullet}$OH adduct radical is readily oxidized in the presence or absence of oxygen, whereas only the C^4-$^{\bullet}$OH adduct radical of adenine reacts easily with oxygen (Cooke *et al.* 2003). Adenine is also susceptible to an $^{\bullet}$OH attack at the C^2 position and can be subsequently oxidized.

The reactions following the formation of the adduct radicals of purines and pyrimidines result in the formation of numerous modified bases. Figure 1 illustrates the major products formed from OH adduct radicals (Dizdaroglu *et al.* 2002). The formation of base lesions within the DNA strand or in the deoxynucleotide pool tends to be mutagenic by misincorporation of bases yielding transition and transversion mutations (Table 1) (Wang *et al.* 1998) upon replication which can affect gene coding, hydrogen bonding, DNA conformation, and Polymerase fidelity (Kehrer 2000).

In addition to base mutations it has been observed that some lesions, such as thymidine glycol, are capable of blocking replication at flanking bases. Deletions are

also incorporated into the DNA molecule during the base excision repair process of 5-(hydroxymethyl)uracil by Hydroxymethyluracil DNA glycosylase (Cooke *et al.* 2003).

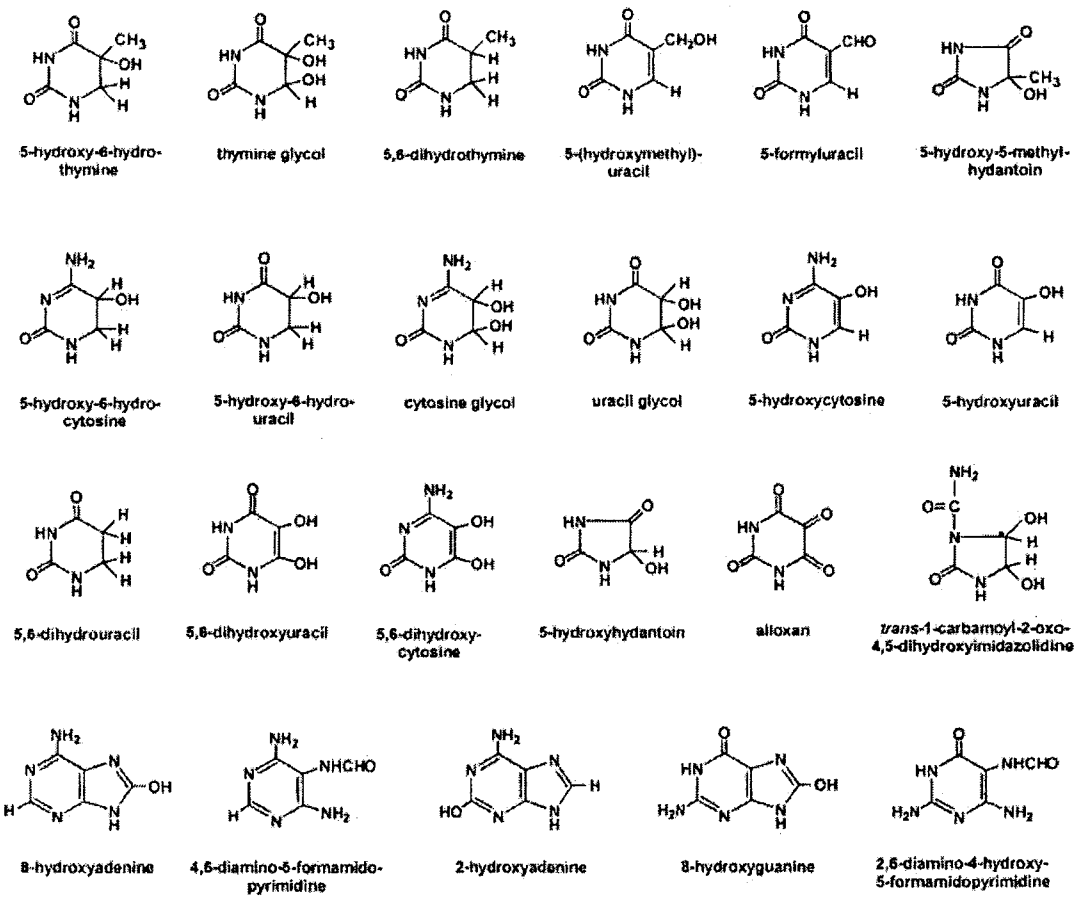

Figure 1. Structures of modified base products formed from OH adduct radicals. (Dizdaroglu *et al.* 2002)

The hydroxyl radical also interacts with the carbon atoms of the sugar moiety, producing altered sugar products, apurinic/apyrimidinic (AP) sites, and strand nicks (Dizdaroglu *et al.* 2002). The reaction of a hydroxyl radical at the C^4 position yields an alkoxyalkyl radical with a phosphate group in the β-position. The loss of either of the phosphate group results in a strand break and the modified sugar products 2,3-

dideoxypentose-4-ulose (3' loss) and 2,5-dideoxypentose-4-ulose (5'loss) after further reactions with the addition of hydroxide (Evans *et al.* 2004).

Table 1. Base substitutions incorporated from induced modified base (Wang *et al.* 1998).

Base Pair Substitution	Associated DNA lesion
GC→AT	5-OH-Cyt, 5-OH-Ura, Ug
GC→TA	8-OH-Gua
GC→CG	5-OH-Cyt
AT→CG	8-OH-Gua, 8-OH-Ade
AT→GC	8-OH-Ade, 2-OH-Ade, Tg
AT→TA	2-OH-Ade

Oxidation of the C^4 and C^1 radical followed by the addition of OH^- results in the loss of the base group forming 2-deoxypentonic acid lactone and 2-deoxypentose-4-ulose respectively (Figure 2)(Evans *et al.* 2004).

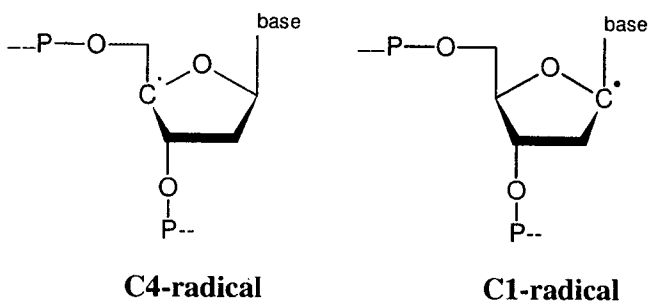

C4-radical **C1-radical**

Figure 2. C^4 and C^1 radical product structure of the sugar moiety.

The C^5 sugar radical is capable of inducing intramolecular cyclisation by an addition reaction with the C^8 position of purines and the C^6 position of pyrimidines. These lesions change the backbone torsion angles and weaken hydrogen bonding as the base rotates around the glycosidic bond to form the C^5 to C^8 covalent bond (Jaruga and Dizdaroglu 2008). These alterations have been identified as being responsible for blocking transcription, DNA polymerases, and transcription binding factors (Jaruga and Dizdaroglu 2008). These products have been only found to date to occur in adenine and guanine (Figure 3) from oxidation reactions (Bjelland and Seeberg 2003).

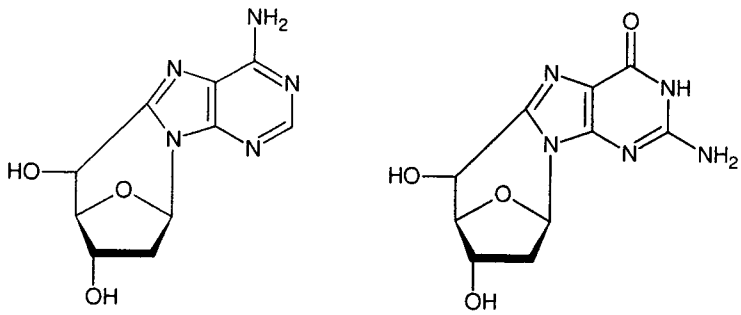

cdA **cdG**

Figure 3. Structures of 8,5'-cyclo-2'-deoxyadenosine (cdA) and 8,5'-cyclo-2'-deoxyguanosine (cdG) formed from intramolecular cyclization.

Alkylating damage agents have both endogenous and exogenous origins and are responsible for mutagenic, cytotoxic, and carcinogenic insults to the cell (Falnes 2004). Endogenous alkylating agents are numerous; however, the individual functions and abundance have not yet been fully characterized.

S-Adenosylmethionine (SAMe) is a commonly found methylating agent that is involved in many necessary biochemical methylating processes yet has also been observed to react with DNA (Altieri *et al.* 2008). In addition, bile acids have the potential to be transformed into alkylating compounds inducing numerous methyladenine and methylguanine adducts in colonic and rectal tissues (Kang 1994). An extensive amount of exogenous alkylating sources are found in environmental gases (i.e. methane), food chemicals, tobacco smoke, and pharmaceuticals (Drablos *et al.* 2004).

These agents primarily react with purine bases (Singer 1979) targeting their N^1, N^3, and N^7 positions and the O^6 atom in guanine (Mitra 2007). The formation of N^3 and N^7 alkylpurines affects the stability of the glycosidic bond, generating an AP site (Mitra 2007). The genotoxic base adduct O^6-alkylguanine (Drablos *et al.* 2004) forms an AT→GC transition mutation and can cause pauses in DNA replication (Mitra 2007).

In pyrimidines, the N^3 and O^2 atoms of cytosine and thymine, and the O^4 atom of thymine, are the predominant sites of alkylation reactions (Mitra 2007). The most common alkylthymine, O^4-alkythymine, is both highly mutagenic and genotoxic due to G:T mispairing, and helix instability from typical Watson-Crick base pairing with adenine (Cruzeiro-Hansson and Goodfellow 1994).

Alkylating species are generally strong electrophiles (Mol *et al.* 1999) or are converted to electrophilic compounds which react with the nucleophilic DNA species in S_N1 and S_N2 reactions (Figure 4) (Mitra 2007)

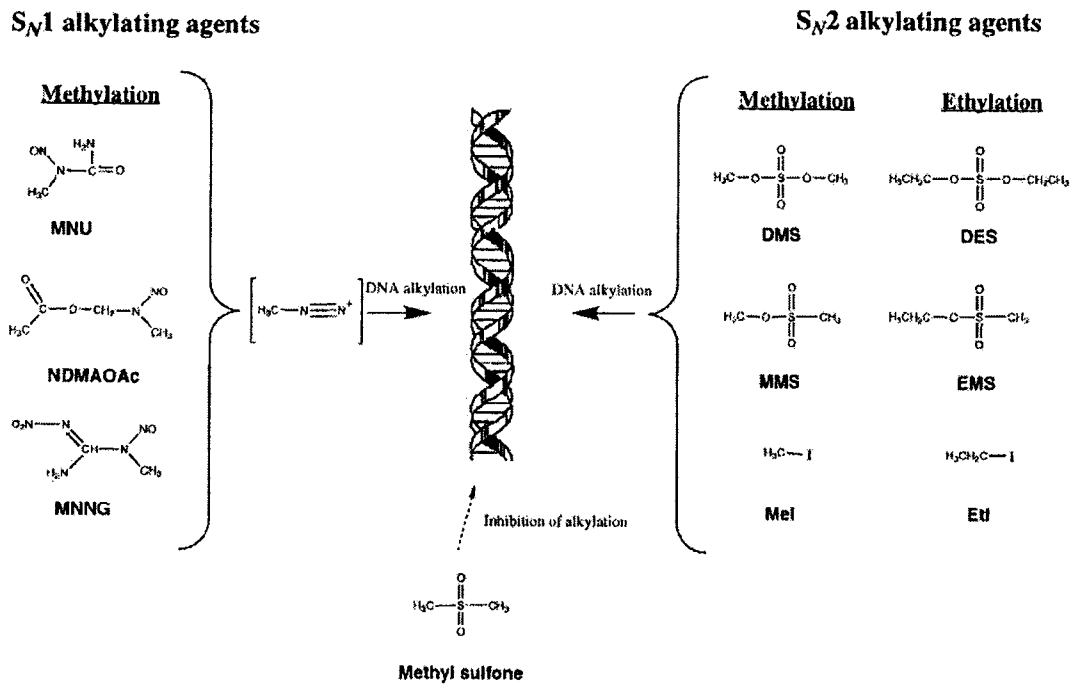

Figure 4. Structures and corresponding substitution reaction pathways for various alkylating agents (Cloutier *et al.* 2001).

. The S_N1 reactions preferentially alkylate the oxygen and nitrogen groups of nucleotides (Drablos *et al.* 2004)and due to S_N1 reaction conditions, can occur in areas of greater steric hindrance such as guanine homopolymeric stretches (Cloutier *et al.* 2001). The S_N2 reactions tend to alkylate only the nitrogen groups (Singer 1977) and due to

steric hindrance are affected by the sequence content, DNA conformation, (Cloutier *et al.* 2001) and chemical structure of the alkylating agent (Mhaskar *et al.* 1981).

Hydrolytic reactions in the cell are responsible for the deamination of the DNA bases and the creation of AP sites through spontaneous and glycosylase catalyzed hydrolytic reactions. The deamination of DNA bases does occur more frequently in pyrimidines than in purines however both are equally mutagenic and genotoxic causing base mismatches resulting in mutations and AP sites (Mol *et al.* 1999). In the mammalian genome, the majority of CpG cytosines are in the methylated form of 5-methylcytosine (Waters and Swann 2000) which functions in gene silencing (Robert *et al.* 2003). The deamination of 5-methylcytosine results in the formation of thymine generating a G to A transition mutation (Waters and Swann 2000). The deamination of an unmodified cytosine base by an addition-elimination reaction with hydroxyl or water at C^4 generates uracil (Frederico *et al.* 1993). These reactions result in an U:G mispair leading to a GC→AT transition mutation and have also been identified as acting in retroviral infection defense (Kavli *et al.* 2007). The deamination of the purines, guanine and adenine, form the mutagenic lesions of xanthine and hypoxanthine, respectively. Xanthine, which can pair with thymine induces a GC→AT mutation whereas hypoxanthine pairs with cytosine leading to a AT→GC transition mutation (Lim *et al.* 2006).

Hydrolysis of the DNA structure at the N-glycosidic bond (Figure 5) results in the formation of abasic sites at an estimated rate of 10000 bases per cell per day (Lindahl and Nyberg 1972). These hydrolytic lesions arise from spontaneous loss, DNA glycosylases,

and previously destabilized N-glycosyl bonds from damaging agents (Dianov *et al.* 2003). If these nucleotide gaps are not repaired they can arrest DNA synthesis,

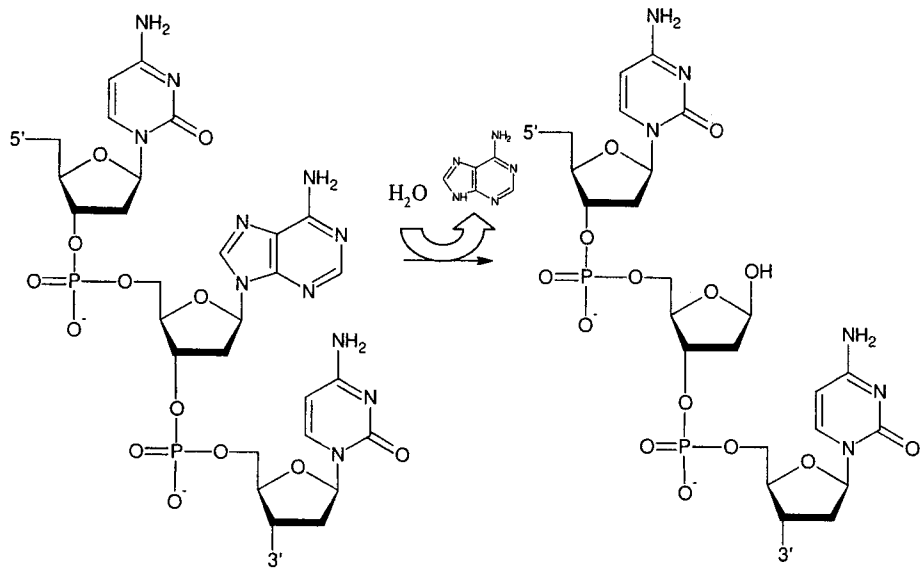

Figure 5. The formation of an abasic site created from the hydrolysis of the N-glycosidic bond of DNA.

transcription, and result in the default misincorporation of adenine opposite to the lesion (Ide *et al.* 1993).

Ultraviolet radiation (UVR) emitted from the sun exists in the wavelength groups of UVA (320-400nm), UVB (280-320nm), and UVC (200-280nm) (Pfeifer *et al.* 2005). The majority of UVC and short wavelength UVB (280-295nm) is blocked by the atmosphere and does not affect cellular components (Douki *et al.* 2003). Long wavelength UVB (295-320) contributes to less than 10% of the UV emission reaching the earth's surface in comparison to the 90 % contribution from UVA (Runger and Kappes 2008). The exposure to this radiation has been recognized as a major risk factor in the development of non-melanoma and malignant melanoma skin cancer (Runger and Kappes 2008).

Despite the large percentage of exposure contributed by UVA it is less cytotoxic as it is poorly absorbed by DNA (Douki *et al.* 2003). UVA induced damage to DNA occurs indirectly by the absorption and transfer of the emitted photons by cellular photosensitizers (Pfeifer *et al.* 2005). These sensitizers can transfer the charge diretly to DNA (type I photosensitization) or can transfer this charge to oxygen resulting in the formation of ROS (type II photosensitization) capable of reacting with DNA (Douki *et al.* 1999) and other cellular components. It is expected that guanine is the primary target because it has the lowest ionization potential leading to the formation of 8-OH-Gua (Douki *et al.* 2003). This product will result in the mispairing of adenine with 8-OH-Gua resulting in a G→T transversion, or an A→C transversion if an 8-OH-Gua modified dNTP is incorporated opposite to adenine (Cheng *et al.* 1992). In addition to 8-OH-Gua, the formation of cyclobutane pyrimidine dimers (CPDs), specifically TT, is reported as being the primary form of UVA radiation damage (Mouret *et al.* 2006). The CPD products are formed from the 5,6, bonds of two adjacent pyrimidine bases resulting in C→T transition mutations.

The wavelength of light emitted from long wavelength UVB is readily absorbed by the DNA molecule and is responsible for the majority of UVR induced mutations. The main products of UVB radiation are CPDs, pyrimidine (6-4) pyrimidone photoproducts (6-4PPs) and Dewar valence isomers (DewPPs) (Figure 6).

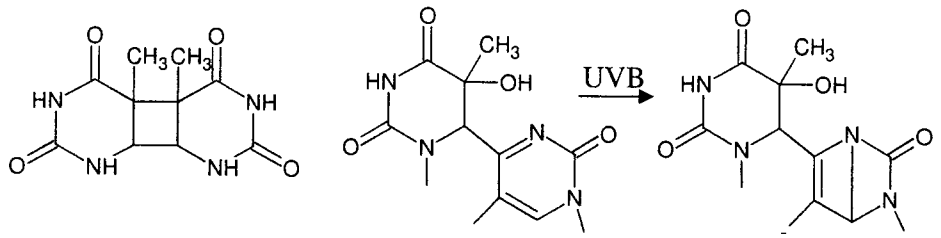

Figure 6. Structures of photoproducts induced by ultraviolet radiation (Cadet *et al.* 2005)

The CPD products primarily occur at TT sites, followed in occurrence by TC and CC sites (Cadet *et al.* 2005). These lesions generate the trademark C→T and CC→TT tandem mutations associated with UVB damage. It is also observed that 5-methylcytosine bases located at CpG positions are vulnerable to deamination when incorporated into a CPD based on its increased energy absorption (You *et al.* 1999).

The wavelength range of UVC occurs at the maximum absorption wavelength of naked DNA (260nm) which results in the production of the greatest yield of photoproducts (Runger and Kappes 2008). Despite not contributing to the UVR reaching the earth's surface, UVC light is used in disinfection of laboratory and hospital surfaces for airborne bacteria and fungal spores (Kujundzic *et al.* 2006). Treatment with UVC induces CPD mutations (Runger and Kappes 2008) as seen in UVA and UVB and also single and double stranded breaks (Bogdanov *et al.* 1997). Double stranded breaks, left unrepaired, will lead to genetic alterations and cellular death (Peak and Peak 1990).

1.3 Damage Defense Mechanisms

To cope with the onslaught of DNA damaging agents the cell is equipped with defense mechanisms to reduce cytotoxic, mutagenic, and carcinogenic outcomes. The major defense mechanisms in the cell accommodate oxidative radicals with enzymatic

and non-enzymatic antioxidants. Enzymatic antioxidants include superoxide dismutase (SOD), glutathione peroxidase (GPX), and catalase, whereas the non-enzymatic antioxidants consist of α-tocopherol (vitamin E), ascorbic acid (vitamin C), glutathione (GSH), carotenoids, and vitamin A (Mates *et al.* 1999).

Superoxide dismutase is present in the inner mitochondrial space in the form of MnSOD and in the outer mitochondrial space and cytoplasm as Cu/ZnSOD (Landis and Tower 2005). This enzyme is responsible for the conversion of superoxide free radicals into oxygen and hydrogen peroxide via a series of redox reactions in the presence of the transition metal (Equation 4) (McCord and Fridovich 1969).

Equation 4. The enzymatic conversion of superoxide free radicals

$$O_2^{\bullet -} + O_2^{\bullet -} + 2\,H^+ \xrightarrow{SOD} O_2 + H_2O_2$$

Glutathione peroxidase exists in a selenium dependant form (GPx) and a selenium independent form (glutathione-S-transferase,GST) contrasted by reaction mechanisms (Valko *et al.* 2006). The GPx enzymes have the capability to reduce organic hydroperoxides and H_2O_2 by oxidizing glutathione (Equation 5 & 6) (Mates *et al.* 1999). This reaction is critical to reduce hydroperoxides contributing to Fenton type reactions which produce reactive hydroxyl radicals.

Equation 5. The glutathione peroxidase reaction of hydrogen peroxide

$$2\,GSH + H_2O_2 \xrightarrow{GPx} GSSG + 2\,H_2O$$

Equation 6. The glutathione peroxidase reaction of organic hydroperoxides

$$2\,GSH + ROOH \xrightarrow{GPx} GSSG + ROH + H_2O$$

The catalase enzyme is localized within the peroxisome and reacts with H_2O_2 in a high efficiency reaction to yield molecular oxygen and water (Valko *et al.* 2006). Similar

to GSH, it is an important reaction to reduce the concentration of the potentially reactive hydroperoxides (Equation 7 & 8) (Mates *et al.* 1999).

Equation 7. Reaction to reduce reactive hydrogen peroxide

$$2\ H_2O_2 \xrightarrow{CAT} 2\ H_2O + O_2$$

Equation 8. Reaction to reduce organic hydroperoxides

$$ROOH + AH_2 \xrightarrow{CAT} H_2O + ROH + A$$

Vitamin C is renowned for its significant antioxidant capabilities by scavenging numerous forms of oxidative species (Sies *et al.* 1992) and decreasing the formation of N-nitroso compounds (Valko *et al.* 2006). Vitamin C is also involved in the protection of membrane oxidation by increasing the efficiency of tocopherol radical scavenging (Barclay *et al.* 1985). Vitamin C, in vivo, is present in the form of $AscH^-$ (Figure 7) and following reaction with the radical species is transformed to a non-reactive form (Valko *et al.* 2006).

The lipid peroxidation antioxidant properties of vitamin E can be attributed to its solubility in lipids and its membrane binding capabilities (Valko *et al.* 2006). The Vitamin E antioxidant group is comprised of tocopherols and tocotrienols with α-tocopherol (Figure 7) observed to be the most active (Sies and Stahl 1995). The antioxidant reaction occurs by the transfer of hydrogen from the hydroxyl group at C^6 of the chromane ring (Sies *et al.* 1992).

Beta-carotene is the most common of the carotenoids and its antioxidant properties are due to a long chain of double bonds in its structure (Figure 7) (Sies and Stahl 1995). The major function of β-carotene is the scavenging of singlet oxygen with further capacity for reactions with superoxide, peroxyl, and hydroxyl radicals (Valko *et al.* 2006).

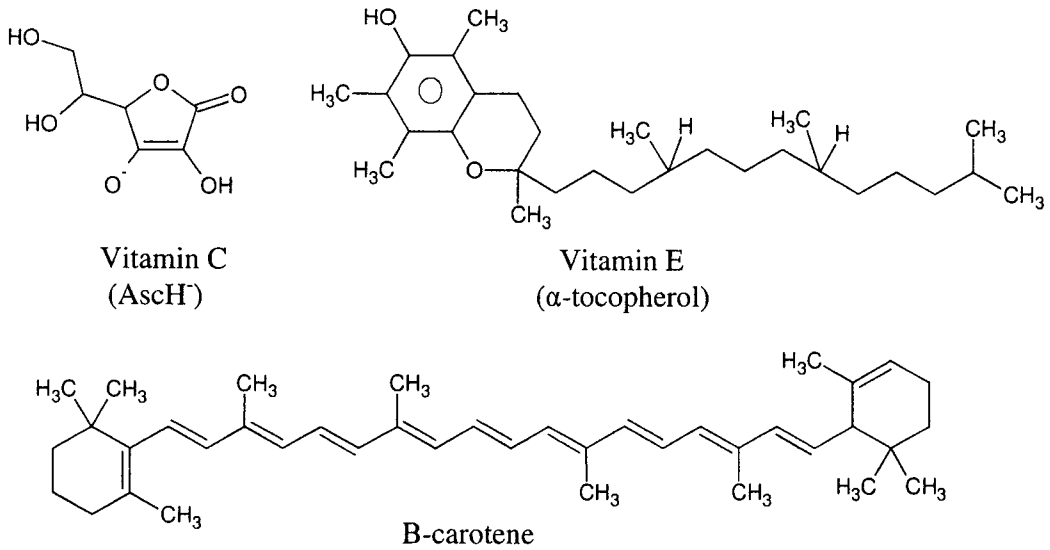

Figure 7. Structures of important non-enzymatic antioxidants (Sies *et al.* 1992).

1.4 DNA Repair Mechanisms

Upon damage to DNA, cells utilize repair mechanisms to repair or remove the offending lesion as failure to do so may lead to cytotoxic results (Krokan *et al.* 1997). The complementary nature of DNA enables efficient recovery of genomic information from the unaffected strand if the other strand is damaged (Altieri *et al.* 2008). The prominent pathways of repair are base excision repair (BER), nucleotide excision repair (NER), mismatch repair (MMR), and direct reversal (Krokan *et al.* 1997). Both the mitochondrial and nuclear genomes possess these repair mechanisms, with the exception of the absence of NER in the mitochondria (Kang and Hamasaki 2002). If these mechanisms fail or cannot meet the necessary repair requirements the cell will eventually begin the apoptotic pathway of cellular suicide.

The most frequently used repair method is the base excision repair (BER) which uses specific recognition to target modified base products to excise from the DNA strand

(Altieri *et al.* 2008). The damage profiles repaired by the BER are those typically formed in deamination of cytosine, oxidative and alkylating damage, SSBs, and abasic sites (Slupphaug *et al.* 2003). The initial step in BER is the recognition of a modified lesion followed by the hydrolysis of the N-glycosyl bond by a DNA N-glycosylase. The glycosylases tend to be specific for a certain modified base though some target purine or pyrimidine base groups (Altieri *et al.* 2008).

Glycosylases exist in monofunctional and bifunctional processing forms. Monofunctional glycosylases are only capable of base removal by the hydrolysis of the N-glycosidic bond to create an abasic site. Bifunctional glycosylases have the capacity to remove the modified base and cleave the DNA backbone at the 3' end of the abasic site by AP lyase activity generating a 3' and 5'-phosphate group (Kang and Hamasaki 2002). Both products undergo processing by AP endonuclease activity to create a 5'-phosphate and 3'OH nucleotide strand break (Altieri *et al.* 2008). In mammalian cells the processed gap is filled in by short patch BER addition of one nucleotide by Polβ polymerase activity (Polγ in mitochondria) and the excision of the 5'-deoxyribosephosphate (dRP) via the dRPase function of Polβ (Sung and Demple 2006). An alternate pathway observed in yeast cells replaces two to ten nucleotides with Polδ or Polε by displacing and excising overlapping bases (Hakem 2008). Finally, the DNA strand is joined by the ligase activity of the XRCC1/ligase III (LigIII) complex in short patch BER and DNA ligase I (LigI) in long patch BER (Hakem 2008).

The nucleotide excision repair (NER) pathway is primarily utilized for the removal of larger adducts such as CPDs, 6-4PPs, and helix distorting alterations (Batty and Wood 2000). This pathway which identifies structure abnormalities has also been

observed to contribute in the removal of modified bases that do not alter the helix significantly, suggesting its importance as a backup system to the BER pathway (Altieri *et al.* 2008).

The helical distorting damage is first observed by the XPC/HR23B NER protein complex and the recognition efficiency is dependent on the severity of distortion induced (Altieri *et al.* 2008). Local strand opening begins surrounding the lesion and is further increased by TFIIH in an ATP-mediated reaction (Wood 1997). The unwound strand is nicked 3' and 5' to the lesion by the XPG and ERCC1 nucleases, respectively, resulting in the loss of approximately 25-30 single stranded nucleotides containing the lesion (Wood 1996). The resulting gap is filled by either DNA Polδ or DNA Polε, determined by initial damage mechanism, with the proliferating cell nuclear antigen (PCNA) followed by ligation by DNA ligase I (Wood 1997).

During DNA replication base pairing errors can be created by the DNA polymerase and are not detected by the proofreading abilities of the polymerase (Altieri *et al.* 2008). It is these errors that are repaired by the mismatch repair (MMR) pathway. This repair pathway has been fully characterized in detail in *Escherichia coli* (*E.coli*), however only some homolog proteins and processes have been identified in yeast and mammals (Table 2), therefore the proteins and mechanisms for *E.coli* are discussed.

Table 2. "Mut" Genes of Escherichia coli in MMR and corresponding homologs (Buermeyer *et al.* 1999).

Escherichia coli	*Saccharomyces cerevisiae*	*Homo sapiens*
MutS	Msh2, Msh6, Msh3	Msh2 [a], Msh6 [a], Msh3
	Msh1	-[b]
	Msh4, Msh5	Msh4, Msh5
MutL	Mlh1	Mlh1 [a]
	Pms1	Pms2 [a]
	Mlh2, Mlh3	Pms1 [a]
MutH	-[b]	-[b]
MutU	-[b]	-[b]

[a] Mutations found in cancer families

[b] Not identified

The initial step in MMR is the identification of the mismatch by MutS (Buermeyer *et al.* 1999) which binds to the DNA and compares adjacent nucleotides following polymerase incorporation (Altieri *et al.* 2008). When the mismatch is identified, MutS interacts with MutL to initiate strand selectivity by MutH (Buermeyer *et al.* 1999). MutH distinguishes the newly synthesized and incorrect strand by the lack of methylation and is also responsible for the cleaving of this strand at a local hemimethylated site (Altieri *et al.* 2008). The MutU helicase protein localizes at the site of MutH cleavage and initiates duplex unwinding followed with fragment removal by DNA exonucleases (Iyer *et al.* 2006). The gap is then filled by DNA polymerase and joined with DNA ligase.

In BER, NER, and MMR there is a complete removal of the lesion along with surrounding bases. In direct repair (DR) the species that is responsible for the mutagenic properties of the base is removed in a single step process. An example of DR is the demethylation of the lesion O^6-methylguanine by O^6-methylguanine-DNA methyltransferase (MGMT) back to guanine (Hakem 2008). The reaction occurs by the transfer of the O^6-methyl group to a cysteine residue of MGMT resulting in a reversal of

the lesion (Figure 8) (Mitra 2007). Each MGMT contains only one active site which is methylated upon O^6-alkylG reversal resulting in inactivation and protein degradation (Hakem 2008).

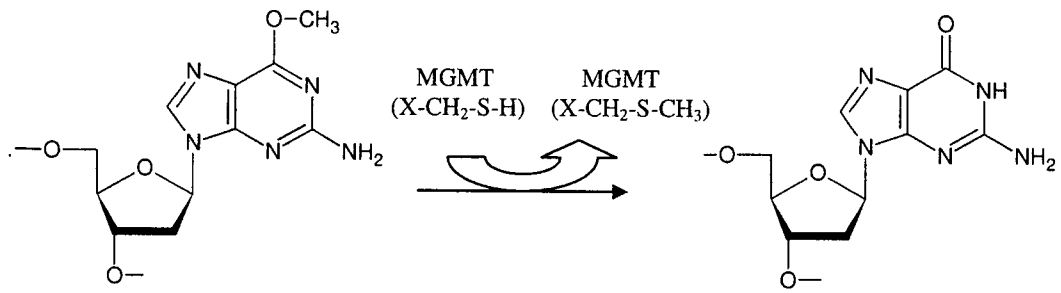

Figure 8. Direct reversal of O6-alkylG to guanine by MGMT (Mitra 2007).

1.5 Methods of Damage Detection

The occurrence of DNA lesions has been observed to correspond with the prevalence of a plethora of diseases, cancers, and disorders (Cooke *et al.* 2003). The measurement of these lesions could potentially be utilized as biomarkers for risk assessment, diagnosis, and treatment. Assays created for the detection of DNA damage must however display acceptable sensitivity, specificity, and reproducibility. In addition these methods must limit any artifactual damage that is a result of DNA isolation, sample preparation, and during the detection analysis itself (Halliwell 1998). Currently the major methods utilized for the detection of DNA damage are gas chromatography-mass spectrometry (GC-MS), high performance liquid chromatography-mass spectrometry (HPLC-MS), HPLC-electrochemical detection (ECD), Comet assay, ^{32}P-Postlabelling, Immunochemical detection (ID), and the Polymerase Chain Reaction (PCR).

GC-MS and HPLC-MS

The use of GC-MS has been frequently and successfully used in the detection of undamaged and modified bases and sugar moieties (Dizdaroglu *et al.* 2002). The samples are initially hydrolyzed with formic acid to separate the sugar and base by the cleavage of the glycosidic bonds followed by derivitization to convert the species into volatile products for gas chromatography and electron ionization (Dizdaroglu 1994). These processes, if not performed cautiously, can lead to overestimation of DNA damage by producing artifact lesions (Cadet *et al.* 1998). Despite this nuance, which can be eliminated with proper techniques (Dizdaroglu 1998), GC-MS is highly sensitive, specific, quantifiable, and can provide structural details of the analyte (Poulsen *et al.* 1999). The use of selected ion monitoring (SIM) can further increase the sensitivity of the method (Hwang and Bowen 2007) by essentially focusing on certain ions at pre-determined retention times.

To reduce possible artifacts produced from acid hydrolysis and derivitization, LC-MS processing by enzymatic hydrolysis with no derivitization is suggested (Hwang and Bowen 2007). This method is successful in the detection of modified base products at a respectable limit, however to match the sensitivity of GC-MS an increased concentration of DNA template is necessary (Dizdaroglu *et al.* 2001).

HPLC-Electrochemical Detection (ECD)

HPLC coupled with electrochemical detection is widely used in the identification of 8-OH-Gua (Poulsen *et al.* 1999). This method yields presumably no artifacts (Cadet *et al.* 1998) since bases are liberated from the sugar by enzymatic hydrolysis, separated by HPLC, and identified and measured through a redox reaction by electrochemical

detection (van Delft *et al.* 1993). The method is regarded as being a highly sensitive, despite possible underestimation from enzymatic hydrolysis, (Guetens *et al.* 2002) and very reproducible assay (ESCODD 2003). A limitation to this assay is that it can only detect species with low oxidation potential and many bases are not electrochemically active. This results in a measure of oxidative damage solely by 8-OH-Gua which may include a percentage of artifactual formation (Hwang and Bowen 2007).

Comet Assay

The Comet assay has been regarded as being a simple, quick, and sensitive method (Hwang and Bowen 2007) for the detection of double and single stranded breaks, abasic sites, and specific base lesions (Cooke *et al.* 2006). The assay is performed by initially lysing cells embedded in agarose followed by electrophoresis with an alkaline buffer solution of varying pH dependent on the type of damage investigated (Collins *et al.* 2008). The gels are then visualized by fluorescence after staining and measured (Moller 2006). The undamaged DNA in the nucleosome does not migrate through the gel at the extent that smaller damaged fragments will, creating the comet like appearance (Guetens *et al.* 2002). Some major drawbacks of this assay are the decreased specificity, forms of measurement, and lack of genome specification. The DNA can be treated with glycosylases and Endonuclease III targeting DNA lesions and creating strand breaks to add to the comet tail. However, glycosylase activity can vary depending on helical conformation/glycosylase accessibility, and the distribution of lesions on the strand (Poulsen *et al.* 1999). Also, as in the case of formamidopyrimidine-DNA glycosylase (Fpg) which cleaves 8-OH-Gua, Fapy-Gua, Fapy-Ade, and 8-OH-Ade, glycosylases are not necessarily lesion specific (Guetens *et al.* 2002). This also restricts the ability to

distinguish between the contribution of strand breaks, abasic sites, and different base lesions in one gel. The scoring of these comets is achieved by measuring the length of the tail, visual inspection, tail moment, and image analysis software (Collins *et al.* 2008). From this, problems concerning reproducibility, consistency, and exact measurement are inherent.

^{32}P-Postlabelling

The use of ^{32}P-postlabelling is one of the most sensitive techniques with the ability to detect 1 lesion/10^7-10^{10} using approximately 1-10μg of DNA (Hwang and Bowen 2007). In ^{32}P-postlabelling the samples are enzymatically digested to 3'mononucleotides followed by the transfer of ^{32}P from γ^{32}P-ATP with T4 polynucleotide kinase (PNK) to the 5'OH position of the base lesion (Phillips and Arlt 2007). The labeled products are then separated and detected by HPLC. This assay, though sensitive, is relatively time consuming (Poulsen *et al.* 1999), requires optimal chromatographic conditions for each adduct being studied (Hwang and Bowen 2007), and synthetic internal standards have not yet been developed to achieve exact quantification (Phillips and Arlt 2007).

Immunochemical Detection

Immunochemical detection measures DNA lesions by the use of monoclonal antibodies (mABs) via a competitive enzyme-linked immunosorbent assay (ELISA) (Guetens *et al.* 2002). In this reaction a lesion specific mAB binds with the modified base antigen of interest followed by the addition of a secondary antibody which is specific for the mAB (Guetens *et al.* 2002). The concentration is determined by plotting the fluorescence against a standard curve of known lesion concentrations. This assay is

sensitive under conditions of low template and the brief sample processing decreases formation of artifacts (Hwang and Bowen 2007). However, the use of antibodies to detect lesions such as 8-OH-Gua, lack the specificity by reacting with species of similar characteristics (Poulsen *et al.* 1999).

Polymerase Chain Reaction Amplification

The polymerase chain reaction (PCR) has been utilized for the detection of DNA damage based on the premise that DNA lesions block PCR amplification (Govan *et al.* 1990). Though a relative quantification can be achieved through gel imaging and standard concentrations, the use of quantitative PCR (qPCR) has resulted in a more sensitive assay represented by the cycle threshold (C_T) (Sikorsky *et al.* 2004). To determine the concentration of a sample the measured C_T is compared to either the C_T of a sample of known concentration or determined by linear regression from a standard curve of known concentrations and relative C_T values (Sikorsky *et al.* 2004). This methodology has demonstrated that an increase in damaged template results in the decrease of amplification characterized by an increased C_T (Sikorsky *et al.* 2007). A benefit of this assay is the ease of genome isolation and the targeting of desired regions by specific primer design (Santos *et al.* 2006). However, this assay may underestimate damage due to polymerase bypass of the lesion and misincorporation of dNTP's opposite of the lesion (Sikorsky *et al.* 2007). In addition, lesion types can only be inferred from base mutations observed post-PCR by sequencing.

1.6 Project Objective

The objective of this study is to evaluate the development of a DNA damage detection system by identifying insults associated with various forms of damage agents using multiple detection assays and to observe damage profile differences in isolated genomic content (Figure 9). This project will initially use synthetic DNA template (PCR product, dNTP's) to focus on DNA lesions induced by endogenous, exogenous, and sample processing agents to identify associated damage and demonstrate the versatility of samples that this methodology can be applied.

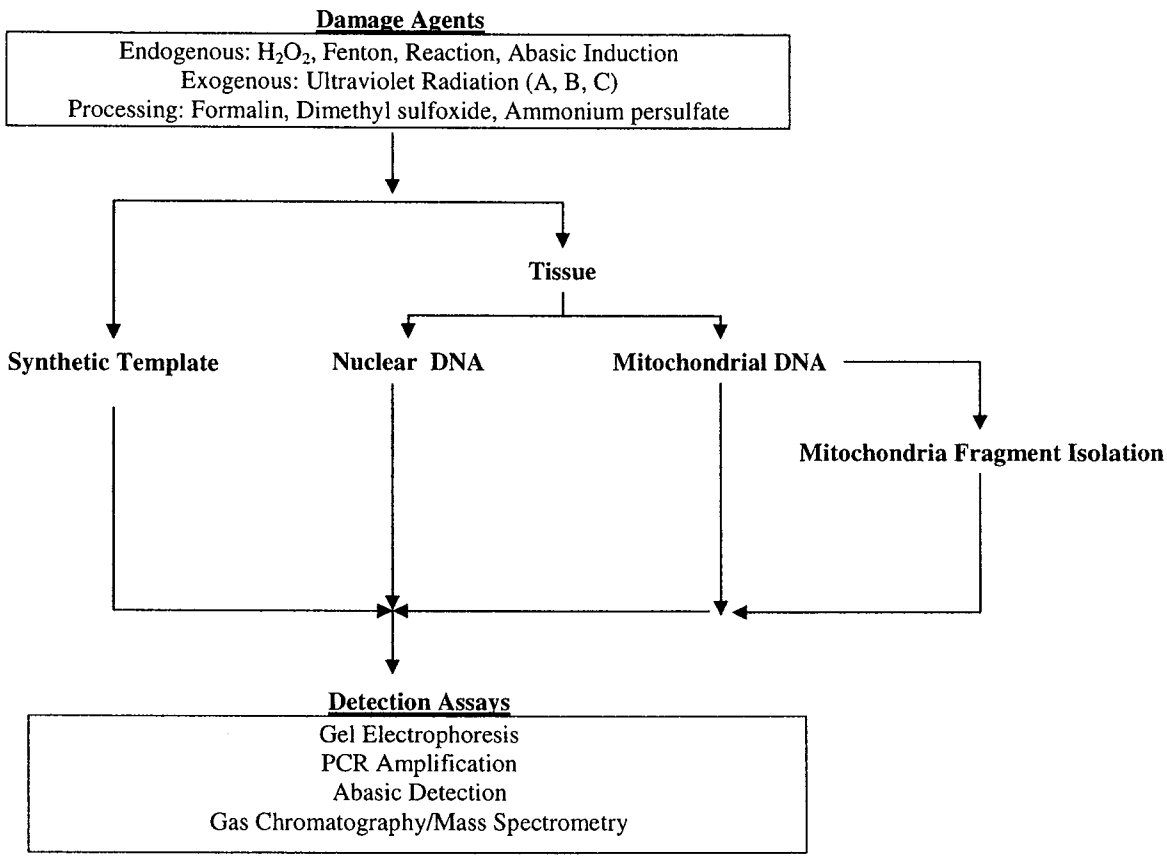

Figure 9. Experimental approach to identify induced damage to DNA control template via multiple detection assays followed by the localization of damage utilizing a genome isolation pathway.

These lesions may include double stranded and single stranded breaks, apurinic/apyrimidinic sites, and modified bases and sugar moieties. Contrary to current research, this study will combine multiple assays to gain insight into the overall causes and effects of damaging agents. The methods utilized to assess this damage include agarose gel electrophoresis, PCR amplification, GC-MS, and additional enzymatic reactions. The combination of the outcomes of each individual reaction will potentially provide insight into the DNA damage profile. In addition, these methods will be employed on DNA template damaged over time intervals to possibly identify damage accumulation and progression profiles. Once this is completed, in an attempt to localize DNA damage, the nuclear and mitochondrial genomic fractions of tissue will be separated, followed by further isolation of selected mitochondrial DNA components.

Finally, this study will attempt to develop a methodology to improve the detection of abasic sites by characterizing individual base loss and distribution.

2.0 Methods and Procedures

2.1 DNA Template and Processing

2.1.1 DNA Extraction

In this study DNA was extracted from buccal swabs using a modified protocol of Proteinase K (PK) extraction method (Hansen 1974) for the creation of DNA damage template.

The buccal swabs are cotton tipped swabs that were scraped on the inside of the cheek approximately twenty times and then placed upright in a swab holder and left to dry for 2 hours.

For each swab a 400µL extraction buffer consisting of 290µL TNE (1M Tris pH 8.0, 0.5M NaCl, 0.5M EDTA), 40µL 20% SDS, 40µL DTT (0.39M), 28µL ddH_2O, and 2µL of Proteinase K (Fisher Scientific) (20mg/mL) was added to a 2mL tube and briefly vortexed. The swab tip was cut and placed in the prepared solution and incubated for 3 hours at 55°C and 350rpm in an Eppendorf® Thermomixer R. For each extraction round, an extraction control (swab with no DNA) was processed.

After incubation the samples were ethanol precipitated with an adapted method from Hansen (1974). For each sample 40µL (10% v/v) of 3M sodium acetate was added and vortexed for 1 minute and zip spun. Next, 1100µL (2.5X sample volume) of cold 95% ethanol was added, vortexed, and then incubated on ice for 30 minutes. Following incubation, the tubes were centrifuged at 13,793 x g for 5 minutes to pellet the DNA. The supernatant was removed being careful not to disturb the pellet, and then air dried for 30 minutes. The DNA was resuspended in 100µL of ddH_2O, vortexed, and incubated for 15 minutes at 37°C and 800rpm with an Eppendorf® Thermomixer R. The DNA

concentration and purity, 260/280, and 260/230 ratios were obtained using a NanoDrop™ 1000 spectrophotometer.

2.1.2 Damage Template Formation

For the generation of PCR product for damage template reactions, an approximate 1kb fragment from the mitochondrial D-loop using the primers 15975F and 429R (Table 3) was amplified with LA Taq™ DNA Polymerase (Takara Bio Inc.) from the previously extracted buccal swabs using the reagent concentrations listed Table 4 in 25µL reactions.

Table 3. Sequence and properties of oligonucleotides used in the amplification template for damage reactions

Primer name and position	Primer Sequence (5'-3')	Length (bp)	GC content (%)	Tm (°C)
15975F	CTC CAC CAT TAG CAC CCA AAG C	22	55	64
429R	CTG TTA AAA GTG CAT ACC GCC A	22	45	60

Table 4. PCR reagent concentrations for template amplification.

Reagent	Volume (µL)	Final Concentration
Takara LA Taq™ DNA Polymerase (5 U/µL)	0.25	1.25U
10X LA PCR Buffer II (Mg^{2+}plus)	2.5	1X
10mM dNTP Mix (2.5mM each)	4	0.4mM each
Buccal Swab Template ~(20ngµL /)	5	100ng
10uM Forward Primer	0.5	0.2uM
10uM Reverse Primer	0.5	0.2uM
Sterile ddH_2O	12.25	-

The template amplification was completed with the following PCR cycling parameters for a total of 35 cycles.

Table 5. PCR cycling parameters for template amplification.

PCR Step	Temperature (°C)	Time (sec)	Cycle
First Denaturing	94.0	180	1
Denaturing	94.0	45	1-35
Annealing	62.0	45	1-35
Extension	72.0	50	1-35
Hold	4.0	-	Hold

Successful amplification was determined by gel electrophoresis using 5μL of each product. Five samples, now containing 20μL each, were added to a 1.5mL tube and purified using the RBC Bioscience HiYield™ Gel/PCR DNA Extraction Kit.

2.1.3 Isolation of Nuclear and Mitochondria Genomes

In this research, two primary methods of genome isolation were utilized on preserved blood samples. Both methods utilize differential centrifugation to separate the nuclear and mitochondrial fractions.

Differential centrifugation via Lim *et al.* (2005)

This procedure was adapted from the isolation of DNA documented in Lim *et al.* (2005). A TES isolation buffer consisting of 100mM Tris pH 7.4, 10mM EDTA, and 250mM Sucrose was prepared. During all steps the reagents and working solutions were kept on ice and the centrifuge temperature was set to 4°C. Two milliliters of blood were added to 38mL of TES buffer (95:5 v/v) in a 50mL centrifuge tube and vortexed for 1 minute to homogenize the solution. This homogenate was then centrifuged for 20 minutes at 959 x g to crudely separate the two fractions. The supernatant was transferred to a new 50mL tube and the original tube containing the first pellet, which is the nuclear component, was held on ice until later steps. The removed supernatant was centrifuged for 20 minutes at 5,524 x g. The supernatant from this step was then transferred to a new 50mL tube and the pellet was stored on ice. This centrifugation step was completed four more times. The remaining supernatant was centrifuged for 20 minutes at 22,095 x g followed by the removal of the supernatant, leaving the mitochondrial pellet. The nuclear pellet was resuspended in 40mL of TES buffer and centrifuged for 20 minutes at 959 x g. The supernatant was discarded and the nuclear pellet was chilled again on ice. The

nuclear component pellet and the mitochondrial pellet were both resuspended in 40mL of TES buffer, vortexed for 30 seconds and centrifuged for 20 minutes at 959 x g and 22,095 x g respectively. The supernatant was removed and the pellets were resuspended in 400μL TNE extraction buffer, extracted, and ethanol precipitated following the procedures previously described in DNA Extraction methods.

QIAamp® DNA Mini Kit

The QIAamp® DNA Mini Kit (Qiagen) was used following the Protocol for Mitochondrial DNA from Platelets to isolate the mitochondrial genome. The protocol was modified to incorporate the isolation of the nuclear genome. Four mililitres of blood was centrifuged in a 15mL centrifuge tube for 15 minutes at 100 x g. The upper layer was transferred to a new tube and centrifuged at 200 x g for 10 minutes. The bottom nuclear layer was set aside. The platelet suspension was added in a 1.5mL microcentrifuge tube with 40μL QIAGEN Protease solution and 400μL Buffer AL. The suspension was vortexed and incubated for 10 minutes at 56°C. Samples were quickly centrifuged, 400μL of ethanol added, vortexed, and zip spun (a brief centrifugation to remove residual liquid from the lid and sides of tube). The lysate was then added to a QIAamp Mini spin column in a 2mL tube. The tube cap was closed and the sample centrifuged for 1 minute at 6000 x g. The spin column was then place in a new 2mL collection tube and the original tube containing the filtrate discarded. Five hundred microlitres of Buffer AW1 were added to the spin column and then centrifuged for 1 minute at 6000 x g. The spin column was removed and placed in a new 2mL tube and the filtrate tube discarded. The column was opened and 500μL of Buffer AW2 was added and the column was then centrifuged for 3 minutes at 20,000 x g. The column was

removed, placed in a new collection tube, and centrifuged for 1 minute at max speed. The column was removed, placed in a new collection tube and 100µL of ddH_2O was added. The sample was incubated for 1 minute at room temperature and then centrifuged for 1 minute at 6000 x g to elute. The isolated nuclear layer was then processed according to the described Lim *et al.* (2005) extraction method with the exception of the mitochondrial fraction processing.

For mitochondrial and nuclear genome separation confirmation, the primers 15975F and 429R (Sigma-Aldrich) were used to amplify the mitochondrial genome and the primers 61942HBB3F and 62257HBBR targeting the *Homo sapiens* hemoglobin, beta (Accession U01317.1) were used for nuclear genome amplification (Table 6).

Table 6. Sequence and properties of oligonucleotides used in the genome separation amplification of nuclear and mitochondrial DNA.

Primer name and position	Primer Sequence (5'-3')	Length (bp)	GC content (%)	Tm (°C)
15975F	CTC CAC CAT TAG CAC CCA AAG C	22	55	64
429R	CTG TTA AAA GTG CAT ACC GCC A	22	45	60
61942HBB3F	TCT TAG AGG GAG GGC TGA GGG TTT	24	54	67
62257HBBR	ACT TCA TCC ACG TTC ACC TTG CCC C	25	56	69

These primer sets have the identified annealing temperatures and extension times, reagent concentrations, and PCR cycling parameters as outlined in Tables 7, 8, and 9 respectively.

Table 7. PCR annealing and extension parameters of genome separation oligonucleotides.

Primer Set	Forward Primer	Reverse Primer	Annealing Temperature (°C)	Extension Time (sec)
Mitochondrial	15975F	429R	62	50
Nuclear	61942HBB3F	62257HBBR	63	30

Table 8. PCR reagent concentrations for genome separation amplification.

Reagent	Volume (µL)	Final Concentration
Takara LA Taq™ DNA Polymerase (5 U/µL)	0.25	1.25U
10X LA PCR Buffer II (Mg^{2+}plus)	2.5	1X
10mM dNTP Mix (2.5mM each)	4	0.4mM each
Template	5	-
10uM Forward Primer	0.5	0.2µM
10uM Reverse Primer	0.5	0.2µM
Sterile ddH_2O	12.25	-

Table 9. PCR cycling parameters for genome separation amplification.

PCR Step	Temperature (°C)	Time (sec)	Cycle
First Denaturing	94.0	180	1
Denaturing	94.0	30	1-35
Annealing	*	30	1-35
Extension	72.0	**	1-35
Hold	4.0	-	Hold

* Annealing temperature is dependant on primer set.
**Extension time is dependent on primer set used as the size of amplicon may differ.

2.1.4 DNA Fragment Isolation

To target a genetic area of interest, restriction enzymes were selected in an attempt to fragment the mitochondrial genome which could be further analyzed for DNA damage and modification. The mitochondrial genome is an ideal candidate for fragment isolation due to the concentration of genes in its relatively small genome (16,569bp) potentially enabling restricted fragments to be identified, isolated, and excised. Due to the difficulties in isolating the nuclear and mitochondrial genomes the fragment isolation was completed using the PCR Damage Template as a "proof of principle" for identifying damaged DNA in specific and isolated DNA fragments. In this research the enzymes tested were MslI, MseI, MscI, KpnI, and HaeIII. All restriction enzymes and accompanying buffer solutions were from New England Biolabs®. In this research HaeIII was primarily used resulting in 3 DNA fragments (482, 435, and 106bp) and

approximately 3-4μg of starting template was necessary to ensure enough DNA concentration was present for damage induction and assessment. Samples are damaged prior to restriction enzyme reactions.

In a 2mL microcentrifuge tube, 1μL of HaeIII (10,000 U/mL) per 1μg of DNA and 5μL of 10X NEBuffer 2 was added to DNA template in a total volume of 50μL. The samples were briefly vortexed and zip spun. The samples were incubated at 37°C and 450rpm (30sec/2min) for 90 minutes on the Eppendorf® Thermomixer R. Following incubation an enzyme heat inactivation step was completed at 80°C for 20 minutes.

The full volume of each sample was loaded into a 1% agarose gel and ran until band resolution was obtained. The bands were gel excised using an X-Acto™ knife and each band was placed into a separate 2mL microcentrifuge tube and gel purified using RBC Bioscience HiYield™ Gel/PCR DNA Extraction Kit and eluted in 45μL of ddH2O. For visual confirmation that the fragment was successfully excised a 5μL aliquot was run on a 1% agarose gel.

2.2 Damage Protocols

In this study PCR template and dNTP's were treated with multiple reagents (H_2O_2, Fenton Reaction, Heat/acid Buffer, UVA/B/C, Formalin, APS, DMSO) in an attempt to induce damage to the DNA structure and nucleotides. PCR product as damage template was selected due to the abundance of template, known base characteristics, and lack of any possible starting damage. For similar reasons, dNTP's were used due to abundance and relatively pure starting template. When damaging PCR template an approximate starting template of 1.2μg is used from a starting concentration of approximately 110ng/μL. After the sample is treated with the damage agent it is placed

on ice until purified by ethanol precipitation or the RBC Bioscience HiYield™ Gel/PCR DNA Extraction Kit to remove damage reagents. A temperature/time control sample containing 10μL 0.01M PBS in place of the damaging reagent is run along side the samples for the maximum reaction time period to ensure any results obtained is due to the damage reagent and not the time duration or temperature exposure. Individual dNTP's (Fermentas) and mixed dNTP's (Takara Bio Inc.) were chilled on ice until all reactions are complete and then lyophilized.

2.2.1 Hydrogen Peroxide

PCR template at a mass of approximately 1.2μg was added to a 1.5mL microcentrifuge tube along with 10μL of 3% H_2O_2 and ddH_2O to achieve a final volume of 50μL. The volume of ddH_2O added was dependant on the concentration of the PCR template added. The samples were vortexed for 15 seconds, zip spun and incubated at 37°C for interval time periods. The samples were cleaned using the RBC Bioscience HiYield™ Gel/PCR DNA Extraction Kit.

For individual dNTP's, tubes were prepared with 100μL of 30% H_2O_2, 96μL of ddH_2O, and 4μL 100mM dNTP to be analysed. The samples were vortexed for 30 seconds and then zip spun down. The tubes were incubated at 37°C and 500rpm (30sec/2min) for the determined length of time on the Eppendorf® Thermomixer R. The time intervals in this research consisted of 0, 0.5, 1, 12, and 48 hour incubation periods. Once incubation was completed the samples were immediately placed on ice and then lyophilized.

For dNTP mixtures 100μL, of 10mM dNTP and 100μL of ddH2O was added to a 1.5mL microcentrifuge tube and vortexed for 30 seconds. The samples were incubated at

37°C and 500rpm (30sec/2min) for the time intervals of 0.5, 1, 24, and 48 hours on the Eppendorf® Thermomixer R. After incubation was complete the samples were held on ice until lyophilized.

2.2.2 Dimethyl Sulfoxide (DMSO)

PCR template at a mass of approximately 1.2μg was added to a 1.5mL microcentrifuge tube with 25% DMSO and ddH_2O to a final volume of 100μL. The volume of ddH_2O added was dependant on the concentration of the PCR template added. The samples were vortexed for 15 seconds, zip spun and incubated at 37°C for 1 hour. The samples were then purified with the RBC Bioscience HiYield™ Gel/PCR DNA Extraction Kit.

For individual dNTP damage reactions, tubes were prepared with 25μL DMSO, 70μL of ddH_2O, and 5μL 100mM of the selected dNTP to be analysed. The samples were vortexed for 30 seconds and then zip spun down. The tubes were incubated at 37°C and 500rpm (30sec/2min) for 1 hour on the Eppendorf® Thermomixer R. Once incubation was completed the samples were immediately placed on ice and then lyophilized.

2.2.3 Formalin

PCR template at a mass of approximately 1.2μg was added to a 1.5mL microcentrifuge tube with 10μL Formalin and ddH_2O in a final volume of 100μL. The volume of ddH_2O added was dependant on the concentration of the PCR template added. The samples were vortexed for 15 seconds and zip spun and incubated. The incubation times of 1, 24, and 48 hours were completed at room temperature. The samples were

cleaned with the RBC Bioscience HiYield™ Gel/PCR DNA Extraction Kit and eluted in 50μL of ddH_2O.

For individual dNTP damage, tubes were prepared with 95μL Formalin and 5μL of the selected 100mM dNTP to be analysed. The samples were vortexed for 30 seconds and then zip spun down. The tubes are incubated at room temperature at a mix speed of 500rpm (30sec/2min) for 1 hour on the Eppendorf® Thermomixer R. Once incubation was completed the samples are immediately placed on ice and then lyophilized.

2.2.4 Ammonium Persulfate (APS)

PCR template at a mass of approximately 1.2μg was added to a 1.5mL microcentrifuge tube with 10% APS and ddH_2O in a final volume of 100μL. In this reaction series the concentration of the 10% APS was adjusted and tested at 50, 20, and 10μL in the 100μL solution for final concentrations of 5, 2 and 1 percent. The volume of ddH_2O added was dependant on the concentration of the PCR template added. The samples were vortexed for 15 seconds and zip spun and incubated at 37°C and a mix speed of 500rpm (30sec/2min) for 1 hour on the Eppendorf® Thermomixer R. The samples were cleaned with the RBC Bioscience HiYield™ Gel/PCR DNA Extraction Kit.

For individual dNTP damage, tubes were prepared with 95μL 10% APS and 5μL of each dNTP (100mM). The samples were vortexed for 30 seconds and then zip spun down. The tubes were incubated on the Eppendorf® Thermomixer R at 37°C and a mix speed of 500rpm (30sec/2min) for 1 hour. Once incubation was completed the samples were immediately placed on ice and held until lyophilized.

2.2.5 UVR treatment

In this study UVA/B/C with wavelengths of 365, 312, and 254nm respectively, generated by a UVP 3UV™ Transilluminator were used to induce damage to the DNA structure and to modify individual bases.

The PCR template of approximately 1.2μg of DNA was added to a 1.5mL microcentrifuge tube with ddH_2O to achieve a final volume of 50μL. The samples were vortexed for 15 seconds and zip spun. The tubes were inserted into an open bottom sample rack and placed on a transilluminator with the bottom of the tube approximately 4mm from the transilluminator surface. An illuminator shroud was placed over the samples and surface area to prevent light escape. The tip of a thermometer was placed within the working area to ensure the temperature does not exceed 37°C. The UVR light was turned on and the samples were treated for 1 and 2 hour exposure times. The samples were placed on ice to cool and then processed with the RBC Bioscience HiYield™ Gel/PCR DNA Extraction Kit.

For mixed dNTP damage, 100μL of 10mM dTNP's were placed in a 1.5mL microcentrifuge tube. The samples were placed in an open bottom sample rack and placed on the transilluminator with the tubes approximately 4mm from the glass surface. The tip of a thermometer was placed within the working area to ensure the temperature did not exceed 37°C. The UVR light was turned on and the samples were treated for a 2 hour exposure time. Once the exposure was completed, the tubes were placed on ice to cool followed by lyophilization.

2.2.6 Sodium Citrate - Heat/Acid Buffer

Following the methods of Nakamura *et al.* (1998), an acid buffer solution was prepared consisting of 10mM sodium citrate, 10mM NaH_2PO_4, and 10mM NaCl at pH 5.0. Template of approximately 1.2µg of DNA was placed in a 1.5mL microcentrifuge tube and dried down. The DNA was suspended in 100µL of the acid buffer, vortexed for 30 seconds and zip spun. The samples were incubated on the Eppendorf® Thermomixer R at 70°C at a mix speed of 500rpm (30sec/2min) for 5, 10, 15, 20, 30, 40, and 60 minute intervals. Once incubation was completed the samples were immediately placed on ice to stop the reaction. Once cooled, the samples were purified via ethanol precipitation and suspended in 50µL ddH_2O.

Individual dNTP's at a volume of 4µL was added to a 1.5mL microcentrifuge tube and desiccated. The dNTP's were resuspended in 200µL of the acid buffer, vortexed for 30 seconds and zip spun. The samples were then incubated at 70°C at a mix speed of 500rpm (30sec/2min) for 1 hour using the Eppendorf® Thermomixer R. Once completed, the tubes were immediately placed on ice to cool followed by lyophilization.

2.2.7 Fenton Reaction

In this study the previous methods outlined in Feig *et al.* (1994) and Henle *et al.* (1996) were used and adjusted to induce damage via the Fenton reaction. Following the methods of Feig *et al.* (1994), in a 1.5mL microcentrifuge tube 1.2µg of PCR damage template was added with the final concentrations of 10mM Tris·HCL (pH 7.5), 750µM $FeSO_4 \cdot 7H_2O$, 15mM H_2O_2, 1.5mM ascorbic acid in a total volume of 200µL. The samples were vortexed for 30 seconds and quickly zip spun. The samples were then placed in the Eppendorf® Thermomixer R and incubated at 37°C at a mix speed of

500rpm (30sec/2min). In this study the time intervals of 15, 30, 45, 60, and 120 minutes were completed. After incubation the samples were cleaned using the RBC Bioscience HiYield™ Gel/PCR DNA Extraction Kit.

Adapting the methods of Henle *et al.* (1996), PCR template with a mass of 1.2μg was combined in a 1.5mL microcentrifuge tube with the final concentrations of 2mM H_2O_2, 1mM $FeSO_4 \cdot 7H_2O$, and Tris·HCL was added to achieve pH 5.7. The samples were vortexed, zip spun, and placed in an Eppendorf® Thermomixer R to incubate at 37°C with a mix speed of 500rpm (30sec/2min). In this study the time intervals of 15, 30, 45, 60, and 120 minutes were completed. After incubation the samples were cleaned using the RBC Bioscience HiYield™ Gel/PCR DNA Extraction Kit.

2.3 Damage Detection Protocols

2.3.1 Template Integrity

To observe the integrity of the template DNA post damage horizontal agarose Gel Electrophoresis was used in this research. A volume of 1X TAE buffer suitable for the size of gel apparatus being used was poured into an Erlenmeyer flask and agarose was added to achieve a 1% gel concentration using the formula; Agarose(g) = [%Gel/100] x [TAE volume(mL)]. The flask was heated to a boil to dissolve the agarose and then left to cool to approximately 50-60°C. Once cool enough to handle, 2μL of 10mg/mL of ethidium bromide were added and stirred into solution. An appropriate gel comb was added to the gel tray in the casting position of the buffer chamber. The agarose was then poured and allowed to cool for 30-45 minutes at room temperature. Once the gel had solidified the gel tray is positioned so that the wells are placed towards the negative electrode to ensure that the DNA will migrate towards the positive electrode once the

current is added. The chamber was filled with 1X TAE buffer and the combs removed. Six microlitres of DNA ladder with a concentration of 0.1μg/μL was added in one well to each row of samples. The samples were mixed with 6X loading buffer in a ratio of 5:1 (v/v) respectively and loaded into the wells. The power supply was then connected to the gel apparatus and set to 100V. Once completed the gel was visualized using the Kodak EDAS 290 gel imaging system and analyzed with Kodak 1D imaging software.

2.3.2 Damaged Template Amplification

After damage was induced to the PCR product a hemi-nested amplification was completed using the original forward primer and the reverse primer 16420R resulting in a 445bp product (Table 10).

Table 10. Sequence and properties of oligonucleotides used in the amplification of mitochondrial DNA.

Primer name and position	Primer Sequence (5'-3')	Length (bp)	GC content (%)	Tm (°C)
15975F	CTC CAC CAT TAG CAC CCA AAG C	22	55	64
16420R	TGA TTT CAC GGA GGA TGG TG	20	50	60

For the damaged samples amplification, *Taq* DNA polymerase (New England Biolabs®) was selected due to it being one of the most frequently used DNA polymerases with average fidelity and a lack of 3'-5' exonuclease (proofreading) ability. These characteristics make it an ideal candidate to observe any damage, in terms of amplification efficiency, present in the treated template. The concentrations of reagents used in the *Taq* DNA Polymerase Kit from New England BioLabs® are listed in Table 11.

Table 11. PCR reagent concentrations for damaged template amplification.

Reagent	Volume (µL)	Final Concentration
Taq DNA Polymerase (5 U/µL)	0.15	0.75U
10X Standard Taq Reaction Buffer	2.5	1X
10mM dNTP Solution Mix	0.5	0.2mM
Template ~(20ng/µL)	5	100ng
10uM Forward Primer	0.5	0.2µM
10uM Reverse Primer	0.5	0.2µM
Sterile ddH_2O	15.85	-

The damage amplification was completed using the PCR cycling parameters listed in Table 12 for a total of 30 cycles.

Table 12. PCR cycling parameters for damaged template amplification.

PCR Step	Temperature (°C)	Time (sec)	Cycle
First Denaturing	94.0	180	1
Denaturing	94.0	30	1-30
Annealing	60	30	1-30
Extension	72.0	*	1-30
Hold	4.0	-	Hold

*Extension time is dependent on primer set used as the size of amplicon may differ.

2.3.3 Abasic Detection

Endonuclease IV Detection System

To cleave the phosphodiester bond 5' to an AP site and create a 3' hydroxyl group 10units of Endonuclease IV (New England Biolabs®) and 1X NEBuffer 3 were added to 1µg of DNA template in a 2.0mL centrifuge tube. The sample was vortexed and quickly spun down to remove residue on the side of the tube. The sample was then placed in the Eppendorf® Thermomixer R at 300rpm for 3 hours at 37°C. To confirm and observe the extent of the abasic sites the sample was visualized with agarose gel electrophoresis.

The samples to be further processed for ddNTP incorporation are split in equal volumes into new 2mL centrifuge tubes to serve as a positive and negative sample controls. The sources of ddNTP's are from individual fluorescent ddNTP's (PerkinElmer Inc.) and pooled nucleotides in the ABI Prism® SNaPshot™ Multiplex Kit (Applied

Biosystems). The properties of these fluorescent dyes and ddNTP's are listed below in Table 13.

Table 13. Properties of individual and SNaPshot™ Multiplex Kit fluorescent ddNTP's.

Individual Fluorescent Dideoxynucleotides				
ddNTP	Dye Label	Extinction coeff.($M^{-1}cm^{-1}$)	Excitation (nm)	Emission (nm)
A	R6G	108000	525	550
C	ROX	82000	580	605
G	R110	78000	500	525
T	TAMRA	91000	552	575
SNaPshot™ Multiplex Kit Fluorescent Dideoxynucleotides				
ddNTP	Dye Label	Extinction coeff.($M^{-1}cm^{-1}$)	Excitation (nm)	Emission (nm)
A	R6G	108000	525	550
C	TAMRA	91000	552	575
G	R110	78000	500	525
T	ROX	82000	580	605

Positive samples containing approximately 1μg of DNA template were mixed with 1 unit/5μL of Klenow Fragment DNA Polymerase (New England Biolabs®) and 8.25μM of each individual fluorescent-ddNTP (PerkinElmer Inc.), or 10μL of the SNaPshot™ Multiplex Ready Reaction Mix (Applied Biosystems). The tubes were briefly vortexed and zip spun to remove any remaining solution on the sides. Samples were then incubated for 2 hours at 37°C. Negative sample controls do not contain any Klenow Fragment DNA Polymerase and this volume is substituted with an equivalent volume of ddH_2O. Post incubation, samples were allowed to cool to room temperature and processed with RBC Bioscience HiYield™ Gel/PCR DNA Extraction Kit to remove any non-incorporated ddNTP's. The samples were eluted in 40μL of ddH_2O and then concentrated to 10μL.

GeneScan Analysis

An amount of 1μL of sample was combined with 12μL of deionized formamide and 0.5μL of GENESCAN-500 LIZ® (Applied Biosystems) as the internal standard, denatured at 95°C for 5 minutes followed by cooling on ice for 5 minutes. To determine the length of DNA fragments and amount of fluorescent nucleotides that were incorporated an ABI Prism Genetic Analyzer™ 3100 (POP-4 polymer) with GeneScan ™ (Applied Biosystems) software was utilized. The electropherograms of the samples and controls were analyzed for size of amplicon and fluorescent signal.

Nanodrop Quantitation

A Nanodrop ND-1000 Spectrophotometer (Thermo Fischer Scientific) was used to detect the fluorescence signal emitted by the ddNTP's. The fluorescent properties of each ddNTP used were entered into the Dye/Chromophore editor. Using the MicroArray application module the ddNTP of interest was selected from the dye drop down menu. After blanking the instrument with ddH_2O, 2μL of each sample was added to the measurement pedestal and the absorbance is measured and recorded. The absorbance and spectrum for all positive and negative samples were analyzed.

2.3.4 Gas Chromatography-Mass Spectrometry Analysis

Samples were initially dried under vacuum in a 2mL autosampler vial, without heat, using an Eppendorf Concentrator 5301. Following the methodology outlined by Dizdaroglu (1994) the vials were evacuated with nitrogen gas and heated at 140°C for 30 minutes in 60% (v/v) formic acid and then immediately lyophilized. The products were purged with nitrogen, sealed with a teflon septa, and then derivitized by heating 80μL

bis(trimethylsilyl)trifluoroacetamide (with 1% trimethylchlorosilane) (Sigma-Aldrich) and 20μL of acetonitrile (Sigma-Aldrich) at 120°C for 30 minutes.

After derivitization the samples were analyzed using a Varian CP-3800 gas chromatograph and Varian 1200 Quadrupole Mass Spectrophotometer. Using an autosampler, 1μL of sample was injected into the injection port at a temperature of 280°C with helium as the carrier gas in a DB-5 column. The column oven temperature was set to 50°C for one minute and increased to 280°C at a rate of 10°C/minute and then held for 6 minutes. Electron ionization is utilized at an electron energy of -70eV and full scan ion monitoring is started at 5.0 minutes to avoid detecting the derivitizing agents. Output files were analyzed using Varian MS Workstation Version 6 and the NIST 98 Mass Spectral Database.

3.0 Results

3.1 Template Processing

3.1.1 Genome Separation

Using the protocols listed in Lim *et al.* (2005) to separate the nuclear and mitochondria fractions the initial reactions failed as mitochondria product was observed in the nuclear fraction and nuclear product in the mitochondria fraction (Figure 10).

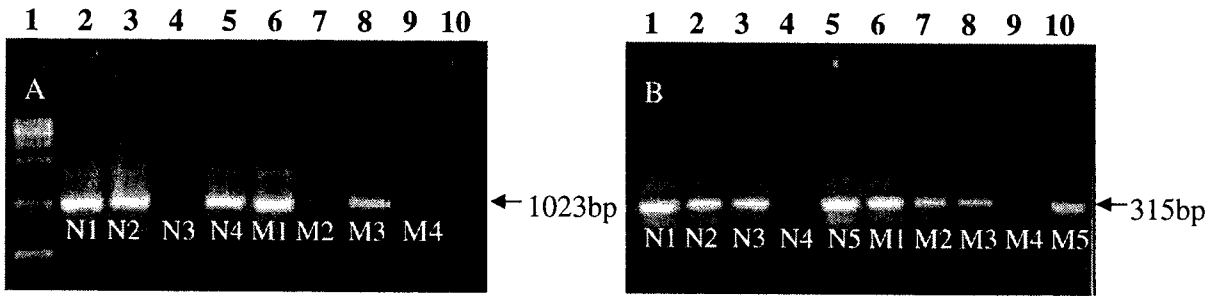

Figure 10. Amplification of nuclear (N) and mitochondrial (M) fraction samples using A. mitochondrial and B. nuclear primer sets. Gel A. Lane 1: DNA Ladder; Lane 2: Nuclear fraction trial 1; Lane 3: Nuclear fraction trial 2; Lane 4: Nuclear fraction trial 3; Lane 5: Nuclear fraction trial 4; Lane 6: Mitochondria fraction trial 1; Lane 7: Mitochondria fraction trial 2; Lane 8: Mitochondria fraction trial 3; Lane 9: Mitochondria fraction trial 4; Lane 10: Empty; Gel B. Lane 1: Nuclear fraction trial 1; Lane 2: Nuclear fraction trial 2; Lane 3: Nuclear fraction trial 3; Lane 4: Nuclear fraction trial 4; Lane 5: Nuclear fraction trial 5; Lane 6: Mitochondria fraction trial 1; Lane 7: Mitochondria fraction trial 2; Lane 8: Mitochondria fraction trial 3; Lane 9: Mitochondria fraction trial 4; Lane 10: Mitochondria fraction trial 5.

Due to the failure of the above reactions, a QIAamp® DNA Mini Kit was used following the kit protocols for isolating mitochondrial DNA from platelets. This reaction was also unsuccessful as the targeted nuclear DNA was detectable in the mitochondrial component (Figure 11).

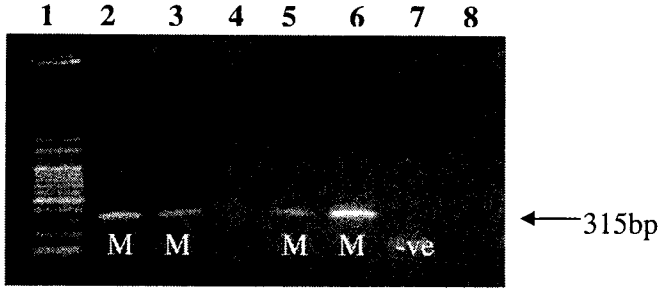

Figure 11. Amplification of mitochondrial (M) fractions using the nuclear primer set after extraction with the QIAamp® DNA Mini Kit. Lane 1: 100bp Sharp Ladder (RBC Bioscience); Lane 2: Mitochondria fraction trial 1; Lane 3: Mitochondria fraction trial 2; Lane 4: Empty; Lane 5: Mitochondria fraction trial 3; Lane 6: Mitochondrial fraction trial 4; Lane 7: PCR Negative; Lane 8: Empty.

The method from Lim *et al.* (2005) was revisited again, however extra centrifugation steps were added in an attempt to purify the divided fractions. Adding these steps resulted in mitochondrial fractions that were void of nuclear DNA. Figure 12 demonstrates mitochondrial fractions amplifying primarily mitochondria DNA in a multiplex PCR reaction with mitochondrial (Band A) and nuclear (Band B) primers. Lane 2 represents a mitochondrial fraction before extra centrifugation steps.

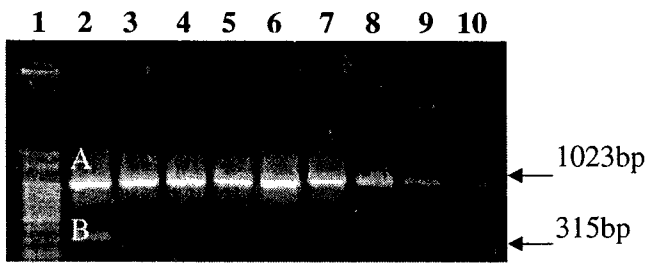

Figure 12. Multiplex PCR reaction of nuclear and mitochondria primers using A. Mitochondrial primers and B. Nuclear Primers. Lane 1: 100bp Sharp Ladder (RBC Bioscience); Lane 2 is original method. Lanes 3-10 have been treated with extra centrifugation steps. Lanes 8-10 are 1:10 template dilutions.

Each separation yielded approximately 1µg of mitochondrial DNA per separation reaction as determined by using the Nanodrop™ 1000 spectrophotometer. The DNA from six reactions was pooled, for a total of 6µg, and used in subsequent reactions.

3.1.2 Fragment Isolation

As previously mentioned, due to difficulties in the isolation of the nuclear and mitochondrial genomes, the fragment isolation was completed using the PCR Damage Template. Using the restriction enzyme HaeIII on the 1023bp template, three fragments with a length of 482, 435, and 106bp (Figure 13) were produced.

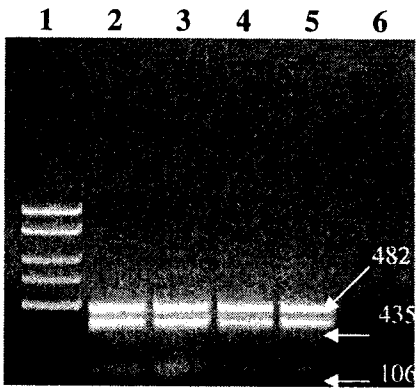

Figure 13. Amplicons produced post HaeIII treatment of 1023bp PCR Damage Template. Lane 1: GeneRuler™ 50bp Plus DNA Ladder (Fermentas); Lane 2: HaeIII restricted 1023bp template 1; Lane 3: HaeIII restricted 1023bp template 2; Lane 4: HaeIII restricted 1023bp template 3; Lane 5: HaeIII restricted 1023bp template 4; Lane 6: Empty.

The two larger products were successfully gel excised independently from each other and confirmed by electrophoresis (Figure 14). The gel products in lanes 2 & 3, 4 & 5, 6 & 7, and 8 & 9 of Figure 14 correspond to the 482 and 435bp products in Lane 2, 3, 4, and 5 respectively of Figure 13.

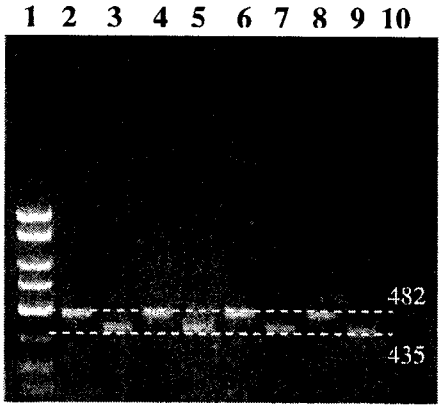

Figure 14. Gel excised products of amplicons 482 and 435 from the original restricted products of the 1023bp PCR template. Lane 1: GeneRuler™ 50bp Plus DNA Ladder (Fermentas); Lane 2: Isolated 482bp Template 1; Lane 3: Isolated 435bp Template 1; Lane 4: Isolated 482bp Template 2; Lane 5: Isolated 435bp Template 2; Lane 6: Isolated 482bp Template 3; Lane 7: Isolated 435bp Template 3; Lane 8: Isolated 482bp Template 4; Lane 9: Isolated 435bp Template 4.

For every 4μg of starting template an average of only 0.5μg per amplicon was recovered after gel excision. For subsequent damage detection reactions it was necessary to pool amplicons of similar fragment size.

3.2 Damage Assessment

3.2.1 Structure Integrity

Agarose gel electrophoresis of the damaged template post damage and purification allowed for the visualization of immediate effects caused to the template. Overall, most samples were not structurally affected as determined by gel visualization of an intact band (Figure 15, 16, & 17) however some samples did exhibit degradation in time course trials and reagent combinations.

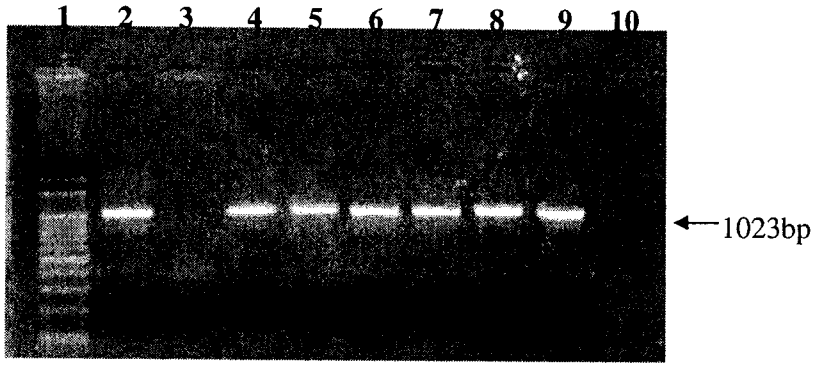

Figure 15. Initial assessment of various damage agents on DNA template. Lane 3 H_2O_2 is absent due to poor DNA yield after purification and not damage related. Lane 1: 100bp Sharp Ladder (RBC Bioscience); Lane 2: PBS Control 37°C 12hr; Lane 3: H_2O_2 12hr; Lane 4: PBS 37°C 24hr; Lane 5: H_2O_2 24hr; Lane 6: UVA 1hr; Lane 7: UVA 2hr; Lane 8: UVB 1hr; Lane 9: Untreated Sample; Lane 10: Empty.

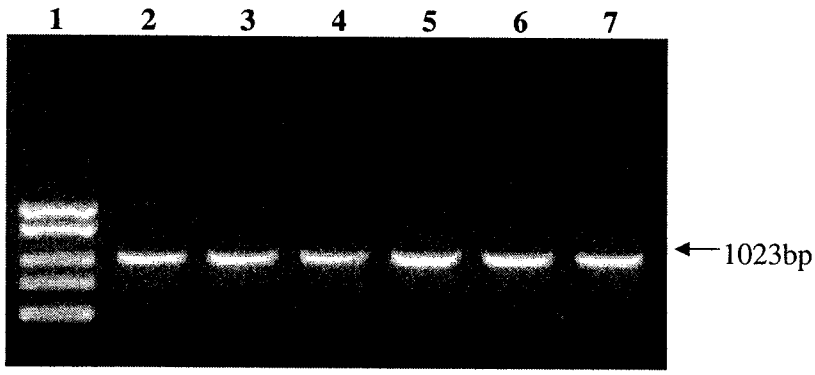

Figure 16. Samples exposed to heat/acid buffer treatment for designated time intervals. Lane 1: 100bp Sharp Ladder (RBC Bioscience); Lane 2: 5min; Lane 3: 20min; Lane 4: 30min; Lane 5: 40min; Lane 6: 60min; Lane 7: PBS 70°C 60min.

In the treatments with 5% and 2% APS for 1 hour no product was observed (Figure 17; Lane 6 &7), though the 1% APS and 1 hour incubation period did yield an intact band (not shown). Extended treatments with formalin also resulted in no visual band at 24 and 48 hour time intervals.

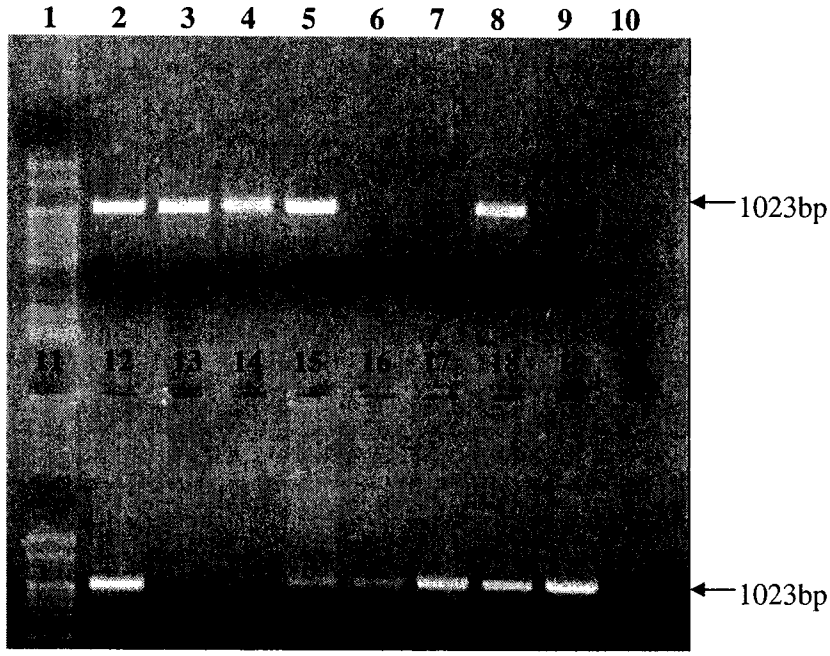

Figure 17. Initial damage assessment on PCR template with various damage agents and conditions. Lane 1: 100bp Sharp Ladder (RBC Bioscience); Lane 2: UVB 1hour; Lane 3: UVB 2hr; Lane 4: UVC 1hr; Lane 5: UVC 2hrs; Lane 6: 5% APS 1hr; Lane 7: 2% APS 2hr; Lane 8: Formalin 1hr; Lane 9: Formalin 2hr; Lane 10: Empty; Lane 11: 100bp Sharp Ladder (RBC Bioscience); Lane 12: UVA 1hr; Lane 13: UVA & H_2O_2 1hr; Lane 14: UVA & H_2O_2 1hr; Lane 15: H_2O_2 5min; Lane 16: H_2O_2 20min; Lane 17: H_2O_2 30min; Lane 18: H_2O_2 40min; Lane 19: Untreated; Lane 20: Empty.

Time interval reactions with UVA generally yielded a visual band, however when combined with H_2O_2 at temperatures observed under UVR conditions the template is not observed. In addition, some Fenton reactions also failed to produce a visible band whereas H_2O_2 alone typically resulted in an unaffected band (not shown).

All time/temperature controls with PBS resulted in a visual unaltered band, along with loaded untreated template. As observed in Lane 3 of Figure 14, it was important to quantify all products using the Nanodrop™-1000 Spectrophotometer before damage reactions and after purification steps to ensure that working and loading template were consistent and that the qualitative results were reliable.

3.2.2 Post Damage PCR Amplification

Utilizing a heminested standard PCR with *Taq* DNA Polymerase on the Damage Template, decreased amplification resulting from template damage can be observed.

Samples damaged with H_2O_2 displayed significantly reduced amplification over the damage time intervals. The experimental control in Lane 8 of Figure 19 (PBS, 37°C for 3 hours) had no observable difference from the PCR positive control in Lane 9 of Figure 19, indicating that any results are not produced from any time and/or temperature affects. The amplification difference was minimal within the first hour (Figure 18), followed by a decrease in product yield for extended time intervals, and eventually no significant product at the 3 hour mark (Figure 19).

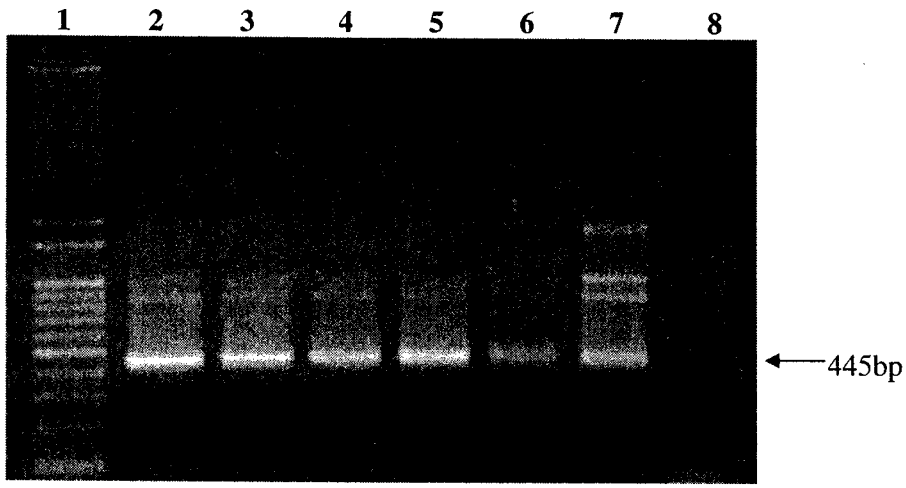

Figure 18. Heminested PCR amplification of H_2O_2 damage focused on short time intervals below 1 hour. Lane 1: 100bp Sharp Ladder (RBC Bioscience); Lane 2: 10min H_2O_2 37°C; Lane 3: 30min H_2O_2 37°C; Lane 4: 45min H_2O_2 37°C; Lane 5: 60min H_2O_2 37°C; Lane 6: 120min H_2O_2 37°C; Lane 7: Positive Control; Lane 8: PCR negative.

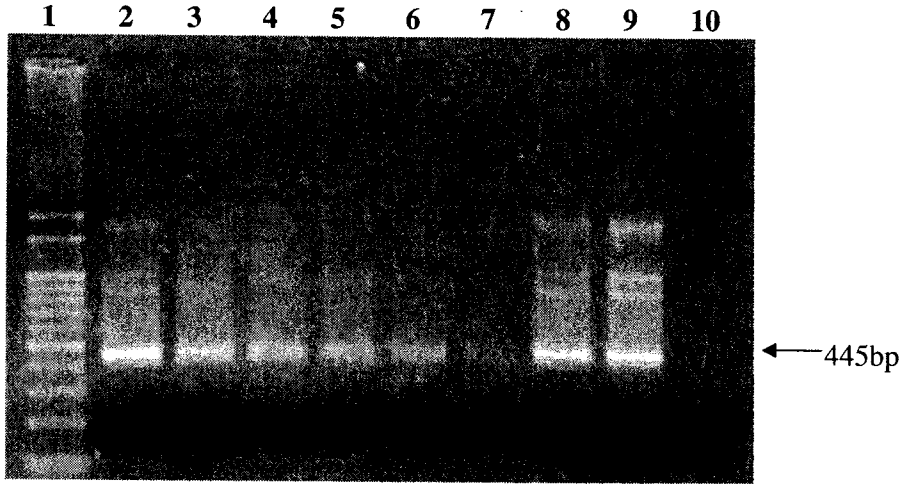

Figure 19. Heminested PCR amplification of extended length time interval H_2O_2 damage. Lane 1: 100bp Sharp Ladder (RBC Bioscience); Lane 2: 10min H_2O_2 37°C; Lane 3: 1.0hr H_2O_2 37°C; Lane 4: 1.5hr H_2O_2 37°C; Lane 5: 2.0hr H_2O_2 37°C; Lane 6: 2.5hr H_2O_2 37°C; Lane 7: 3.0hr H_2O_2 37°C; Lane 8: 3.0hr PBS 37°C; Lane 9: Positive Control; Lane 10: PCR negative.

Samples treated with formalin for 1hour with intact product failed to amplify and as expected those with no observable template product also did not amplify. All other damaged templates which did not have visible product pre-PCR also failed to produce a PCR amplicon.

In the UVR series, UVA (Figure 20) and UVC at both 1 and 2 hour exposure times amplified with the exception of UVA and H_2O_2 damaged samples. Exposure with UVB for one hour resulted in decreased amplification of the target band and a preferential amplification of an unspecific product that is approximately 200bp and is not primer dimer. Despite visible template, UVB samples treated for 2 hours failed to amplify any product (Figure 21).

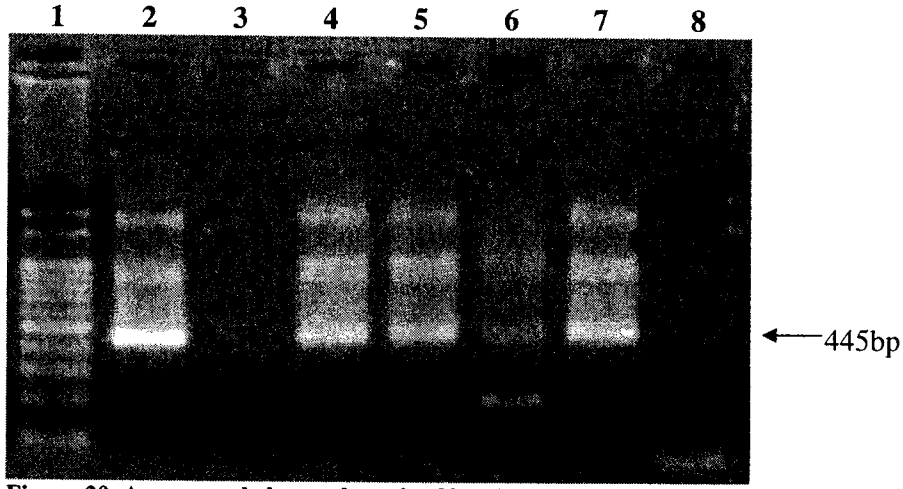

Figure 20. Agarose gel electrophoresis of heminested PCR amplification from damaged template. Lane 1: 100bp Sharp Ladder (RBC Bioscience); Lane 2: PBS 37°C 24hr; Lane 3: H_2O_2 37°C 24hr; Lane 4: UVA 1.0hr; Lane 5: UVA 2.0hr; Lane 6: UVB 1.0hr; Lane 7: Positive Control; Lane 8: PCR negative.

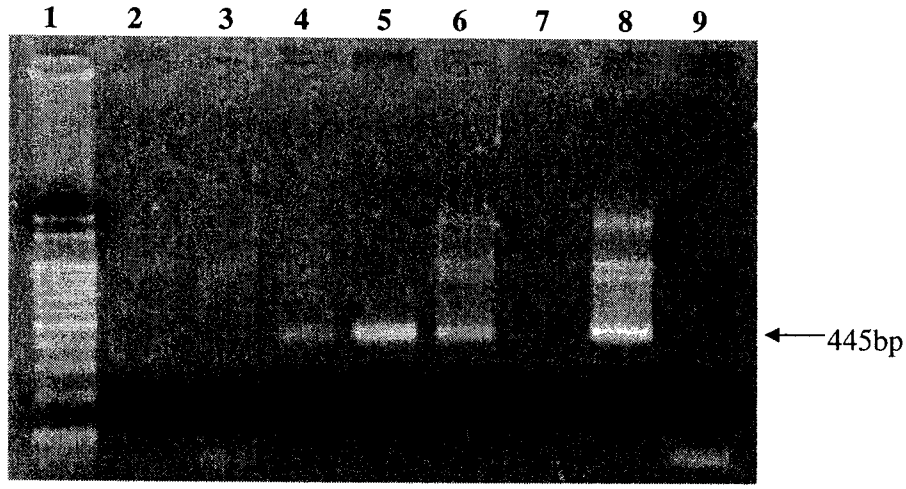

Figure 21. Agarose electrophoresis of heminested PCR amplification from damaged template. Lane 4, labeled with an X, is disregarded due to an error in gel loading. Lane 1: 100bp Sharp Ladder (RBC Bioscience); Lane 2: UVB 2.0hr; Lane 3: UVB 2.0hr; Lane 4: Load Error; Lane 5: 1% APS 37°C; Lane 6: 0.5% APS 37°C; Lane 7: Fenton; Lane 8: Positive Control; Lane 9: PCR negative.

In Figure 22, the Fenton reaction according to Henle *et al.* 1996 did faintly amplify at 1 and 2 hour incubation times whereas both 1 and 2 hour incubations following the concentrations listed in Feig *et al.* 1994 initially failed to amplify. All

Fenton reactions had residual $FeSO_4 \cdot 7H_2O$ indicated by an orange precipitate, which may have inhibited the PCR.

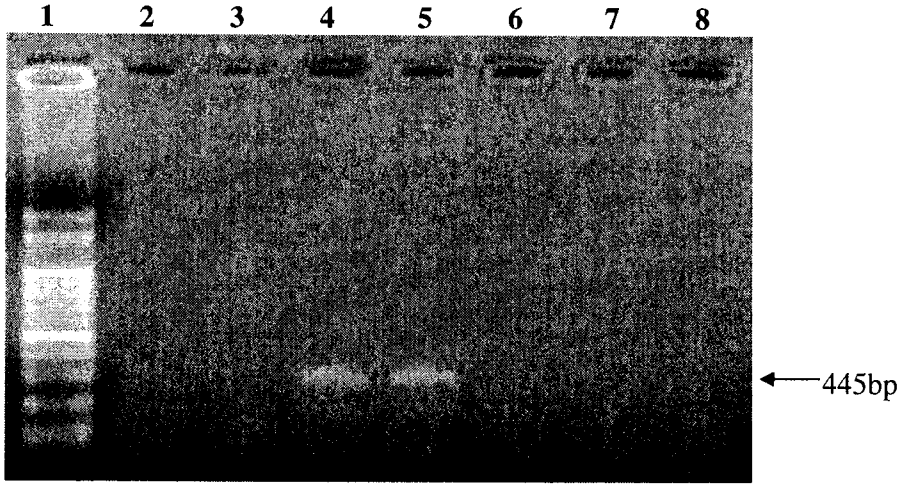

Figure 22. Heminested PCR amplification of template treated with Fenton reaction conditions. Lane 1: 100bp Sharp Ladder (RBC Bioscience); Lane 2&6: 1hr Feig *et al.* (1994); Lane 3&7: 2hr Feig *et al.* (1994); Lane 4: 1hr Henle *et al.* (1996); Lane 5: 2hr Henle *et al.* (1996); Lane 8: PCR negative.

With increased purification steps, the Feig *et al.* 1994 concentrations successfully amplified at incubation times of 15, 30, 60, and 90minutes (Figure 23), however the precipitate was still present.

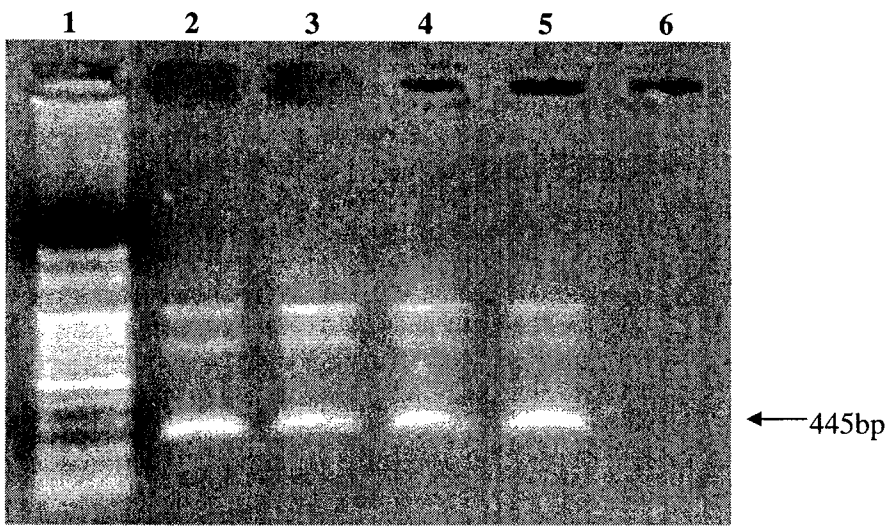

Figure 23. PCR amplification of Fenton reaction treated samples with Feig *et al.* (1994) reaction conditions. Lane 1: 100bp Sharp Ladder (RBC Bioscience); Lane 2: 15min Feig *et al.* (1994); Lane 3: 30min Feig *et al.* (1994); Lane 4: 60min Feig et al (1994); Lane 5: 90min Feig *et al.* (1994); Lane 6: PCR negative.

Samples treated with the heat/acid buffer solution to induce abasic sites demonstrated a decrease in amplification over time intervals observed by agarose gel electrophoresis (Figure 24) and the trend is confirmed in Figure 25 via quantitative PCR. In Figure 25, curve A corresponds to the 5 minute heat/acid buffer treatment followed 1.5 cycles later by the overlapping curves of B and C, 10 and 15 minutes respectively. Curve D, 30 minute treatment, is approximately 8.2 cycles greater than the 5 minute treatment, indicating a significant decrease in amplification with increased damage time. Curve E corresponds to the PBS time/temperature control which represents unaltered DNA.

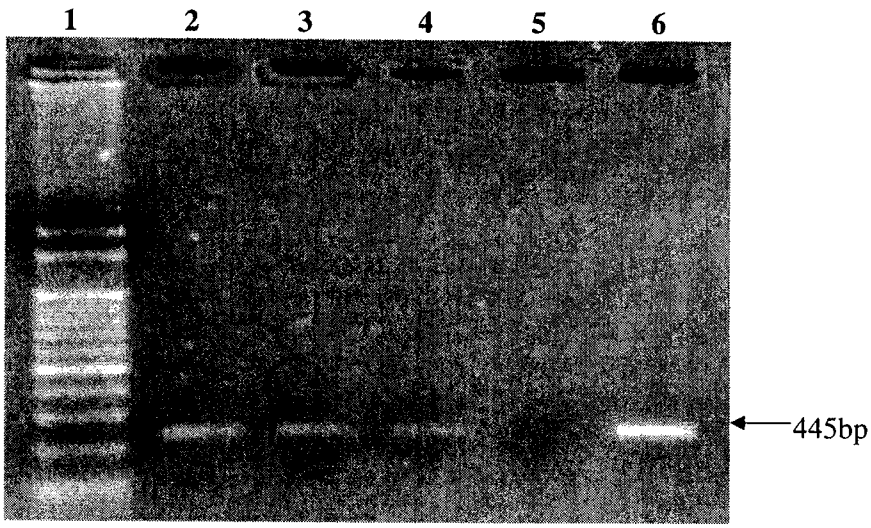

Figure 24. Heminested PCR results of time interval heat/acid buffer solution treatment inducing abasic sites. Lane 1: 100bp Sharp Ladder (RBC Bioscience); Lane 2: 5min; Lane 3: 10min; Lane 4: 15min; Lane 5: 30min; Lane 6: 30min PBS 70˚C.

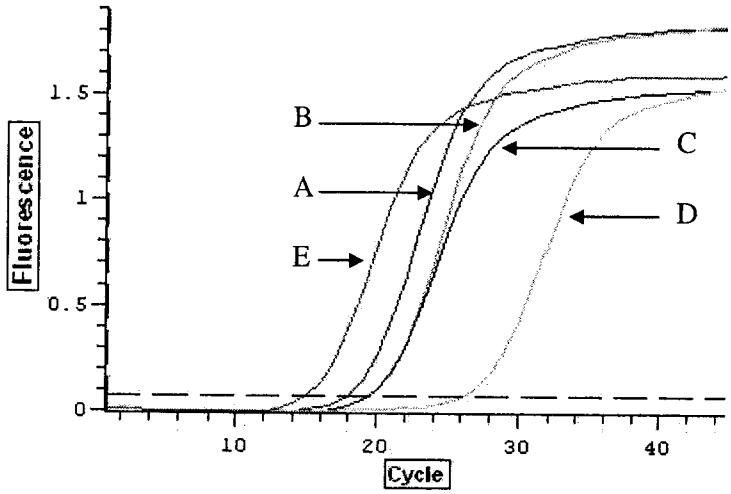

Figure 25. Quantitative PCR of time interval heat/acid buffer solution treatment. Damage time is represented by Curve A. 5min, B. 10min, C. 15min, D. 30min, E. 30min PBS 70°C.

3.2.3 Abasic Detection

Agarose Gel Electrophoresis

To observe if an AP site was created by the damage reagent, the Damage Template samples are treated with Endonuclease IV and then run and visualized on an agarose gel. Endonuclease IV cleaves the phosphodiester bond 5' to the AP site leaving a 3' OH group. Enough of these breaks on the template will eventually yield smaller double stranded products which will be visualized as a smearing pattern on the gel.

When samples are treated in time intervals with the heat/acid buffer solution to induce AP sites, the streaking increases as the product band decreases in intensity until no band is observable (Figure 26).

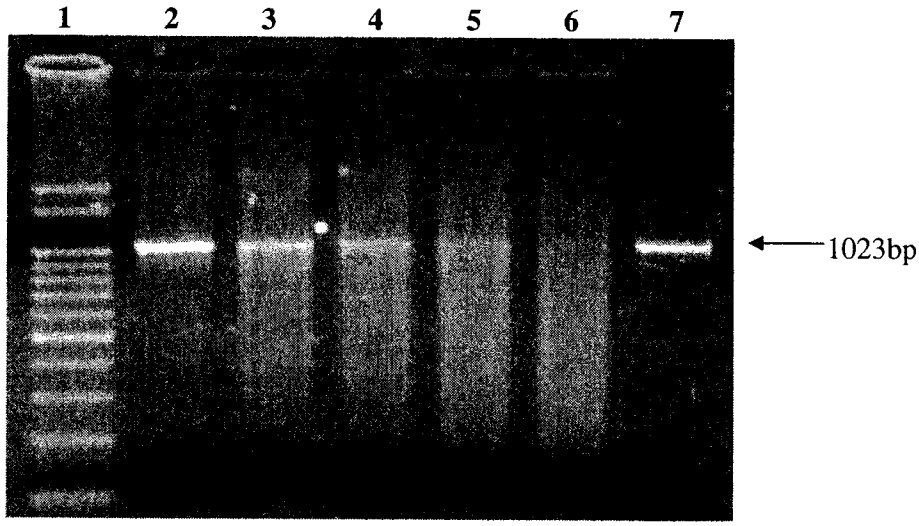

Figure 26. Agarose gel electrophoresis of heat/acid buffer treated samples with Endonuclease IV. Lane 1: 100bp Sharp Ladder (RBC Bioscience); Lane 2: 5min; Lane 3: 20min; Lane 4: 30min; Lane 5: 40min; Lane 6: 60min; Lane 7: PBS 60min.

Samples treated with hydrogen peroxide did not produce any significant observable streaking within 1 hour of damage. A sample which was damaged for 24 hours with H_2O_2 did eventually produce streaking. The 1 hour formalin treated product did not produce any discernable streaking products (Figure 27), nor the DMSO sample.

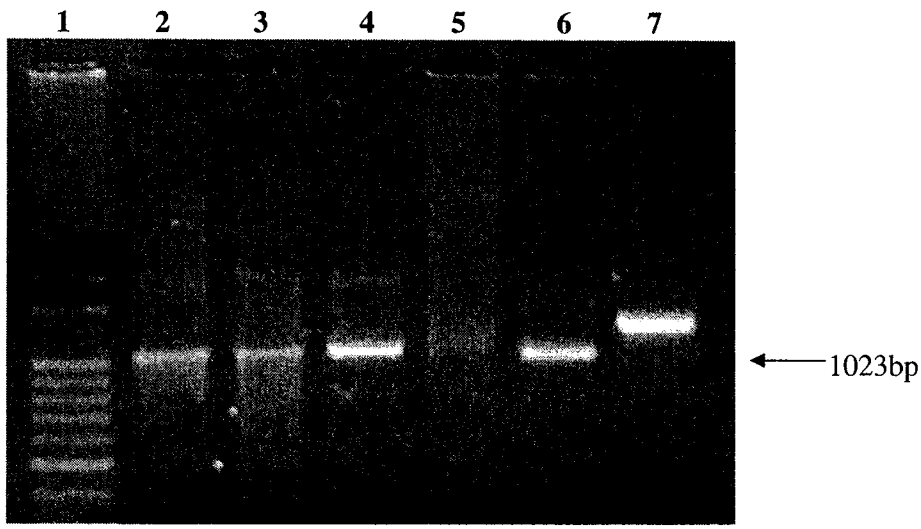

Figure 27. Gel electrophoresis of Endonuclease IV treated damaged samples. Lane 1: 100bp Sharp Ladder (RBC Bioscience); Lane 2: Heat/acid Buffer 15min; Lane 3: Heat/acid Buffer 30min; Lane 4: UVB 1hr; Lane 5: UVC 1hr; Lane 6: Formalin 1hr; Lane 7: Undamaged Control.

In the UVR damage series, UVA exposure did not generally yield any apparent streaking pattern whereas UVC produced a very intense streaking pattern and reduction of DNA template band (Figure 27). Exposure with UVB for 1 hour (Figure 27) did not visually affect the template, however 2 hour exposure yields streaking and reduction of template (Figure 28).

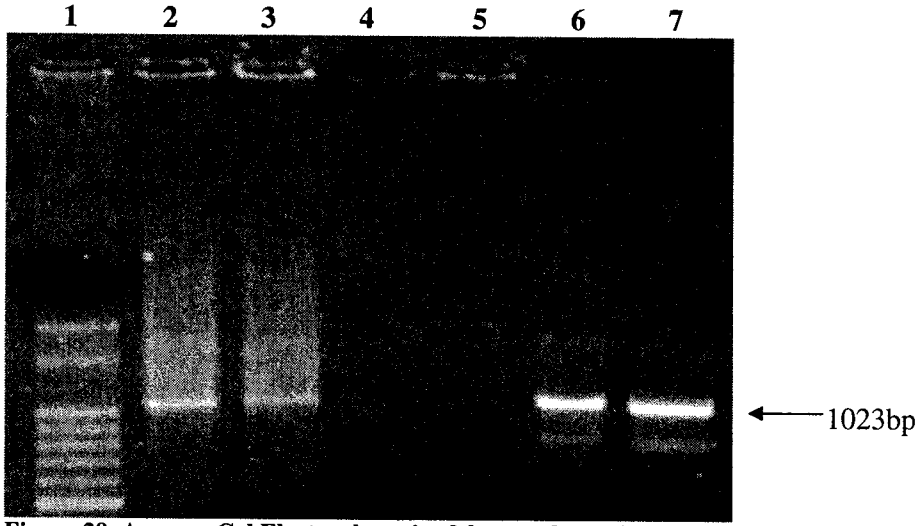

Figure 28. Agarose Gel Electrophoresis of damaged template treated with Endonuclease IV. Lane 1: 100bp Sharp Ladder (RBC Bioscience); Lane 2: UVB 2hr; Lane 3: UVB 2hr; Lane 4: Fenton reaction 1hr; Lane 5: 2% APS; Lane 6: 1% APS; Lane 7: Undamaged Control.

In Figure 28, template damaged with 2% APS is now void of the template band, and the 1% APS sample does not appear to have any streaking or effects to the band intensity.

Samples that were damaged with the heat/acid method and subsequently used in fragment isolation resulted in an observable increase in streaking and decrease in product in time interval reactions after treatment with Endonuclease IV (Figure 29).

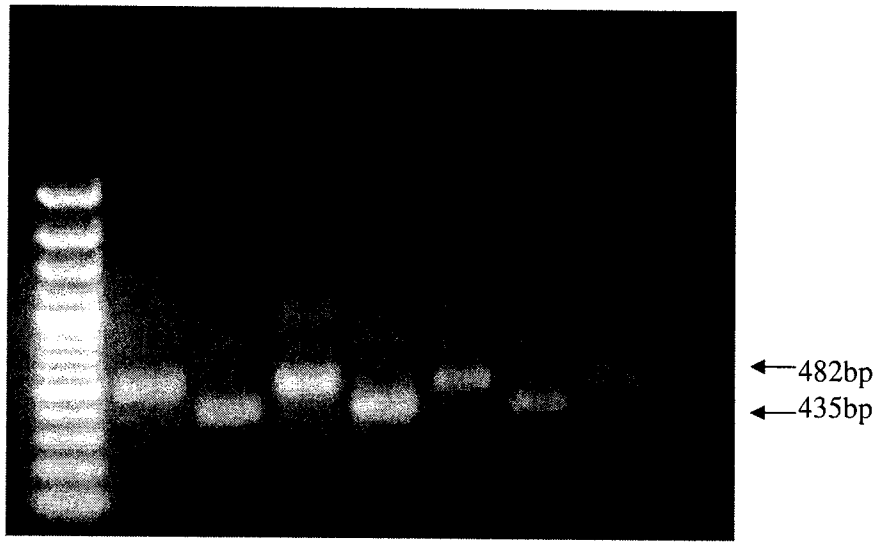

Figure 29. Fragment isolated samples from heat/acid buffer time interval reactions treated with Endonuclease IV. Lane 1: GeneRuler™ 100bp Plus DNA Ladder (Fermentas); Lane 2: 1hr treated sample, 482bp fragment; Lane 3: 1hr treated sample, 435bp fragment; Lane 4: 4hr treated sample, 482bp fragment; Lane 5: 4hr treated sample, 435bp fragment; Lane 6: 7hr treated sample, 482bp fragment; Lane 7: 7hr treated sample, 435bp fragment; Lane 8: 10hr treated sample, 482bp fragment; Lane 9: 10hr treated sample, 435bp fragment.

Spectrophotometer Detection

This methodology was tested as a feasibility study for detection of AP sites in a relatively easy and inexpensive manner. The initial detection was completed with TAMRA-ddUTP on heat/acid buffer treated time interval samples. The times selected were between15-60 minutes since these products contained both streaking and intact template. This indicates that both full length template with AP sites and cleaved double stranded products with 5' overhangs exist for the labeling reaction with the Klenow fragment.

For comparative reference a spectrum of the individual fluorescent ddNTP was initially characterized to compare their respective excitation wavelength (Figure 30).

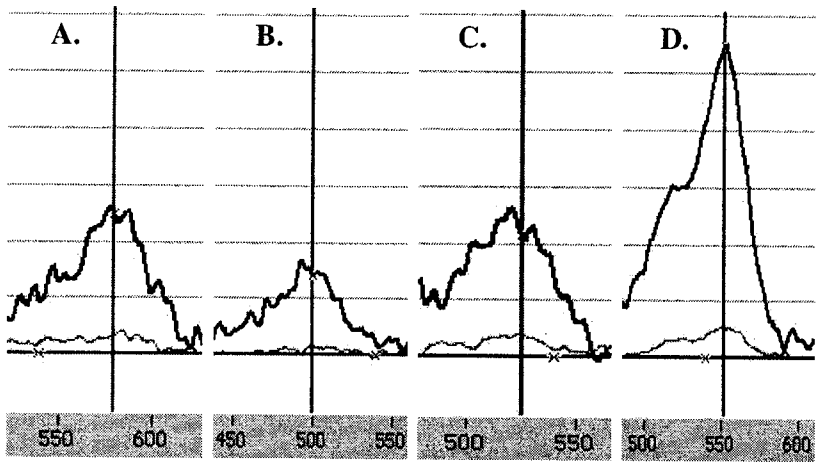

Figure 30. Spectrums of individual fluorescent dideoxynucleotide analogs. A. ROX-ddCTP, B. R110-ddGTP, C. R6G-ddATP, D. TAMRA-ddUTP.

In Figure 31, an AP positive template treated with Klenow and TAMRA-ddUTP which was damaged by heat/acid buffer for 15 minutes yielded an absorbance of 0.02 and concentration of 2.1pmol/μL at the wavelength of 552nm. The parallel control (no Klenow) measured an absorbance of 0.002 and 0.2pmol/μL, indicating that the purification column successfully removed unincorporated fluorescent dideoxynucleotides.

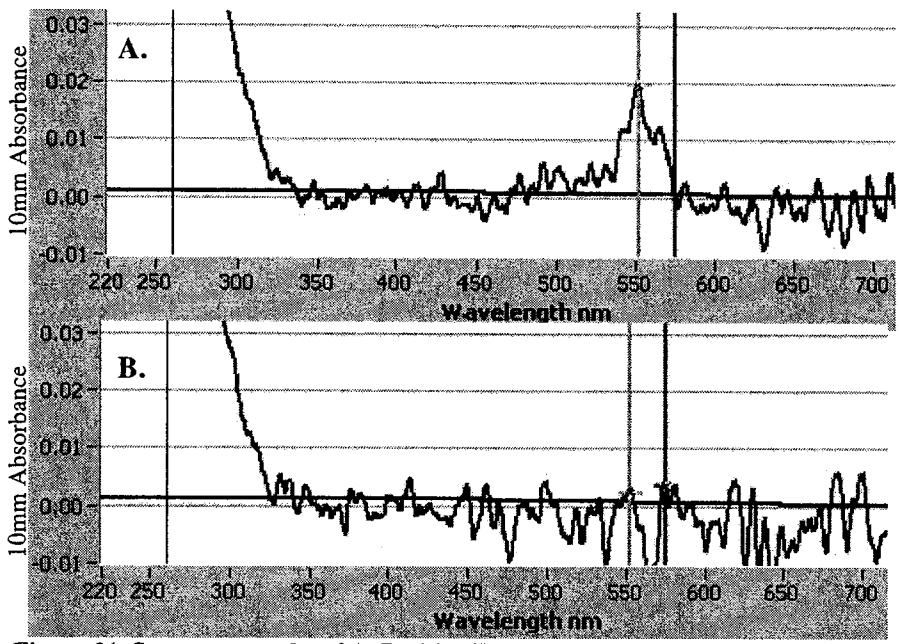

Figure 31. Spectrum results of A. Positive Template, and B. Parallel Control, AP template (15min) treated with TAMRA-ddUTP.

The results of further AP template (15 and 20 minutes) treated with individual TAMRA-ddUTP with is listed in (Table 13).

Table 13. Absorbance and concentration of positive and parallel control samples of AP template (15 and 20min) treated with TAMRA-ddUTP.

AP Template 15min-B	10mm Absorbance	Concentration (pmol/μL)
Positive	0.012	1.3
Parallel Control	0.003	0.4
AP Template 20min-A	**10mm Absorbance**	**Concentration (pmol/μL)**
Positive	0.009	1.0
Parallel Control	0.001	0.1

AP template was then tested using one combination of TAMRA-ddUTP and ROX-ddCTP and a second combination of R6G-ddATP and R110-ddGTP. The first combination produced a clear spectrum for TAMRA-ddUTP however ROX-ddCTP had decreased absorbance and resolution of the wavelength peak (Figure 32) (Table 14).

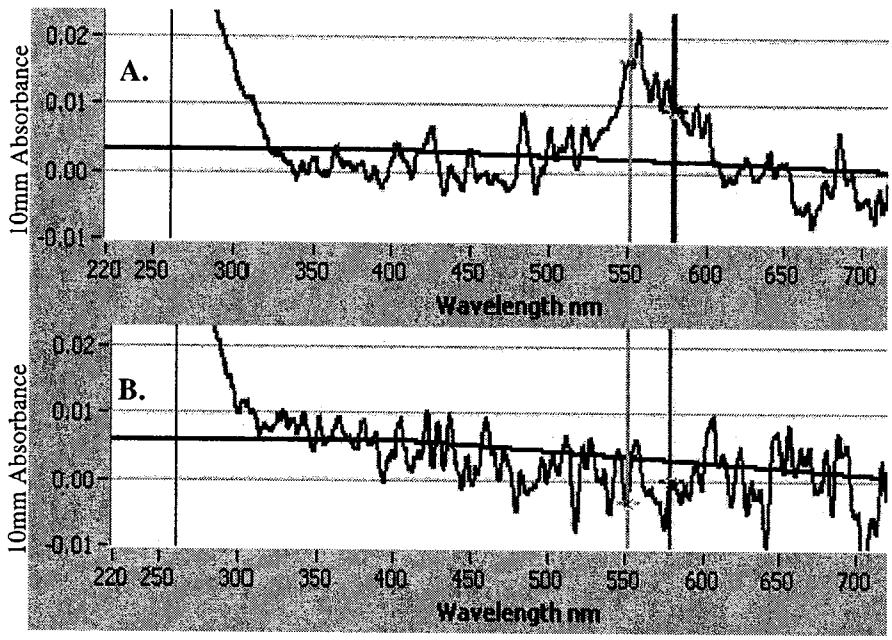

Figure 32. Spectrum results of A. Positive Template, and B. Parallel Control, AP template (20min) treated with TAMRA-ddUTP (552nm) and ROX-ddCTP (580nm).

Table 14. Absorbance and concentration of positive and parallel controls of AP time interval template treated with TAMRA-ddUTP and ROX-ddCTP

	TAMRA-ddUTP		ROX-ddCTP	
AP Template 20min	**10mm Absorbance**	**Concentration (pmol/μL)**	**10mm Absorbance**	**Concentration (pmol/μL)**
Positve	0.019	2.1	0.011	1.3
Parallel Control	-0.009	-1.0	-0.002	-0.2
AP Template 30min	**10mm Absorbance**	**Concentration (pmol/μL)**	**10mm Absorbance**	**Concentration (pmol/μL)**
Positve	0.015	1.6	0.008	1.0
Parallel Control	-0.003	-0.3	0.002	0.3

Samples reacted with R6G-ddATP and R110-ddGTP did not produce as successful of results as only few samples yielded absorbance values above baseline with low resolution between peaks (Table 15).

Table 15. Absorbance and concentration of positive and parallel controls of AP time interval template treated with R6G-ddATP and R110-ddGTP.

	R6G-ddATP		R110-ddGTP	
AP Template 20min	**10mm Absorbance**	**Concentration (pmol/μL)**	**10mm Absorbance**	**Concentration (pmol/μL)**
Positve	0.001	0.1	-0.003	-0.3
Parallel Control	-0.006	-0.5	-0.006	-0.7
AP Template 20minB	**10mm Absorbance**	**Concentration (pmol/μL)**	**10mm Absorbance**	**Concentration (pmol/μL)**
Positve	0.016	1.5	0.009	1.2
Parallel Control	-0.004	-0.4	-0.008	-1.0
AP Template 60min	**10mm Absorbance**	**Concentration (pmol/μL)**	**10mm Absorbance**	**Concentration (pmol/μL)**
Positve	0.009	1.1	0.005	0.6
Parallel Control	-0.003	-0.4	-0.008	-1.0

When initially testing the SNaPshot fluorescent dideoxynucleotide mix, the resolution was poor and the absorbance at stock concentration was too low to provide useful results after dilution in the reaction volume (Figure 33); therefore, further testing with this mixture was aborted.

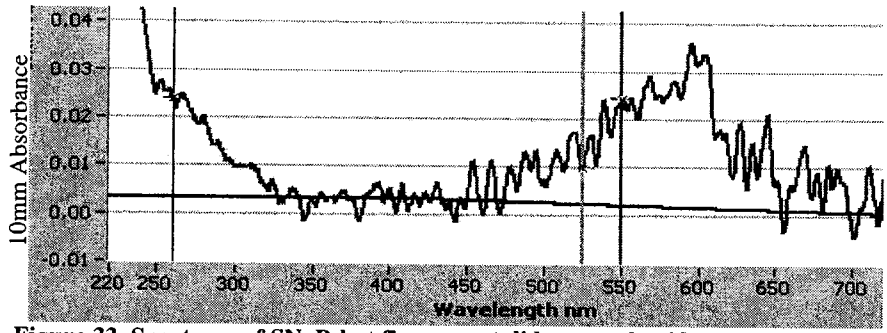

Figure 33. Spectrum of SNaPshot fluorescent dideoxynucleotides at stock concentration.

GeneScan™ Software

This method utilized AP damaged template created with the heat/acid buffer reaction and pre-processed with Endonuclease IV to generate a hydroxyl group at the 3' end. The two initial testing samples were damaged for 15 and 20 minutes and labeled with ROX-ddCTP. Both samples produced products at 78 and 160bp. In Figure 34 the products at the 73bp and 160bp for the 15 minute sample (A.) has a higher RFU than that of 20 minutes by approximately 2500RFU. No peaks were observed in the control sample.

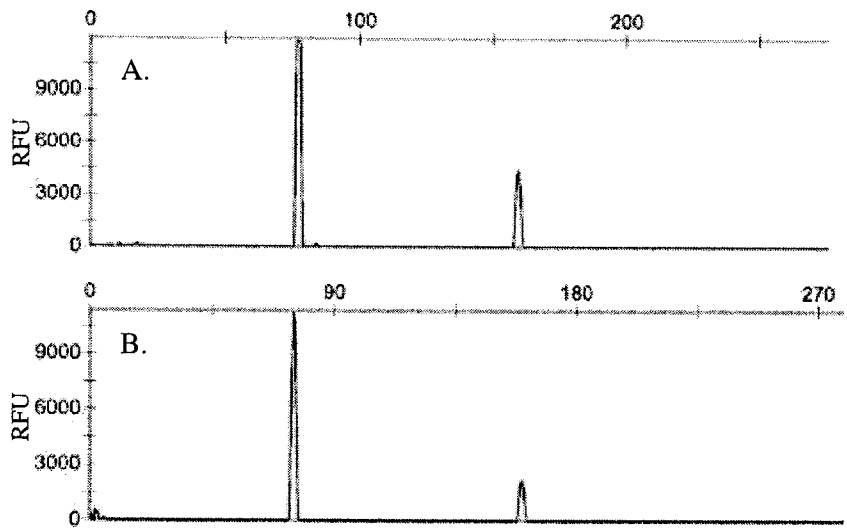

Figure 34. Relative fluorescent units and fragment sizes detected using ROX-ddCTP of template damaged with heat/acid buffer solution for A. 15min and B. 20min.

Samples damaged with heat/acid buffer for 30 minutes and 4 hours were treated with ROX-ddCTP and TAMRA-ddUTP. Despite the difference in damage times the samples were visually similar when viewed by agarose electrophoresis after Endonuclease IV treatment. Figure 35 displays the six products detected with ROX-ddCTP and five products with TAMRA-ddUTP with comparable fluorescence between the samples as listed in Figure 36 and 37.

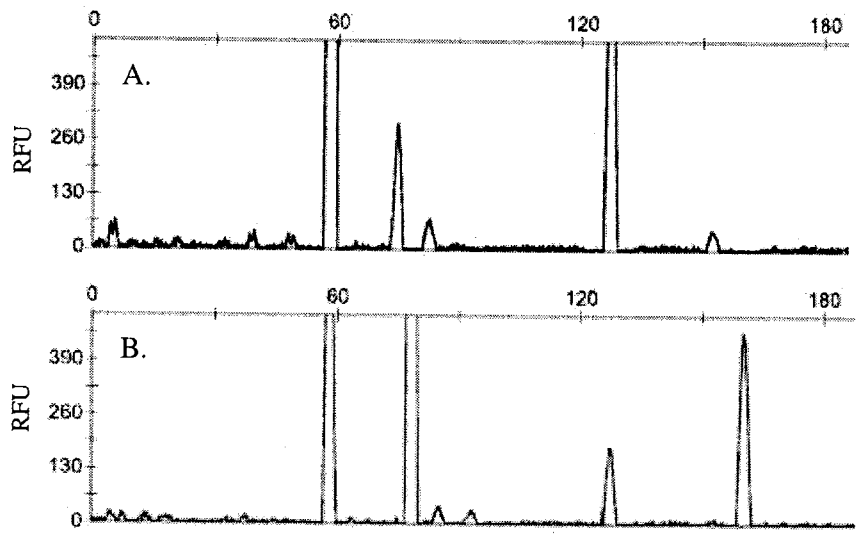

Figure 35. Relative fluorescent units and fragment sizes detected using A. TAMRA-ddUTP and B. ROX-ddCTP of template damaged with heat/acid buffer solution for 4 hours. Electropherogram y-axis is zoomed in to observe fragments producing lower fluorescence.

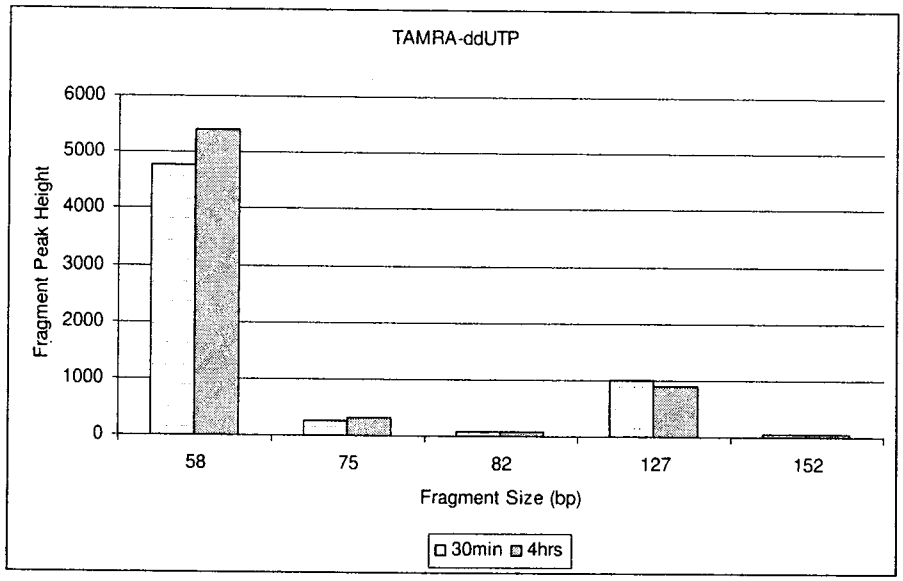

Figure 36. Fragment peak height comparison of 30min and 4hr heat/acid buffer treatment intervals using TAMRA-ddUTP.

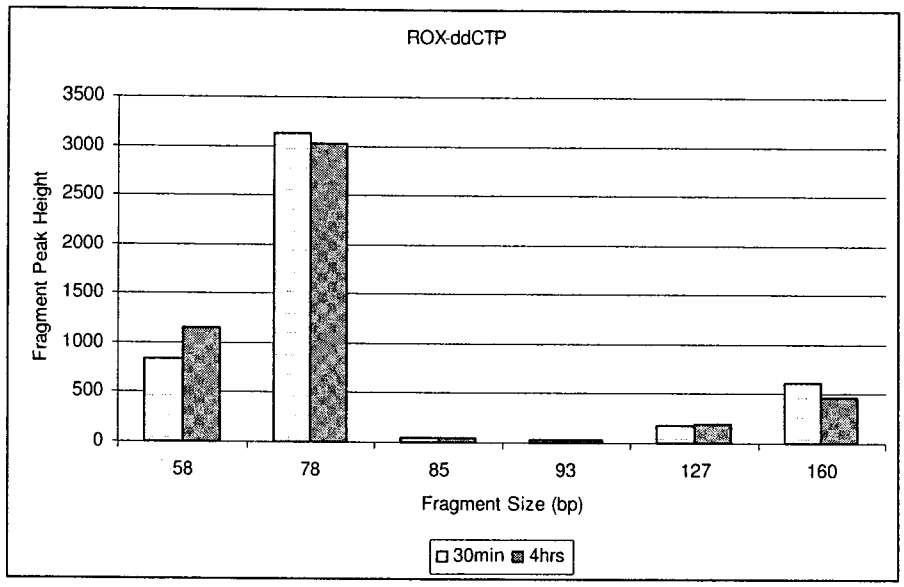

Figure 37. Fragment peak height comparison of 30min and 4hr heat/acid buffer treatment intervals using ROX-ddCTP.

Comparing the initial ROX-ddCTP 15 and 20 minute samples to the 30 minute and 4 hour samples, the fluorescence of the overlapping fragments (78 &160) reduced approximately one third, however, four new fragment sizes were detected. No peaks above background were observed in the control sample.

3.2.4 Gas Chromatography / Mass Spectrometry (GC-MS)

The mass spectra from the ion profiles of unmodified and modified bases are identified by a molecular ion (M^+), and an $(M-15)^+$ ion. Other ions created by fragmentation of the species, and an $(M-1)^+$ ion generated from the loss of an H atom from the molecular ion, are also used for the determination of modified products. For identification of products created by damage reagents an initial ion profile and mass spectrum for each individual nucleotide as a TMS derivative was created (Figure 38).

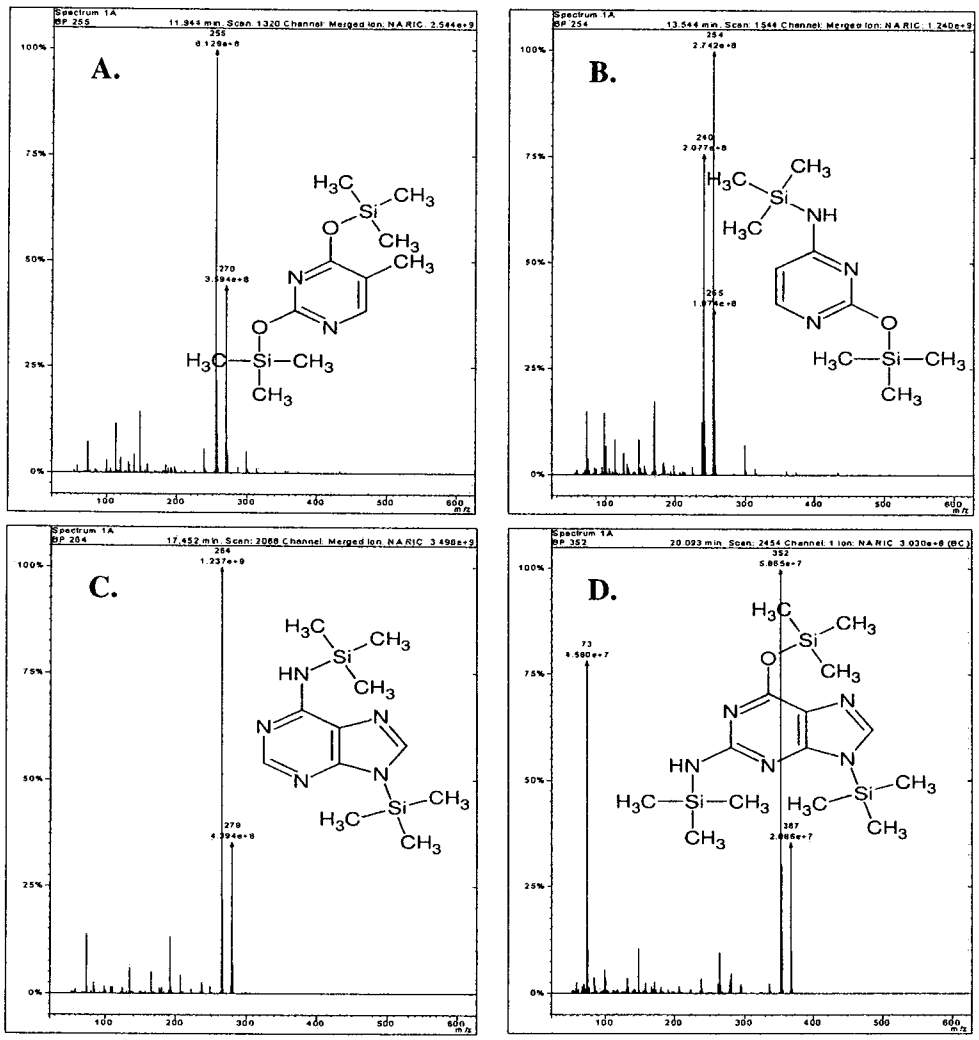

Figure 38. Mass spectrum (M+/(M-15)+) and product structure of TMS derivitized unmodified nucleotides. A. Thymine (270/255), B. Cytosine (254/240), C. Adenine (279/264), D. Guanine (367/352).

This undamaged sample is also run to ensure that the methodology of pre-processing, such as hydrolysis and derivitization, does not produce artifactual base products which may be interpreted as damage induced results. All undamaged samples in this study produced no detectable artifactual fragments.

To observe the efficiency of the hydrolysis and derivitization the phosphate and sugar moiety height count and area were compared between control reactions (Figure 39). The yield of counts and area for both sugar and phosphate were all within 1.5 standard deviations of the average value.

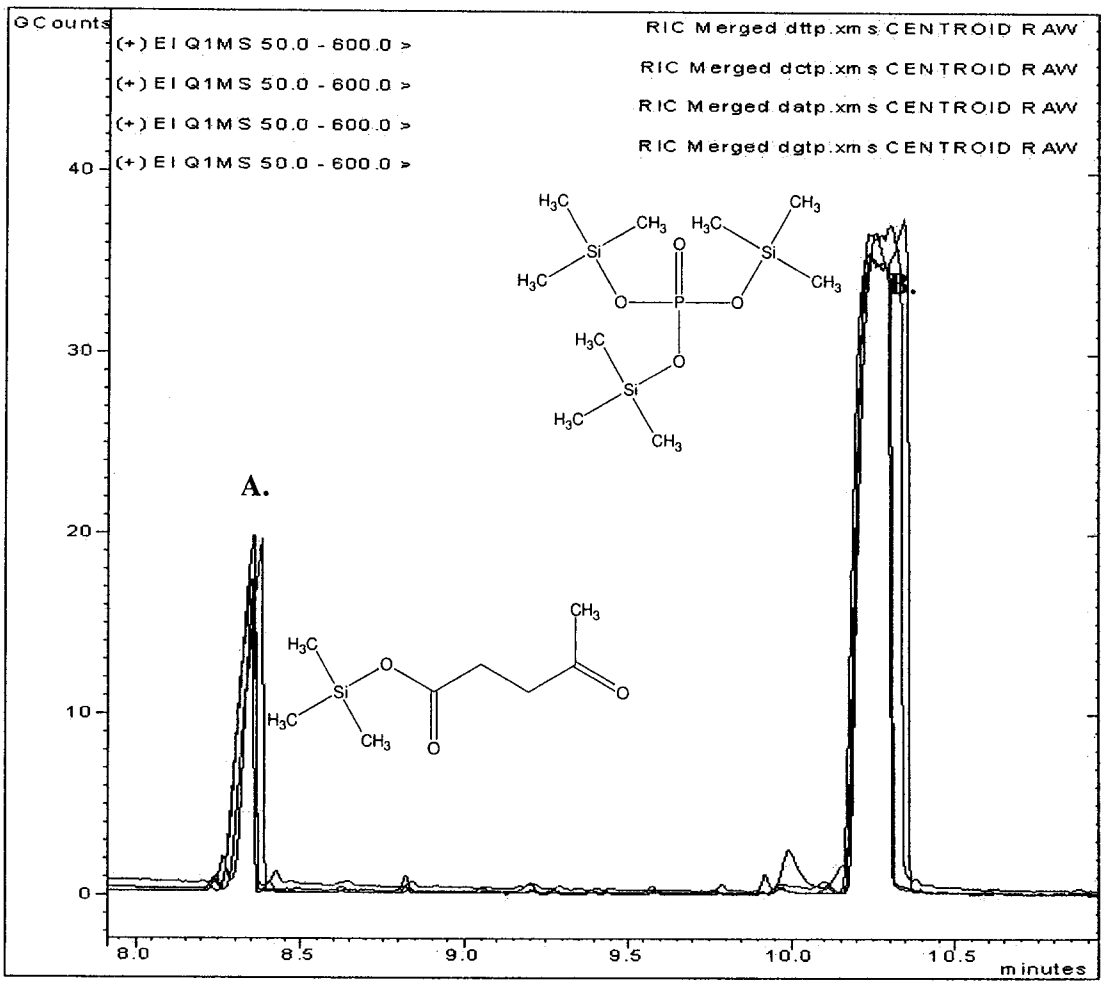

Figure 39. Ion profile and structure of TMS-derivitized A. sugar and B. phosphate moiety displaying comparable values between nucleotides.

Damage with H_2O_2 yielded modified bases in all nucleotides, as well as variation in peak area and height count between the different time intervals. An indication of the increasing concentration of modified bases is observed in the decrease of the base product over the time durations (Figure 40). In Figure 40, the base peak of guanine is not present at the 12 hour damage interval which could be attributed to the lack of solubility that guanine has in an aqueous solution.

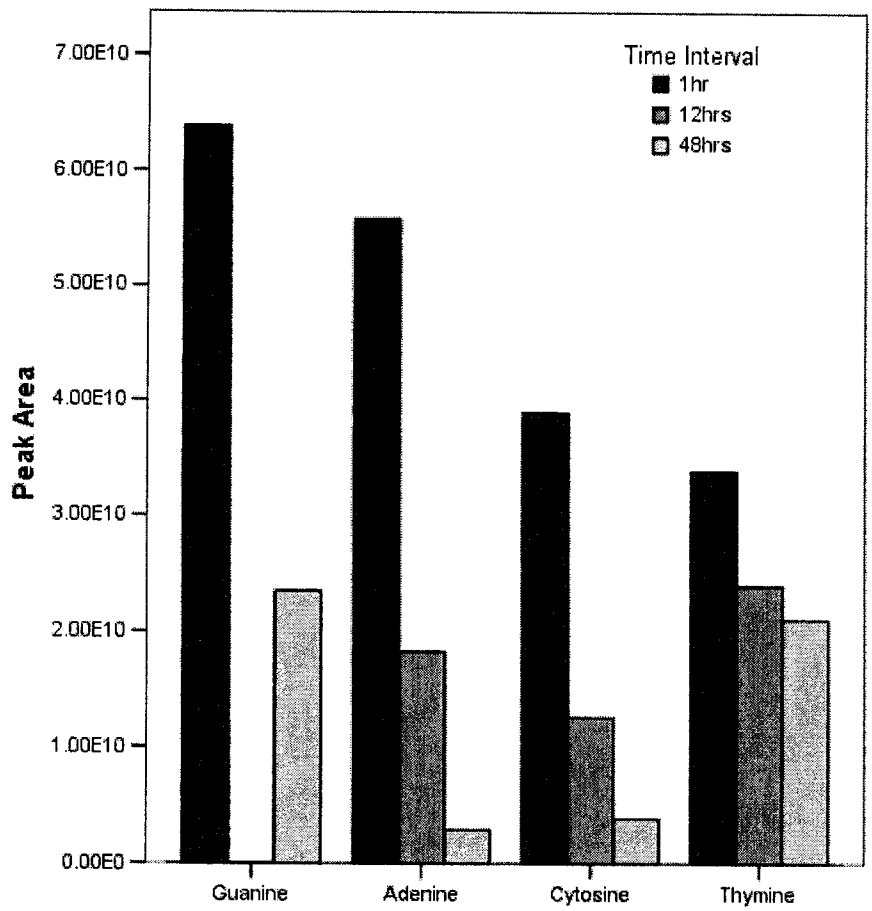

Figure 40. Decrease of base peak for nucleotides when damaged with H_2O_2 for the time intervals of 1, 12, and 24 hours. *Guanine base peak in 12 hours had no product.

Thymine samples treated with hydrogen peroxide yielded seven observable modified bases with *cis* and *trans* forms of thymine glycol reported independently (Figure 41).

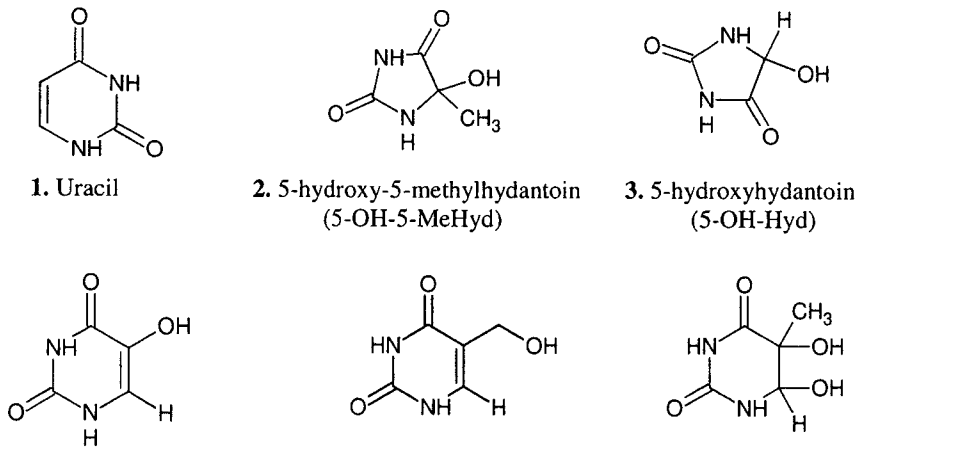

Figure 41. Structure of thymine modified products formed from treatment with H_2O_2 identified by M^+/ $(M-15)^+$ ions.

Thymine glycol was identified by an M^+ and $(M-15)^+$ at m/z 448 and 433 respectively with an intense ion at m/z 259. Due to hydrolysis, *cis*-thymine glycol is isomerized to *trans*-thymine glycol yielding two products separated in the chromatogram. In the first hour, the sum of *cis* and *trans* Tg was the most abundant, contributing to 78% of total modified bases. This abundance decreased in the 12 and 48 hour intervals to 27% and 34% respectively (Figure 42).

The product produced from the thymine C^6-OH-adduct radical, 5-OH-5-MeHyd, generated a mass spectra with an $M^+/(M-15)^+$ of m/z 346/331. Low levels accounting for 6% of 1 hour modified bases were observed followed by increasing contributing yields of 13% and 25% for 12 and 48 hours respectively (Figure 42).

The mass spectrum of 5-OHMeUra was characterized by an intense $(M-1)^+$ of m/z 357, an M^+ and $(M-15)^+$ at m/z 358 and 343 respectively. This product which is formed from an allyl radical of thymine has no detectable product at 1 hour incubation. Compared to other thymine adduct derived products it accounts for only 6% and 9% of 12 and 48 hour modified base products (Figure 42).

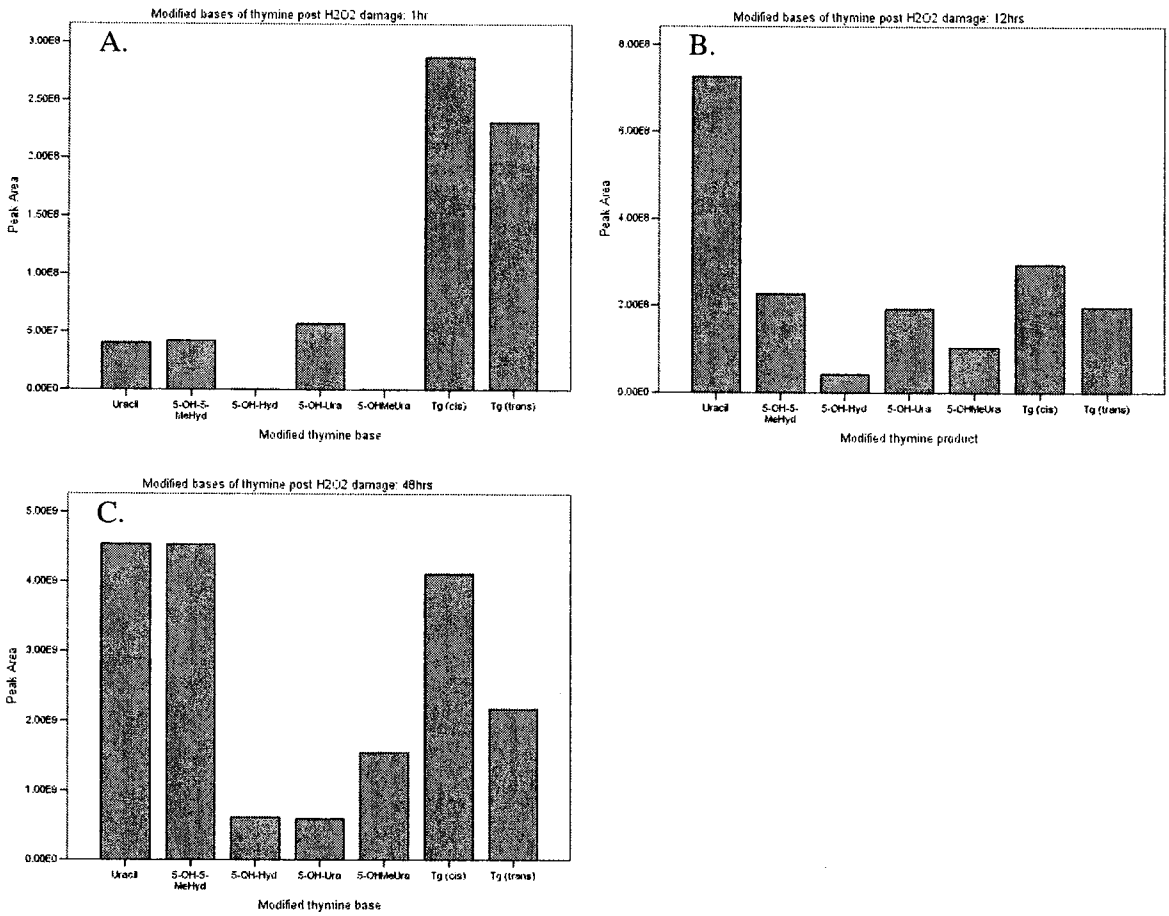

Figure 42. Peak area values of modified bases of thymine formed from treatment with H_2O_2 for A. 1 hour, B. 12 hours, and C. 48 hour

A mass spectrum with an M^+ and $(M-15)^+$ of m/z 256 and 241 was identified and following a search of the NIST spectral database a match of 2,4-oxypyrimidine (uracil) was returned (Figure 43), which is formed by the demethylation of thymine. Uracil

increased from 6% in the 1 hour interval to 41% of the 12 hour total modified base yield, however decreased to 25% at 48 hours (Figure 42).

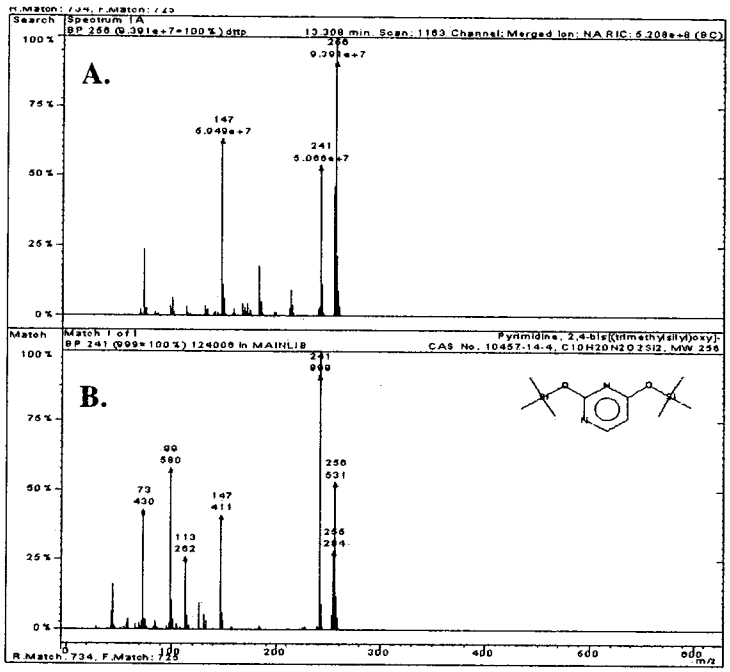

Figure 43. Mass spectra of A. thymine modified base and B. NIST library search result spectrum including structure of 2,4-oxypyrimidine.

This formation of uracil allowed for the creation of thymine derived modified bases with the absence of the C^5 methyl group. The oxidized based product 5-hydroxyuracil, identified by an M^+ and $(M-15)^+$ of m/z 344 and 329, was present in the 1 hour incubation at levels equivalent to uracil, however only consisted of 11% of the 12 hour modified base yield and following the trend of uracil, decreased in the 48 hour incubation, contributing to only 3% of the interval total modified bases.

The lowest contributing yield product at all time intervals was 5-hydroxyhydantoin (m/z 317).

Treatment of dCTP resulted in ten modified bases of cytosine, seven of which are identified (Figure 44) and three unknown base structures.

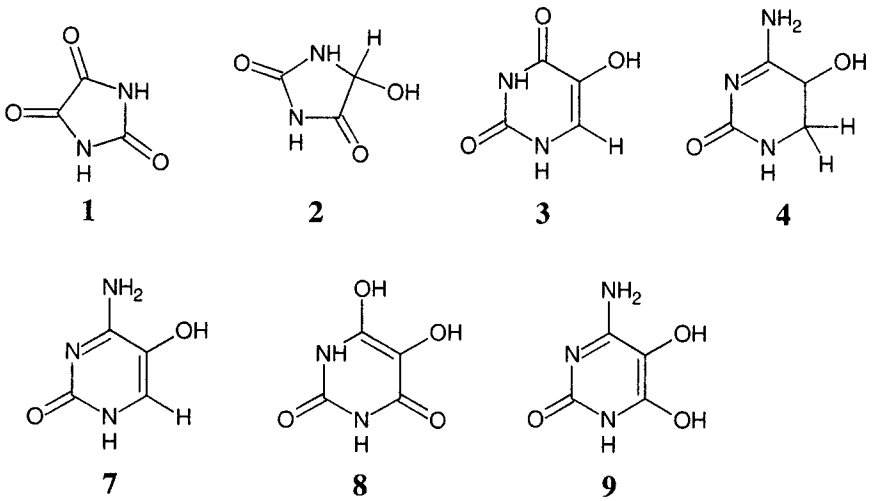

Figure 44. Identified modified base products of cytosine determined by M+/(M-15)+ of TMS derivitized product. Product numbering is dependent on product retention. 1. Parabanic Acid (258/243), 2. 5-hydroxyhydantoin (317), 3. 5-hydroxyuracil (344/329), 4. 5-hydroxy-6-hydrocytosine (345/330), 7. 5-hydroxycytosine (343/328), 8. 5,6-dihydroxyuracil (432/417), 9. 5,6-dihydrocytosine (431/416).

The unidentified structures were classified as cytosine modified products due to their absence in other nucleotide damage profiles and based on the fragmentation pattern in their mass spectra. Cytosine product 5 is characterized by an $M^+/(M-15)^+$ at m/z 327/312 with fragmentation ions at m/z 100, 170, 240, and 254 (Figure 45).

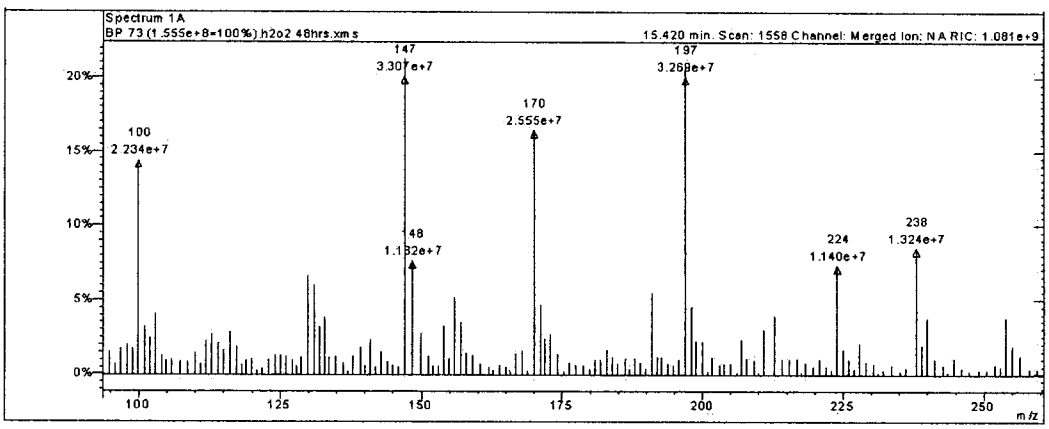

Figure 45. Fragmentation ions of cytosine product 5 characterized by an $M^+/(M-15)^+$ at m/z 327/312.

Cytosine modified product 6 is defined with an $M^+/(M-15)^+$ at m/z 334/319 with fragmentation ions at positions 100 and 133 (Figure 46).

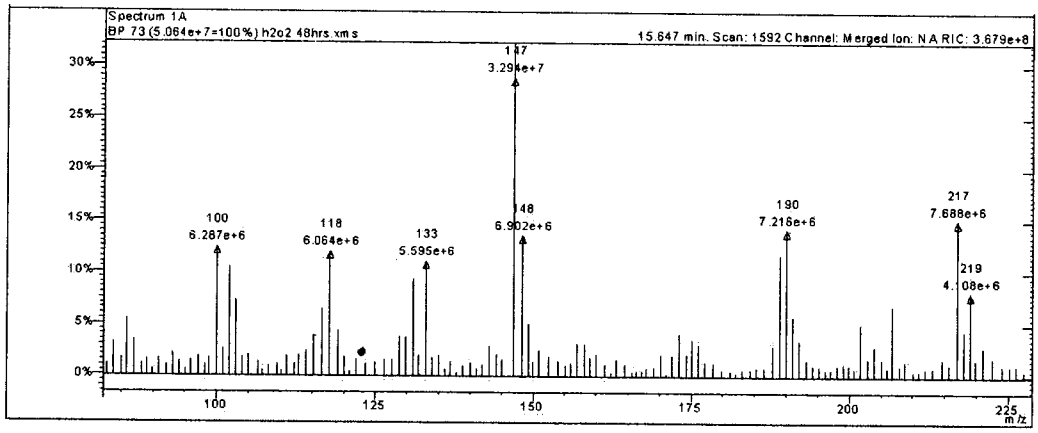

Figure 46. Fragmentation ions of cytosine product 6 characterized by an M+/(M-15)+ at m/z 334/319.

Cytosine modified product 10 is characterized by $M^+/(M-15)^+$ at m/z 459/444. The fragmentation pattern (Figure 47) at m/z 343 and 328 are observed as $M^+/(M-15)^+$ ions in known modified bases such as 5-hydroxycytosine.

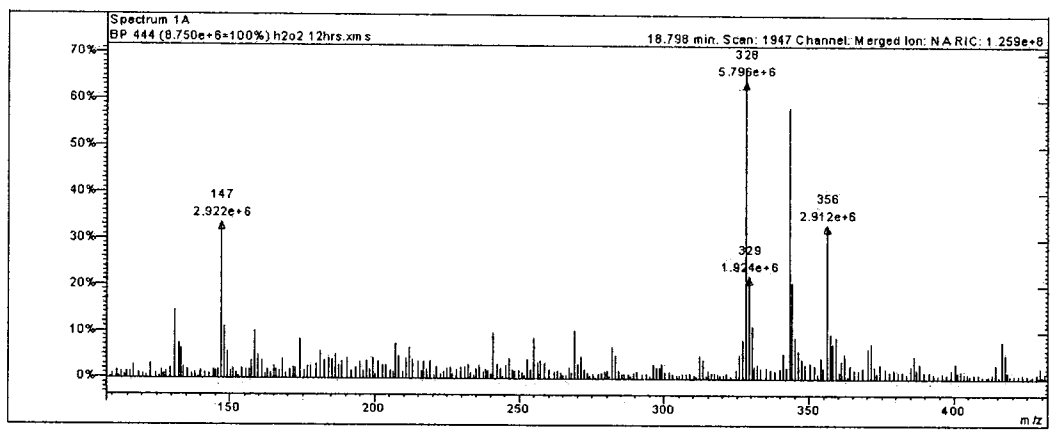

Figure 47. Fragmentation ions of cytosine product 10 characterized by an M+/(M-15)+ at m/z 459/444.

In the first hour of damage the identified products of the cytosine C5-OH radical, 5-hydroxyhydantion and 5-hydroxycytosine, along with the unidentified Cytosine 5, yielded the largest contribution to the modified bases. In the 12 hour interval the major

product was 5-hydroxyhydantoin whereas Cytosine 5 and 5-hydroxycytosine decreased yielding result similar to lower level bases.

In the 48 hour interval all ten modified bases identified in the cytosine reactions are present with varying contribution. At 48 hours, 5-OH-Hyd is not only producing the largest yield of the total modified bases but is also greater in peak area than the cytosine base (Figure 48).

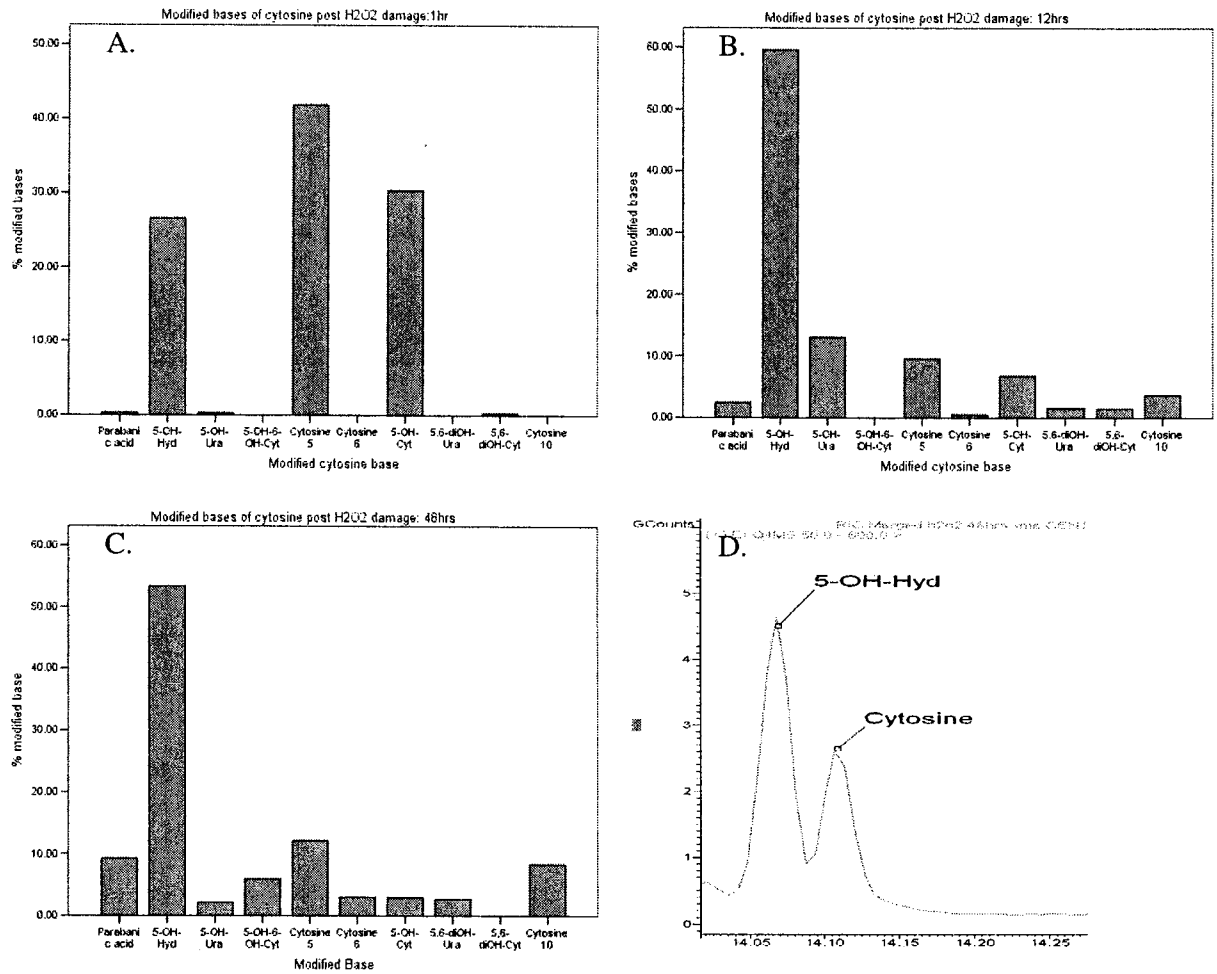

Figure 48. Percent of peak area values of modified bases of cytosine formed from treatment with H_2O_2 for A. 1 hour, B. 12 hours, and C. 48 hours. Panel D represents 5-OH-Hyd with greater peak area than cytosine at 48hr damage interval.

Treatment of dATP resulted in the creation of two nucleotide derivatives of adenine (Figure 49).

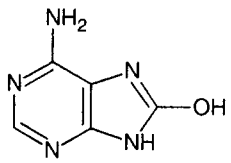

8-hydroxyadenine
(8-OH-Ade)

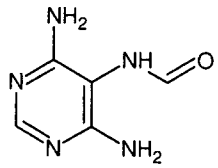

4,6-diamino-5-formamidopyrimidine
(FapyAde)

Figure 49. Structure of adenine modified base products formed from treatment with H_2O_2.

The product of FapyAde is identified by $M^+/(M-15)^+$ at m/z 369/354 and is observed to increase in overall presence throughout the time interval reactions (Figure 50). 8-OH-Ade however is only observed at 48 hours by $M^+/(M-15)^+$ at m/z 367/352.

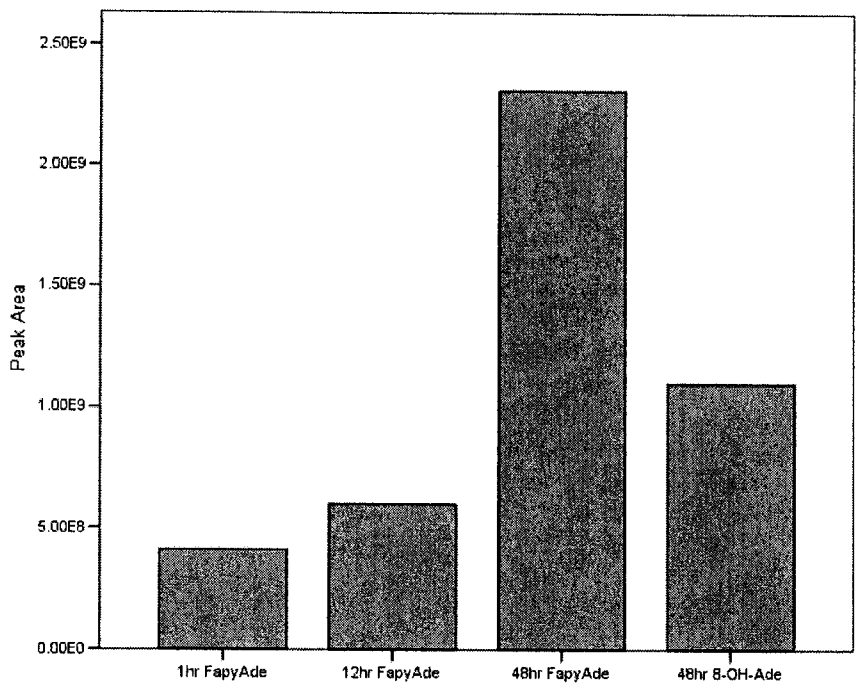

Figure 50. Peak Area of modified base products of adenine produced in H_2O_2 time series reactions of 1, 12, and 48 hours.

In the 48 hour interval, a fragmented form of adenine with a $M^+/(M-15)^+$ at m/z 409/394 is identified as a silanamine via a search of the NIST database (Figure 51). The low level of adenine and modified base products, in addition to the presence of silanamine, suggests fragmentation via degradation of the base.

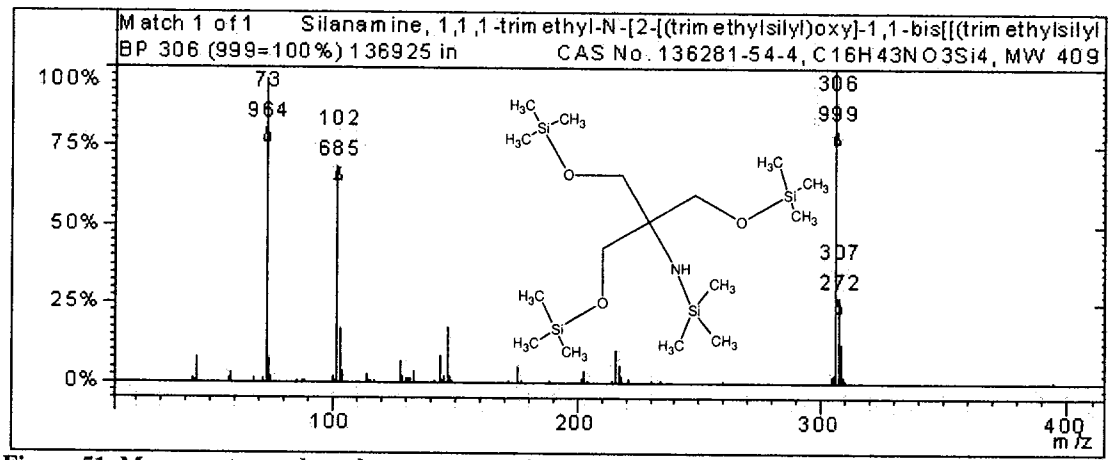

Figure 51. Mass spectra and product structure of silanamine adenine base fragment.

In the guanine reactions, there is limited unmodified guanine and no base lesions present at 12 hours which is most likely due to the insolubility of guanine in an aqueous solution. In this section only the 1hour and 48hour reaction times will be compared. The primary modified base resulting from treatment with H_2O_2 is 8-hydroxyguanine, identified with an $M^+/(M-15)^+$ at m/z 455/440 (Figure 52) and 367/352 ions in the mass spectra resulting from the loss of an OTMS group.

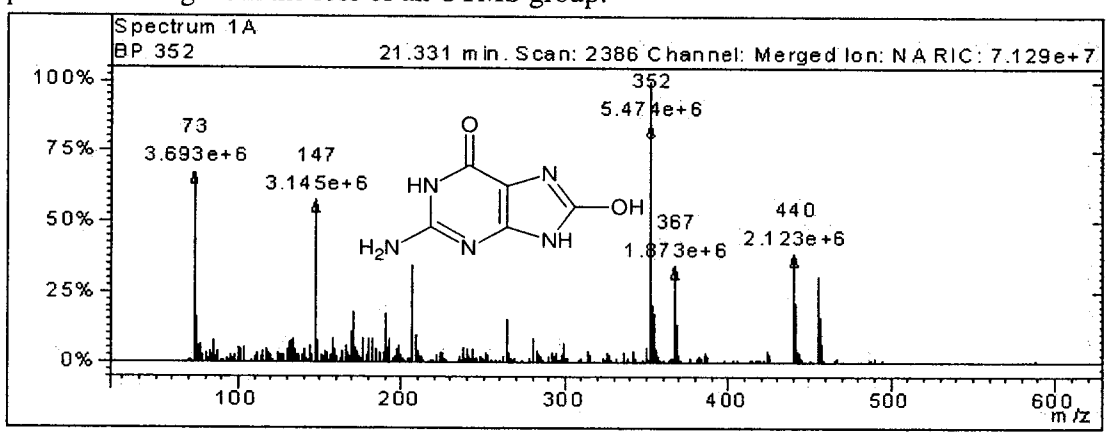

Figure 52. Mass spectrum and underivitized product structure of 8-hydroxyguanine.

A product identified with an $M^+/(M-15)^+$ at m/z 295/280 with an ion at m/z 264 is comparable to a modified adenine product. This product may be due to the loss of the NH-TMS group and an underivitized oxidized C8 position.

The product yield of 8-OH-Gua increased approximately 77% from 1 to 48 hours, whereas the 295/280 product decreased approximately 92%, suggesting that the 295/280 product may be an intermediate modified base (Figure 53).

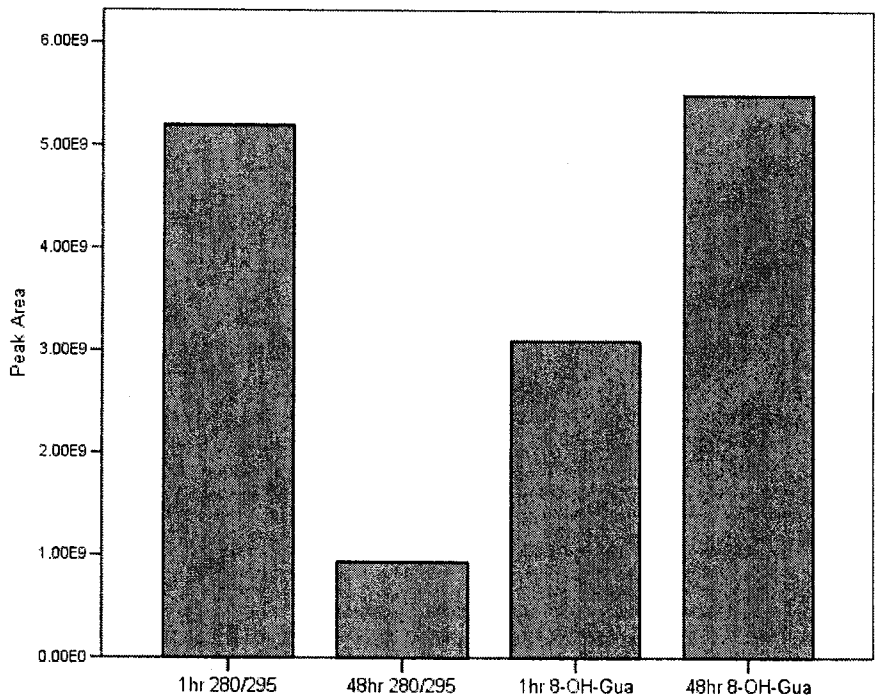

Figure 53. Identified modified products 295/280 and 8-OH-gua produced from the treatment of dGTP with H_2O_2 for 1 and 48 hour time intervals.

Following individual nucleotide damage, mixed dNTP's were treated with hydrogen peroxide and modified bases were identified from mass spectra data and retention times characterized from single nucleotide reactions. The majority of previous identified bases were detected in the dNTP mixture reaction (Figure 54).

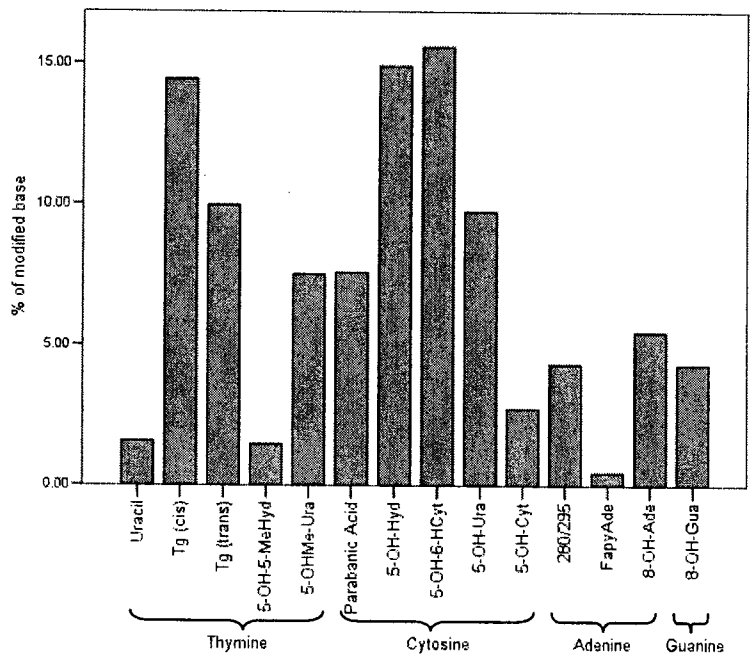

Figure 54. Percent of total identified modified bases from dNTP mixture treated with H_2O_2 for 48 hours.

As previously observed in individual nucleotide damage, the pyrimidine bases produce a significant yield of modified bases in respect to the natural nucleotide, and conversely a low percentage of purines are converted to modified base lesions (Figure 55).

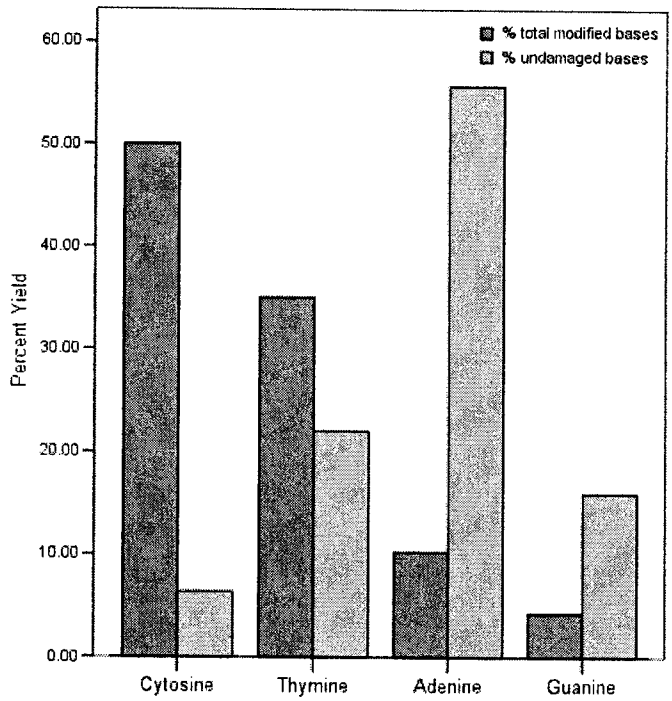

Figure 55. Percent of total modified base yield per nucleotide and percent of remaining undamaged nucleotide in H_2O_2 reactions.

Treatment of mixed dNTP's with UVA and UVB yielded eight similar base modified products. The mass spectral peaks that were identified included 5-OH-Ura, 5-OH-Cyt, Adenine N-oxide 295/280 (2 forms), and a possible 5,6-cyclo-5,6-dihydrothymidine (cdT) structure (Figure 56) characterized by an M^+ at m/z 538.

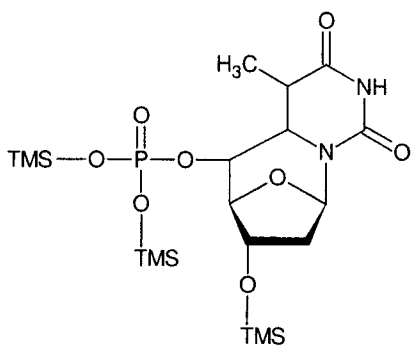

Figure 56. Possible 5,6-cyclo-5,6-dihydrothymidine structure identified by an observed mass spectra M^+ at m/z 538.

The three unknown modified bases produced m/z values at 326/312, 278/263, and 271/255. The two forms of Adenine 295/280 are N-Oxide isomers which are distinguished by retention time and will have 2 of the 3 possible structures depicted in Figure 57.

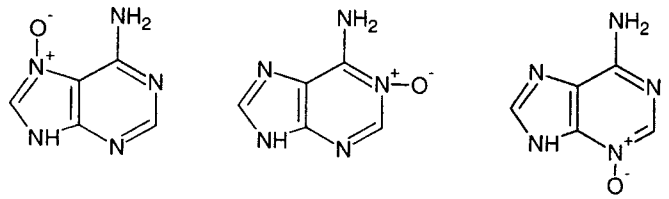

Figure 57. Three possible structures of N-oxide isomers of adenine modified base characterized with an $M^+/(M-15)^+$ at m/z 295/280.

The modified bases that discriminated between the UVA and UVB treatments were the Unknown 271/255, N-Oxide-1 (295/280), and possible cdT (Figure 58).

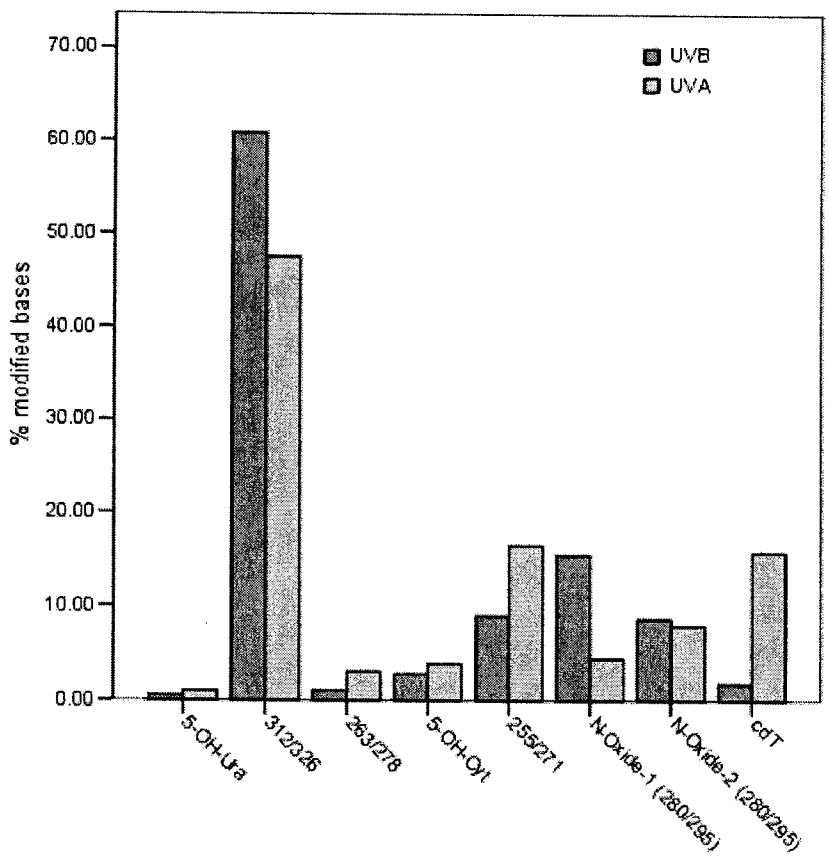

Figure 58. Percent of modified bases formed from the treatment of dNTP mixture samples with UVA and UVB.

Nucleotides treated with DMSO, formalin, and APS did not yield any modified bases, nor were any intact nucleotides observed. The sugar and phosphate moiety were derivitized suggesting that the hydrolysis and derivitization steps were successful, and in the case of DMSO a common unidentified high concentration peak was consistent in all samples likely resulting from the derivitization of DMSO.

Formalin produced repetitive peaks in the chromatogram occurring in approximately 1.5 minute intervals and repetitive ions in the mass spectrum in 30 m/z intervals (Figure 59). These peaks may be attributed to the derivitization of the formaldehyde and methanol components in the formalin.

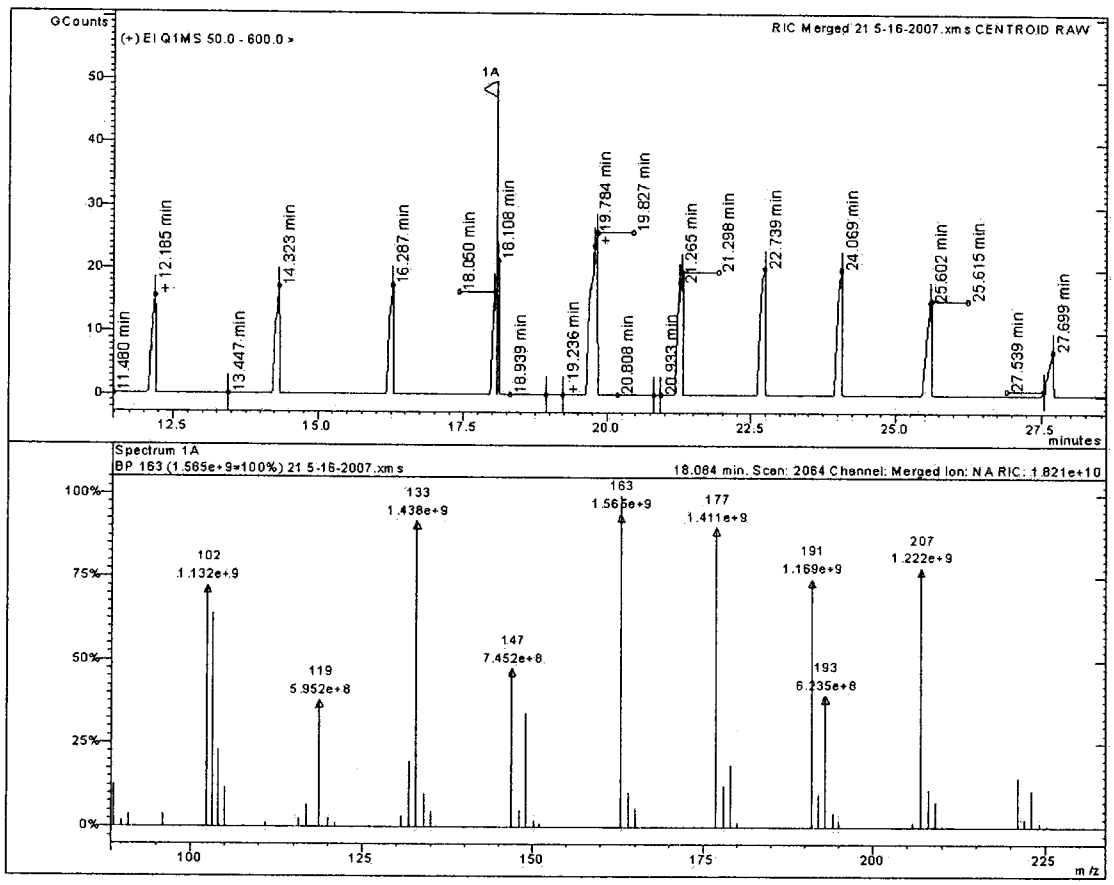

Figure 59. Gas chromatogram and mass spectrum of repetitive elements observed in samples treated with formalin.

Individual nucleotides and PCR template subjected to heat/acid buffer solution did not yield any observable modified bases with the exception of the previously described silanamine product (Figure 51). Products that were observed in these chromatograms and not in control samples included ethanedioic acid and carbonates (Figure 60). These products may be the result of the breakdown of the sugar moiety degradation.

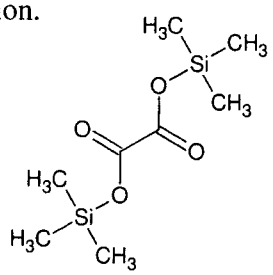

M^+ 234

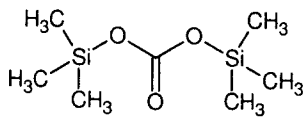

M^+ 206

Figure 60. TMS derivitized product structures and M+ formed in template treated with heat/acid buffer solution. A. Ethanedioic acid, B. Carbonate.

Despite the lack of identified modified bases and sugar groups, a series of unidentified peaks in the chromatogram are observed in the retention time range similar to the unmodified TMS derivitized sugar moiety (Figure 61), and also share related mass spectral fragmentation patterns and ions.

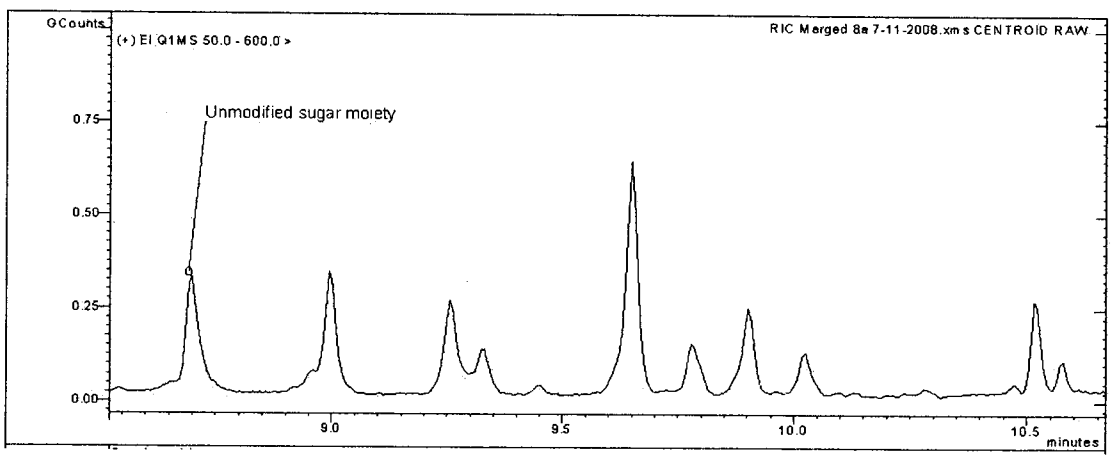

Figure 61. Gas chromatogram of unidentified peaks observed after treatment with heat/acid buffer solution. Peaks are localized near the unmodified TMS derivitized sugar.

In addition, the detection of 2-deoxypentose-4-ulose, a C4-oxidized abasic sugar moiety, and 2-deoxypentonic acid lactone, a C1-oxidized abasic sugar moiety, were detected (Figure 62) sporadically in this study in hydrogen peroxide treated samples and buccal swab concentration experiments (data not reported).

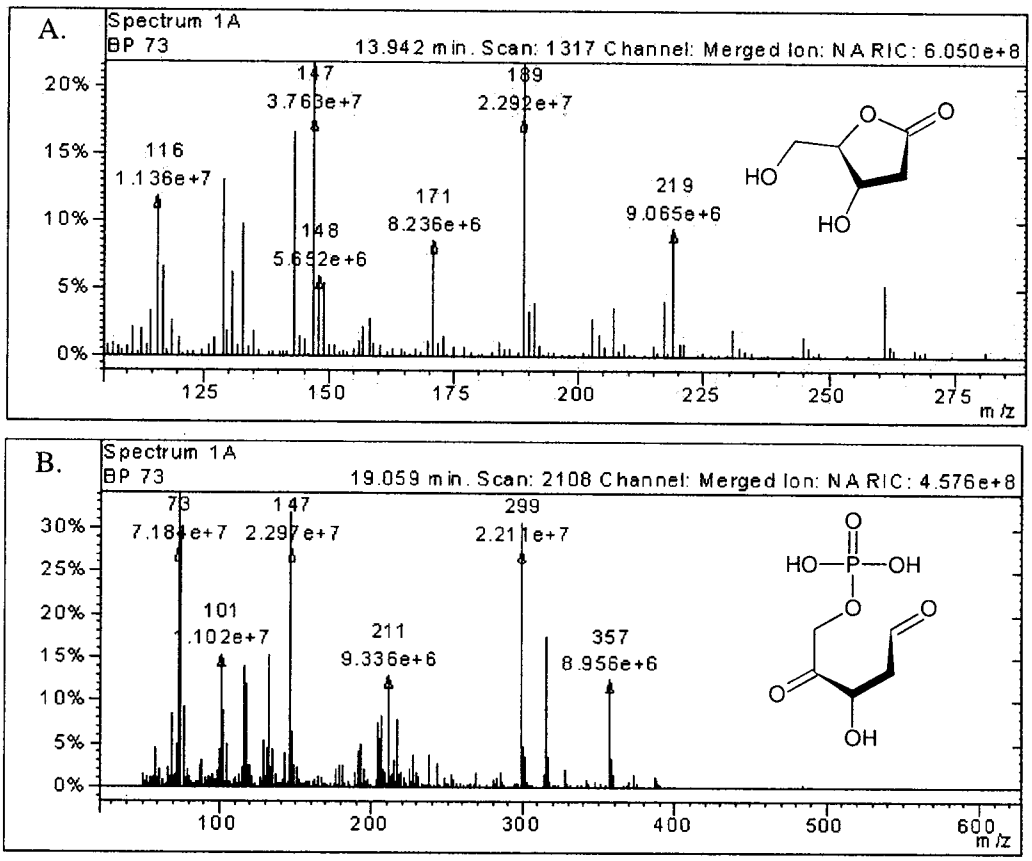

Figure 62. Partial mass spectra and underivitized product structure of A. 2-deoxypentonic lactone, and B. 2-deoxypentose-4-ulose.

Samples treated with hydrogen peroxide and subsequently processed with fragment isolation protocol yielded low, yet identifiable base products in both isolated bands for GCMS scans. Cytosine could not be detected due to an overlapping peak and guanine was not detected due to low levels in the 482 and 435bp fragments. Figure 63 displays the modified bases observed in the 482bp fragment (parabanic acid, 5-OH-5-

MeHyd, silanamine, 5-OH-6-HCyt, 5-OH-Ura, FapyAde, and 8-OH-Ade) and the 435bp fragment (5-OH-5-MeHyd and 5-OH-Hyd). The discrepancies in the modified bases may be attributed to low DNA concentrations and purity post gel excision despite relatively equal values reported by quantification with the spectrophotometer. Samples treated with heat/acid buffer solution and fragment isolation did not yield any modified bases or sugar groups.

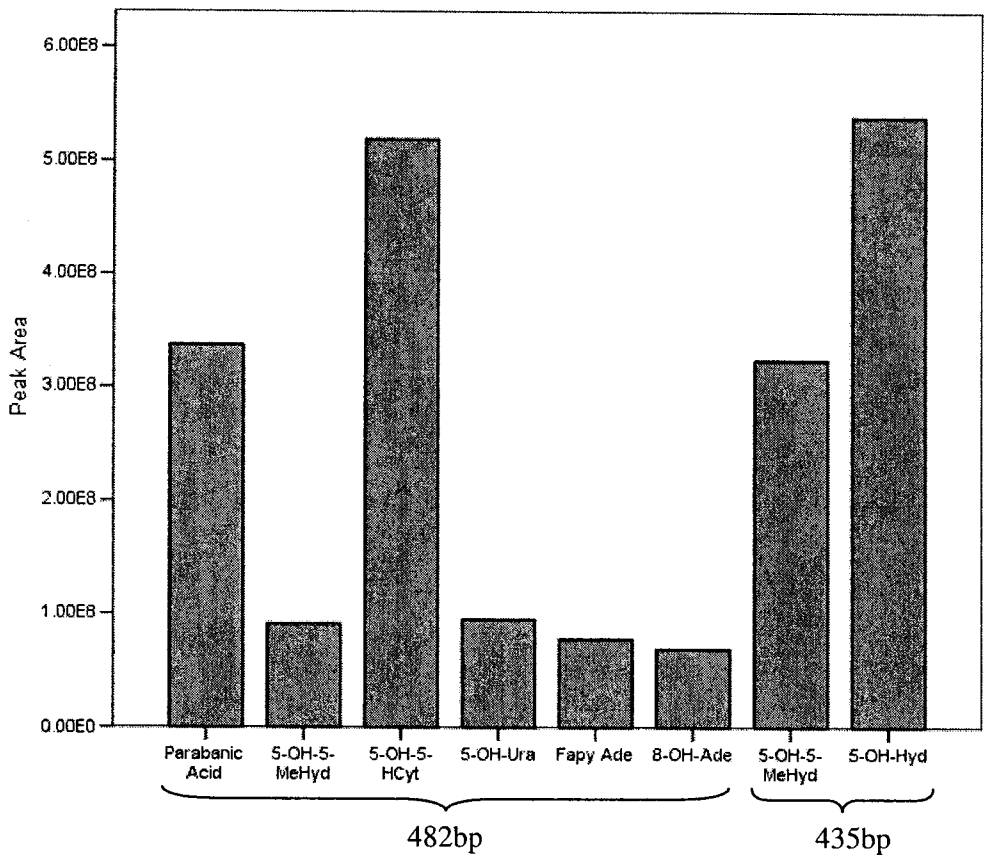

Figure 63. Modified bases identified from PCR template treated with hydrogen peroxide and after fragment isolation of 482 and 435bp fragments.

In the genome separation reactions approximately only 4μg of nuclear and mitochondrial DNA were available for analysis. Typically this concentration should

yield low level results, however due to the lack of purity of the sample only the unmodified base of thymine was detected in the mitochondrial DNA fraction.

Modern samples were analyzed to observe possible modified bases induced from storage conditions and duration. The first two samples did not yield any DNA bases or phosphate and sugar moieties. This however is most likely due to the concentrations of the samples being only 1.2µg and 0.7µg with poor 260/230 and 260/280 ratios. A fresh sample however purified with a Qiagen© Extraction Kit resulting containing only 1µg of DNA allowed the identification of all bases in a full GCMS scan method. This indicates that the sensitivity of the GCMS may be influenced by the extraction and purification methods utilized.

4.0 Discussion

4.1 Template Processing

Genome Separation

The separation protocols of the nuclear and mitochondrial genome were performed to assess differences in damage profiles and concentrations occurring in the nuclear and mitochondrial genome. Due to the vulnerability of mtDNA in respect to structure protection, proximity to ROS, and preferential binding by other DNA damaging agents (Sawyer and Van Houten 1999) it is suggested that oxidative damage may occur at a greater extent than in nDNA (Yakes and Van Houten 1997). The separation of the two genomes is generally accomplished with buffer/centrifugation methods or with cesium chloride (CsCl) gradients with high speed centrifugation (Carr and Griffith 1987). Since CsCl isolation procedures require centrifugation speeds between 55,000 and 100,000rpm for upwards of 5 hours, this method was not explored. Following the methodology of (Lim *et al.* 2005), a TES buffer and differential centrifugation separation was utilized.

The majority of separation trials failed in reliably distinguishing the nuclear and mitochondrial fractions as demonstrated by PCR amplification. Modifying this procedure by adding extra centrifugations at 5,524 x g suggests that remaining nuclei were removed providing a nuclear free mitochondrial fraction, as determined by PCR amplification. Similarly, the increase of centrifugation steps at 959 x g to purify the nuclear fraction allowed for residual mitochondria to be removed in the supernatant as opposed to contaminating the nuclear pellet. The failure to initially separate the genomes may also be attributed to the age of the blood samples used. Degradation of cellular and nuclear membranes over extended periods of storage time may have resulted in the

release of DNA which would possibly make the separation of nucleic acid content via cellular components difficult. In future work the number of centrifugation steps can be optimized on the tissue and sample type and characteristics to ensure efficient separation.

Fragment Isolation

The purpose of genome fragment isolation was to observe the possibility of segmenting the mitochondrial genome into its respective functional components via restriction enzymes to characterize potential damage hot spots. Due to the lack of template produced from the genome separation reactions, a 1kb PCR product corresponding to the mtDNA D-loop was utilized to observe detection potential. Isolation and gel purification of restricted bands was successful with acceptable concentration and purity ratios. The template treated with heat/acid buffer solution resulted in observable smearing and reduction of template band indicating abasic detection capability from isolated fragments. It was also demonstrated that the detection of modified bases and sugar moieties induced by heat/acid buffer or H_2O_2 from isolated DNA fragments via GC-MS detection methods is possible.

Even though GC-MS SIM methods did not perform properly in this component, the use of scan mode was still capable of detecting base lesions in low concentration (<5μg) samples. This concept and methodology can be applied in future studies to target regions of interest within the genome since numerous diseases have been associated with mutations occurring in mitochondrial genes which ultimately contribute to Complex I, III, IV, or V of the OXPHOS subunits (DiMauro and Schon 2001). This information which is currently obtained primarily by DNA sequencing is capable of only showing the result of the damage and not the cause. Positively identifying the lesions responsible for

these mutations may assist researchers in understanding the mechanisms and pathways associated with a specific disease.

4.2 Damage Detection Assay Assessment

The assays selected in this experiment allowed for the observation of the major damage insults to the structure and composition of the treated DNA (Figure 64). Initial gel electrophoresis provided information regarding the integrity of the DNA structure post damage by addressing DSBs and template degradation. The use of PCR is twofold as it not only indicates the presence and extent of polymerase blocking lesions, but also adds insights into the effects that the induced damage may have on replication efficiency. By utilizing Endonuclease IV, abasic lesions that may not be observed in other assays, such as GC-MS, can be identified and assessed. Finally, GC-MS is essential to fill in the blanks and provide priceless information regarding the type of lesions present and to what extent. These methods combined allowed for the following discussion on the mechanisms and effects of the damaging agents tested on the DNA template

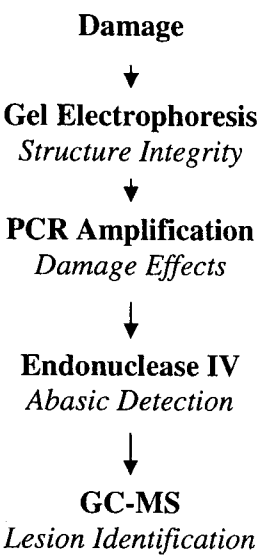

Figure 64. The multiple assay pathway utilized in the assessment of a DNA damage profile.

Treatment with UVA exposure did not visually appear to affect the double stranded template, induce abasic sites, or inhibit PCR amplification. Modified oxidative base products, primarily derivatives of cytosine, thymine, and adenine, were identified via GC-MS. The products 5-OH-Ura and 5-OH-Cyt are characterized as non-blocking lesions (Evans *et al.* 2004) and produce the characteristic C→T mutations associated with UVA damage (Runger and Kappes 2008). The lesions cdT and 5,6-dH-Thy are known to block polymerase activity (Bjelland and Seeberg 2003) however these products were on average only 3% of the undamaged base yield suggesting that a higher concentration of undamaged template was present for successful amplification.

An unknown product of cytosine (m/z: 312/326), not observed by other damaging agents, was identified at high yields similar to that of unmodified bases though did not appear to affect PCR amplification. With the combination of UVA and H_2O_2 no template product was observed post treatment and failure of PCR amplification suggests that an increased conversion of H_2O_2 to •OH via UVA potentially generated multiple single stranded breaks. Contrary to literature, the 8-OH-Gua lesion which is a commonly targeted marker of UVA treatment (Cadet *et al.* 2005) was not identified though guanine was present confirming that solubility was not an issue. Despite this, the observations in this study do support the oxidative damage mediated role of UVA on DNA template.

Treatment with UVB exposure suggests a progression in damage with increased exposure. After 1 hour the template is intact, no abasic sites are induced, and the majority of detected modified bases are at low levels. The presence of a smaller secondary band in PCR amplification indicates a possible premature stop in extension caused by CPDs which can block *Taq* DNA Polymerase (Wellinger and Thoma 1996).

The generation of moderate smearing in the EndoIV treated template and lack of PCR amplification suggests the existence of abasic sites and *Taq* DNA Polymerase blocking lesions.

Exposure to UVC resulted in abasic lesions indicated by significant smearing of the template DNA post Endo IV treatment. Due to the successful amplification of product via PCR it suggests that the polymerase was capable of incorporating bases adjacent to the abasic lesion. At abasic sites, *Taq* DNA polymerases is capable of inserting nucleotides in the frequency of dAMP, dGMP, dCMP, and dTMP (Shibutani *et al.* 1997) and is referred to as the "A-rule" due to the preferential incorporation of dAMP (Kobayashi *et al.* 2005).

The results observed with formalin treatment demonstrate the damaging effects to DNA and the difficulty associated with the measurement of formalin fixed samples (Ferrer *et al.* 2007). Failure in amplification of samples treated for 1 hour is likely due to polymerase blocking by cross-linking lesions such as di-(N^6-deoxyadenosyl)methane induced by formalin treatment (Wang *et al.* 2007). The extended time intervals of 24 and 48 hours did not produce any viable template post treatment suggesting that the non-buffered formalin was oxidized to formic acid (Bonin *et al.* 2003) which in turn degraded the DNA by hydrolysis of the N-glycosidic bond. The pattern of repetitive peaks observed by GC-MS analysis demonstrated that purification steps were not extensive enough in removing the formalin from the samples to obtain reliable results. In future studies, purification protocols will have to be refined in order to eliminate the interference of formalin derivatives.

In the formation of AP sites by the heat/acid buffer, the DNA template remained intact despite the time-dependant increase of induced AP sites as determined by treatment with Endonuclease IV. The amplification of PCR product decreased with increasing damage intervals and eventually resulted in no observable product. This heat/acid buffer solution protocol is estimated to generate approximately 10 AP sites/10^6 nucleotides per minute (Nakamura *et al.* 1998). Based on a 30 minute incubation, ~309 AP sites were created per 10^6 nucleotides on template consisting of approximately $2x10^{15}$ nucleotides. Though *Taq* DNA Polymerase is capable of performing translesional synthesis across an AP lesion (Belousova *et al.* 2006), it is possible that multiple adjacent AP sites may have been created which ultimately blocked the polymerase. In addition, a formation of AP lesions located within primer sites would potentially affect primer annealing and therefore reducing amplification. Despite the lack of positively identified products via GC-MS, a series of uncharacterized high contribution peaks were observed in the chromatographs. These lesions, which appear to be specific to this treatment process, are potentially products and intermediates of oxidative damage to the sugar moiety as described by Evans *et al.* 2004 and will be further investigated.

Upon treatment of DNA template with H_2O_2 over time intervals, the structure did not appear to contain SSBs, DSBs, or abasic sites. The observed decrease in amplification with increasing time can be attributed to the formation of multiple modified base products. Of the products detected, the majority were pyrimidine derivatives, some of which were responsible for the inhibition of amplification. A direct negative correlation exists between amplification success and the presence of the *Taq* DNA polymerase blocking lesions 5-OH-Hyd, Tg, and 5-OH-5-MeHyd (Hoss *et al.* 1996).

These blocking lesions were the dominant species observed from their respective parent base and increased in yield over time intervals. The remaining pyrimidine bases, though not blocking to the polymerase, would be responsible for the incorporation of sequence mutations.

Though the detected purine lesions 8-OH-Gua, FapyAde, and 8-OH-Ade are not capable of inhibiting the PCR amplification, the lesions will result in miscoding and possible structural distortion.

From the time interval studies, a progression of the detectable modified bases is suggested in both purines and pyrimidines. The greatest contributing pyrimidine species throughout the time intervals were those at the end of a reaction mechanism pathway (Evans *et al.* 2004), and it was not until later intervals that intermediate products were detected at contributing levels. This is likely due to rapid reactions of the intermediates, of which finally become detectable during high concentrations of end product formation. Thymine glycol is the dominant detected thymine derivative due to its formation from the favored C^5-OH adduct radical. In initial oxidation, Tg contributes to 70% of modified thymines yet drops to only 35% at the final interval. The lesion 5-OH-MeHyd is formed from the less preferred C^6-OH adduct radical and increases steadily from 6 to 25% in initial and final durations, respectively. These results demonstrated that a ratio of Tg to 5-OH-MeHyd can potentially be utilized to identify oxidative damage stages.

The major cytosine product 5-OH-Hyd formed from a C^5-OH adduct radical consistently contributes to >40% of modified base products and in fact is in greater presence than unmodified cytosine after 48 hours. This is due to both the increased formation of modified cytosine products and a consistent high concentration of 5-OH-

Hyd. This high presence of 5-OH-Hyd can be compared to the unmodified cytosine base to assess oxidative damage.

In agreement with previously published results (Chetsanga and Grigorian 1983) FapyAde was the most abundant adenine lesion and displayed a detectable yield increase throughout the damage time intervals. Though 8-OH-Ade did not display a progression of yield over the time intervals, its emergence after 48 hours displays possible potential as a marker of severe oxidative damage.

In guanine spectra, a species with similar m/z values of an N-oxide isomers initially associated with adenine (Simandan *et al.* 1998) and may potentially be a guanine radical intermediate, was observed to decrease as the concentration of 8-OH-Gua increased. This transitional correlation suggests a possible future opportunity to predict the yield and the rate of formation of 8-OH-Gua.

Samples damaged with APS, DMSO and Fenton reactions did not provide reliable results due to problems in reaction procedures. Amplification was possible with DMSO and APS, however due to no further information provided by EndoIV, and GC-MS reaction failures the types of induced damage could not be determined. The failure of base product detection in DMSO reactions by GC-MS analysis may be due to the formation of base-DMSO adducts at derivitization sites resulting in the blocking of trimethylsilyation. Also, due to the potential formation of numerous artifacts from the reaction of DMSO and BSTFA (Little 1999), it is possible that these reactions may have been favored to base derivitization, especially if DMSO was present in excess. To avoid these artifacts in future reactions, BSA or MSTFA could be used in substitution of BSTFA (Little 1999). Despite attempts with various cleanup procedures such as ethanol

precipitation and the RBC Bioscience HiYield™ Gel/PCR DNA Extraction Kit, precipitate from $FeSO_4 \cdot 7H_2O$ could not be fully removed. Though there was eventually amplification via PCR no further testing was possible due to this persisting residue, therefore comments regarding damage formation is limited.

Damage Assay Considerations

The assays considered for the detection of damage to the synthetic template does have advantages and disadvantages associated with each. The measure of template integrity by gel electrophoresis is an efficient manner to quickly observe a snapshot of the template health. It is necessary to confirm this since despite relatively pure and concentrated spectrophotometer readings post damage the damage may be significantly degraded, as observed in formalin treated at 1hour. To enhance the quantification of this step a multiplex quantitative-PCR reaction of increasing amplicon sizes (preferentially targeting a housekeeper gene) may be utilized, however this is limited by relatively smaller amplicon sizes which may not accurately assess degradation.

The use of PCR amplification is a reliable measure for an understanding of damage results and damage induced, but the use of PCR template may underestimate the amount of damage present due to the high concentration present but if coupled with time interval reactions an effect should still be observed if one does exist. Another consideration is if the damage occurs within the primer site as opposed to within the amplicon. Depending on the nature of the mismatch and the position within the primer site amplification may be reduced. This however, is a non-issue since the primer site accounts for on average approximately 20 bases per primer in an amplicon of 1kb, and in

itself is still a result of the DNA damage. To improve this step though, q-PCR can be substituted to produce measurable and comparable results.

On relatively short DNA template the use of Endonuclease IV to act on abasic sites results in a reliable smearing pattern which increases with the accumulation of abasic sites. This method however is only quantifiable by the measure of the initial product band intensity. To apply this in future research the use of available antibody based methods or GC-MS detection may be utilized.

The use of GC-MS for the detection of modified base and sugar moieties is for the most part a sensitive, specific, and reliable assay. With proper experimental conditions little to no artifactual products should be formed, and by ensuring that the DNA extract is properly purified the sensitivity can be further increased.

GC-MS Detection Considerations

Following the identification of retention times and mass spectra of detected modified bases in this study, two degraded modern samples extracted with ethanol precipitation and one fresh sample extracted with a Qiagen© Extraction kit were analyzed via scan and SIM mode. Though all the samples contained approximately 1μg of DNA, only the sample extracted with the Qiagen© Extraction kit yielded detectable bases.

In addition to this, during sample optimization for this study, buccal samples extracted with both ethanol precipitation and DNA extraction kits with concentrations ranging from 1 to 50μg of DNA were analysed. Ethanol precipitation extractions resulted in the detection of nucleic acids, proteins, purification reagents, and residues from the swab itself. The utilization of DNA extraction kits eliminated this background allowing for

detection of nucleic acids in samples consisting of 1-5μg as opposed to 25-50μg. Thus, it was observed that the limiting factor of GC-MS sensitivity in scan mode was the purity of the sample and not solely DNA concentration. This is of significant interest to molecular diagnostics, ancient DNA analysis, and forensic science where DNA concentration is often limited.

Unfortunately, throughout this research, the analysis of samples with GC-MS SIM mode was unsuccessful, and is most likely due to instrumentation problems. By optimizing GC-MS SIM in combination with the use of DNA extraction kits, the sensitivity of detecting modified bases and sugar moieties is unmatched by other techniques.

Abasic Detection Methodology

The purpose of AP site detection experiments was to test alternate methods of identifying apurinic/apyrimidinic lesions. Most detection methods tend to only identify the concentration of AP sites in total and do not distinguish between the proportions of lost nucleotides or AP site location. Detection with GeneScan™ Software did identify the presence of incorporated fluorescent ddNTP's in AP template. Reactions that contained both TAMRA-ddUTP and ROX-ddCTP exhibited different detectable fragment lengths, however no discernable difference was observed in total fluorescent signal for comparable peaks over the different time intervals. A major drawback of this assay is the identifiable fragment length limit of approximately 500bp due to the size standard. It was assumed that upon treatment of a 1kb AP site containing fragment with EndoIV, a series of varying length double stranded products with both 5' and 3' overhangs would be formed. Treatment with the Klenow fragment of DNA polymerase I

would digest 3' overhangs and incorporate a fluorescent ddNTP to the 3'OH group of a 5' overhang fragment. Despite the sensitivity capabilities of the GeneScan™ Software it is likely that a high percentage of fragments existed in excess of 500bp and those that were within the size limit occurred at random lengths restricting strong fluorescent peaks. Therefore, the detection of AP sites is probable, however AP site location based on the size restriction is only effective when applied to smaller isolated genome fragments.

Following these results, incorporated fluorescent ddNTP's were analyzed by utilizing the Nanodrop spectrophotometer which detects the full signal produced by each nucleotide regardless of fragment size. Initial results with TAMRA-ddUTP, after accounting for the parallel control, indicate that approximately 4 AP sites per 1kb template strand were capable of being detected, and in subsequent reactions a maximum of 13 AP sites were present. This assay was also successful at differentiating between types of nucleotides lost by demonstrating that the AP template contained a higher concentration of thymine to cytosine, and adenine to guanine. This assay is highly specific as the Klenow fragment will add the appropriate complementary nucleotide at the Endonuclease IV prepared 3'OH site, and due to the 3'-H of the ddNTP sugar moiety, elongation will terminate immediately. The only issue encountered in this assay was the limited resolution of the fluorescent spectra. This is likely due to the age of the fluorescent ddNTP's and possible degradation as a result of excessive freeze/thaw cycles. This can be easily overcome by new reagents and selecting different nucleotide-fluorophore combinations to increase greater wavelength separation. This study however, has been successful in identifying a potential assay that is both sensitive and specific to apurinic and apyrimidinic sites. In addition, the reaction can be completed on

extracted DNA samples in only approximately 12 hours with relatively inexpensive commercially available reagents and equipment. In future studies, all four fluorescent ddNTP's will be included in a single reaction and time dependent AP lesion formation will be studied further.

5.0 Conclusion

The detection and interpretation of DNA damage induced by endogenous and exogenous sources is of important interest not only to the study of diseases but in forensic and aDNA applications. The ability to understand damage types and pathways associated with the development of cancers and other diseases is crucial for prevention, early diagnosis, and treatment. The characterization of DNA lesions is also relevant in aDNA and forensic science to confirm the authenticity of point mutations used to identify the ancestry of remains or the identity of an individual.

This study focused on the use of methods to localize regions of DNA damage and to identify the types of induced damage with various analytical techniques. Though difficulties were encountered with genome separation, the concept of combining genome separation with mitochondrial fragment isolation was successful using PCR DNA template and could prove to be useful in isolating gene regions for disease studies or the D-loop for ancient DNA and forensic applications.

This research was successful in the formation of damage and subsequently identifying how this damage affects the structure and composition of the DNA strand, base, and sugar moiety. Though many of the products identified have been previously characterized, the concept of combining multiple assays in a single study is scarce in the literature. In addition, the importance of time interval reactions to observe changing damage spectra was demonstrated.

Also, an adapted method which displays potential as a sensitive and specific method in the detection of apurinic/apyrimidinic sites was introduced, and based on the

positive results of this preliminary study it indicates that with further refinement a significant tool in DNA damage studies may available to researchers.

Finally, though not directly related to DNA damage, upon optimization of GC-MS samples it was observed that the sensitivity of the GC-MS, especially in scan mode, is determined significantly by the purity of the DNA extract.

The study of DNA damage is an important field of research; however it requires extensive and thorough protocol to fully understand the processes involved. This research was conducted to identify challenges and provide insights and focus to be considered in the future research of DNA damage, detection, and repair.

6.0 Future Considerations

The research has provided information regarding the formation, effects, and detection of induced DNA damage. Throughout the discussion the refinement of tests and protocols based on observed results has been suggested for future experiments. Future studies can now focus on more specific hypotheses utilizing the knowledge achieved in this study.

The optimization of genome separation and fragment isolation protocols would be of benefit for future studies focused on OXPHOS deficiencies. Also, the assessment of taphonomic pathways on Ancient DNA template quality, focusing on the typically sequenced mitochondrial D-loop, can be investigated.

As previously mentioned, future studies with specific damaging agents in time course reactions to identify the changes in damage spectrums which could then eventually be applied to disease progression is invaluable.

Further research is also necessary to optimize and validate the AP detection assay introduced in this study. Due to the relative ease and expense, coupled with its sensitivity and specificity, this assay has the potential to significantly contribute to DNA damage detection.

Finally, the damage detection assays of qPCR, AP detection, and GC-MS can be utilized to aid in research focusing on repair mechanisms of this damaged DNA. By positively identifying lesions specific to a damaging agent, an appropriate blocking mechanism or repair system can be optimized.

7.0 References

Altieri F., Grillo C., Maceroni M., Chichiarelli S. (2008) DNA damage and repair: from molecular mechanisms to health implications. Antioxid Redox Signal 10: 891-937

Anderson S., Bankier A.T., Barrell B.G., de Bruijn M.H., Coulson A.R., Drouin J., Eperon I.C., Nierlich D.P., Roe B.A., Sanger F., Schreier P.H., Smith A.J., Staden R., Young I.G. (1981) Sequence and organization of the human mitochondrial genome. Nature 290: 457-65

Barclay L.R.C., Locke S.C., Macneil J.M. (1985) Autoxidation in micelles. Synergism of vitamin C with lipid-soluble vitamin E and water-soluble Trolox. Canadian Journal of Chemisrty 63: 366-374

Batty D.P., Wood R.D. (2000) Damage recognition in nucleotide excision repair of DNA. Gene 241: 193-204

Belousova E.A., Rechkunova N.I., Lavrik O.I. (2006) Thermostable DNA polymerases can perform translesion synthesis using 8-oxoguanine and tetrahydrofuran-containing DNA templates. Biochim Biophys Acta 1764: 97-104

Bjelland S., Seeberg E. (2003) Mutagenicity, toxicity and repair of DNA base damage induced by oxidation. Mutat Res 531: 37-80

Bogdanov K.V., Chukhlovin A.B., Zaritskey A.Y., Frolova O.I., Afanasiev B.V. (1997) Ultraviolet irradiation induces multiple DNA double-strand breaks and apoptosis in normal granulocytes and chronic myeloid leukaemia blasts. Br J Haematol 98: 869-72

Bonin S., Petrera F., Niccolini B., Stanta G. (2003) PCR analysis in archival postmortem tissues. Mol Pathol 56: 184-6

Buermeyer A.B., Deschenes S.M., Baker S.M., Liskay R.M. (1999) Mammalian DNA mismatch repair. Annu Rev Genet 33: 533-64

Cadet J., D'Ham C., Douki T., Pouget J.P., Ravanat J.L., Sauvaigo S. (1998) Facts and artifacts in the measurement of oxidative base damage to DNA. Free Radic Res 29: 541-50

Cadet J., Sage E., Douki T. (2005) Ultraviolet radiation-mediated damage to cellular DNA. Mutat Res 571: 3-17

Carr S.M., Griffith O.M. (1987) Rapid isolation of animal mitochondrial DNA in a small fixed-angle rotor at ultrahigh speed. Biochem Genet 25: 385-90

Cheng K.C., Cahill D.S., Kasai H., Nishimura S., Loeb L.A. (1992) 8-Hydroxyguanine, an abundant form of oxidative DNA damage, causes G----T and A----C substitutions. J Biol Chem 267: 166-72

Chetsanga C.J., Grigorian C. (1983) A dose-response study on opening of imidazole ring of adenine in DNA by ionizing radiation. Int J Radiat Biol Relat Stud Phys Chem Med 44: 321-31

Cloutier J.F., Castonguay A., O'Connor T.R., Drouin R. (2001) Alkylating agent and chromatin structure determine sequence context-dependent formation of alkylpurines. J Mol Biol 306: 169-88

Collins A.R., Oscoz AA, Brunborg G., Gaivao I., Giovannelli L., Kruszewski M., Smith C.C., Stetina R. (2008) The comet assay: topical issues. Mutagenesis 23: 143-51

Cooke M.S., Evans M.D., Dizdaroglu M., Lunec J. (2003) Oxidative DNA damage: mechanisms, mutation, and disease. Faseb J 17: 1195-214

Cooke M.S., Olinski R., Evans M.D. (2006) Does measurement of oxidative damage to DNA have clinical significance? Clin Chim Acta 365: 30-49

Cruzeiro-Hansson L., Goodfellow J.M. (1994) Flexibility and curvature of DNA duplexes containing O4-methylthymine: implications for DNA repair. Carcinogenesis 15: 1525-33

De Bont R., van Larebeke N. (2004) Endogenous DNA damage in humans: a review of quantitative data. Mutagenesis 19: 169-85

Dianov G.L., Sleeth K.M., Dianova, I.I., Allinson S.L. (2003) Repair of abasic sites in DNA. Mutat Res 531: 157-63

DiMauro S., Schon E.A. (2001) Mitochondrial DNA mutations in human disease. Am J Med Genet 106: 18-26

Dizdaroglu M. (1994) Chemical determination of oxidative DNA damage by gas chromatography-mass spectrometry. Methods Enzymol 234: 3-16

Dizdaroglu M. (1998) Facts about the artifacts in the measurement of oxidative DNA base damage by gas chromatography-mass spectrometry. Free Radic Res 29: 551-63

Dizdaroglu M., Jaruga P., Birincioglu M., Rodriguez H. (2002) Free radical-induced damage to DNA: mechanisms and measurement. Free Radic Biol Med 32: 1102-15

Dizdaroglu M., Jaruga P., Rodriguez H. (2001) Measurement of 8-hydroxy-2'-deoxyguanosine in DNA by high-performance liquid chromatography-mass spectrometry: comparison with measurement by gas chromatography-mass spectrometry. Nucleic Acids Res 29: E12

Douki T., Perdiz D., Grof P., Kuluncsics Z., Moustacchi E., Cadet J., Sage E. (1999) Oxidation of guanine in cellular DNA by solar UV radiation: biological role. Photochem Photobiol 70: 184-90

Douki T., Reynaud-Angelin A., Cadet J., Sage E. (2003) Bipyrimidine photoproducts rather than oxidative lesions are the main type of DNA damage involved in the genotoxic effect of solar UVA radiation. Biochemistry 42: 9221-6

Drablos F., Feyzi E., Aas P.A., Vaagbo C.B., Kavli B., Bratlie M.S., Pena-Diaz J., Otterlei M., Slupphaug G., Krokan H.E. (2004) Alkylation damage in DNA and RNA--repair mechanisms and medical significance. DNA Repair (Amst) 3: 1389-407

Epe B. (1996) DNA damage profiles induced by oxidizing agents. Rev Physiol Biochem Pharmacol 127: 223-49

ESCODD (2003) Measurement of DNA oxidation in human cells by chromatographic and enzymic methods. Free Radic Biol Med 34: 1089-99

Evans M.D., Dizdaroglu M., Cooke M.S. (2004) Oxidative DNA damage and disease: induction, repair and significance. Mutat Res 567: 1-61

Falnes P.O. (2004) Repair of 3-methylthymine and 1-methylguanine lesions by bacterial and human AlkB proteins. Nucleic Acids Res 32: 6260-7

Fernandez-Silva P., Enriquez J.A., Montoya J. (2003) Replication and transcription of mammalian mitochondrial DNA. Exp Physiol 88: 41-56

Ferrer I., Armstrong J., Capellari S., Parchi P., Arzberger T., Bell J., Budka H., Strobel T., Giaccone G., Rossi G., Bogdanovic N., Fakai P., Schmitt A., Riederers P., Al-Sarraj S., Ravid R., Kretzschmar H.(2007) Effects of formalin fixation, paraffin embedding, and time of storage on DNA preservation in brain tissue: a BrainNet Europe study. Brain Pathol 17: 297-303

Frederico L.A., Kunkel T.A., Shaw B.R. (1993) Cytosine deamination in mismatched base pairs. Biochemistry 32: 6523-30

Goodfellow J.M., Cruzeiro-Hansson L, Norberto de Souza O, Parker K, Sayle T, Umrania Y (1994) DNA structure, hydration and dynamics. Int J Radiat Biol 66: 471-8

Govan H.L., 3rd, Valles-Ayoub Y, Braun J (1990) Fine-mapping of DNA damage and repair in specific genomic segments. Nucleic Acids Res 18: 3823-30

Guetens G., De Boeck G., Highley M., van Oosterom A.T., de Bruijn E.A. (2002) Oxidative DNA damage: biological significance and methods of analysis. Crit Rev Clin Lab Sci 39: 331-457

Hakem R. (2008) DNA-damage repair; the good, the bad, and the ugly. Embo J 27: 589-605

Halliwell B. (1998) Can oxidative DNA damage be used as a biomarker of cancer risk in humans? Problems, resolutions and preliminary results from nutritional supplementation studies. Free Radic Res 29: 469-86

Hansen J.N. (1974) Isolation of higher molecular weight DNA from Bacillus Cereus T using proteinase K. Prep Biochem 4: 473-88

Hoss M., Jaruga P., Zastawny T.H., Dizdaroglu M., Paabo S. (1996) DNA damage and DNA sequence retrieval from ancient tissues. Nucleic Acids Res 24: 1304-7

Hwang E.S., Bowen P.E. (2007) DNA damage, a biomarker of carcinogenesis: its measurement and modulation by diet and environment. Crit Rev Food Sci Nutr 47: 27-50

Ide H., Akamatsu K., Kimura Y., Michiue K., Makino K., Asaeda A., Takamori Y., Kubo K. (1993) Synthesis and damage specificity of a novel probe for the detection of abasic sites in DNA. Biochemistry 32: 8276-83

Iyer R.R., Pluciennik A., Burdett V., Modrich P.L. (2006) DNA mismatch repair: functions and mechanisms. Chem Rev 106: 302-23

Jaruga P., Dizdaroglu M. (2008) 8,5'-Cyclopurine-2'-deoxynucleosides in DNA: mechanisms of formation, measurement, repair and biological effects. DNA Repair (Amst) 7: 1413-25

Kang D., Hamasaki N. (2002) Maintenance of mitochondrial DNA integrity: repair and degradation. Curr Genet 41: 311-22

Kang J.O. (1994) Methylated purine bases in hepatic and colonic RNA of rats treated with 1,2-dimethylhydrazine. Biochem Med Metab Biol 53: 52-7

Kavli B., Otterlei M., Slupphaug G., Krokan H.E. (2007) Uracil in DNA--general mutagen, but normal intermediate in acquired immunity. DNA Repair (Amst) 6: 505-16

Kehrer J.P. (2000) The Haber-Weiss reaction and mechanisms of toxicity. Toxicology 149: 43-50

Kelly K.A., Havrilla C.M., Brady T.C., Abramo K.H., Levin E.D. (1998) Oxidative stress in toxicology: established mammalian and emerging piscine model systems. Environ Health Perspect 106: 375-84

Kobayashi A., Kitaoka M., Hayashi K. (2005) Novel PCR-mediated mutagenesis employing DNA containing a natural abasic site as a template and translesional Taq DNA polymerase. J Biotechnol 116: 227-32

Krokan H.E., Standal R., Slupphaug G. (1997) DNA glycosylases in the base excision repair of DNA. Biochem J 325 (Pt 1): 1-16

Kujundzic E., Matalkah F., Howard C.J., Hernandez M., Miller S.L. (2006) UV air cleaners and upper-room air ultraviolet germicidal irradiation for controlling airborne bacteria and fungal spores. J Occup Environ Hyg 3: 536-46

Landis G.N., Tower J. (2005) Superoxide dismutase evolution and life span regulation. Mech Ageing Dev 126: 365-79

Lim K.S., Huang S.H., Jenner A., Wang H., Tang S.Y., Halliwell B. (2006) Potential artifacts in the measurement of DNA deamination. Free Radic Biol Med 40: 1939-48

Lim K.S., Jeyaseelan K., Whiteman M., Jenner A., Halliwell B. (2005) Oxidative damage in mitochondrial DNA is not extensive. Ann N Y Acad Sci 1042: 210-20

Lindahl T., Nyberg B. (1972) Rate of depurination of native deoxyribonucleic acid. Biochemistry 11: 3610-8

Linnane A.W., Marzuki S., Ozawa T., Tanaka M. (1989) Mitochondrial DNA mutations as an important contributor to ageing and degenerative diseases. Lancet 1: 642-5

Little J.L. (1999) Artifacts in trimethylsilyl derivatization reactions and ways to avoid them. J Chromatogr A 844: 1-22

Makalowski W. (2001) The human genome structure and organization. Acta Biochim Pol 48: 587-98

Marnett L.J. (2000) Oxyradicals and DNA damage. Carcinogenesis 21: 361-70

Mates J.M., Perez-Gomez C., Nunez de Castro I. (1999) Antioxidant enzymes and human diseases. Clin Biochem 32: 595-603

McCord J.M., Fridovich I. (1969) Superoxide dismutase. An enzymic function for erythrocuprein (hemocuprein). J Biol Chem 244: 6049-55

Mecocci P., MacGarvey U., Kaufman A.E., Koontz D., Shoffner J.M., Wallace D.C., Beal M.F. (1993) Oxidative damage to mitochondrial DNA shows marked age-dependent increases in human brain. Ann Neurol 34: 609-16

Mhaskar D.N., Chang M.J., Hart R.W., D'Ambrosio S.M. (1981) Analysis of alkylated sites at N-3 and N-7 positions of purines as an indicator for chemical carcinogens. Cancer Res 41: 223-9

Mitra S. (2007) MGMT: a personal perspective. DNA Repair (Amst) 6: 1064-70

Mol C.D., Parikh S.S., Putnam C.D., Lo T.P., Tainer J.A. (1999) DNA repair mechanisms for the recognition and removal of damaged DNA bases. Annu Rev Biophys Biomol Struct 28: 101-28

Moller P. (2006) The alkaline comet assay: towards validation in biomonitoring of DNA damaging exposures. Basic Clin Pharmacol Toxicol 98: 336-45

Mouret S., Baudouin C., Charveron M., Favier A., Cadet J., Douki T. (2006) Cyclobutane pyrimidine dimers are predominant DNA lesions in whole human skin exposed to UVA radiation. Proc Natl Acad Sci U S A 103: 13765-70

Nakamura J., Walker V.E., Upton P.B., Chiang S.Y., Kow Y.W., Swenberg J.A. (1998) Highly sensitive apurinic/apyrimidinic site assay can detect spontaneous and chemically induced depurination under physiological conditions. Cancer Res 58: 222-5

Peak J.G., Peak M.J. (1990) Ultraviolet light induces double-strand breaks in DNA of cultured human P3 cells as measured by neutral filter elution. Photochem Photobiol 52: 387-93

Pfeifer G.P., You Y.H., Besaratinia A. (2005) Mutations induced by ultraviolet light. Mutat Res 571: 19-31

Phillips D.H., Arlt V.M. (2007) The 32P-postlabeling assay for DNA adducts. Nat Protoc 2: 2772-81

Poulsen H.E., Weimann A., Loft S. (1999) Methods to detect DNA damage by free radicals: relation to exercise. Proc Nutr Soc 58: 1007-14

Robert M.F., Morin S., Beaulieu N., Gauthier F., Chute I.C., Barsalou A., MacLeod A.R. (2003) DNMT1 is required to maintain CpG methylation and aberrant gene silencing in human cancer cells. Nat Genet 33: 61-5

Robin E.D., Wong R. (1988) Mitochondrial DNA molecules and virtual number of mitochondria per cell in mammalian cells. J Cell Physiol 136: 507-13

Runger T.M., Kappes U.P. (2008) Mechanisms of mutation formation with long-wave ultraviolet light (UVA). Photodermatol Photoimmunol Photomed 24: 2-10

Santos J.H., Meyer J.N., Mandavilli B.S., Van Houten B. (2006) Quantitative PCR-based measurement of nuclear and mitochondrial DNA damage and repair in mammalian cells. Methods Mol Biol 314: 183-99

Sawyer D.E., Van Houten B. (1999) Repair of DNA damage in mitochondria. Mutat Res 434: 161-76

Schmidtke J., Epplen J.T. (1980) Sequence organization of animal nuclear DNA. Hum Genet 55: 1-18

Shibutani S., Takeshita M., Grollman A.P. (1997) Translesional synthesis on DNA templates containing a single abasic site. A mechanistic study of the "A rule". J Biol Chem 272: 13916-22

Sies H., Stahl W. (1995) Vitamins E and C, beta-carotene, and other carotenoids as antioxidants. Am J Clin Nutr 62: 1315S-1321S

Sies H., Stahl W., Sundquist A.R. (1992) Antioxidant functions of vitamins. Vitamins E and C, beta-carotene, and other carotenoids. Ann N Y Acad Sci 669: 7-20

Sikorsky J.A., Primerano D.A., Fenger T.W., Denvir J. (2004) Effect of DNA damage on PCR amplification efficiency with the relative threshold cycle method. Biochem Biophys Res Commun 323: 823-30

Sikorsky J.A., Primerano D.A., Fenger T.W., Denvir J. (2007) DNA damage reduces Taq DNA polymerase fidelity and PCR amplification efficiency. Biochem Biophys Res Commun 355: 431-7

Simandan T., Sun J., Dix T.A. (1998) Oxidation of DNA bases, deoxyribonucleosides and homopolymers by peroxyl radicals. Biochem J 335 (Pt 2): 233-40

Singer B. (1977) Sites in nucleic acids reacting with alkylating agents of differing carcinogenicity of mutagenicity. J Toxicol Environ Health 2: 1279-95

Singer B. (1979) N-nitroso alkylating agents: formation and persistence of alkyl derivatives in mammalian nucleic acids as contributing factors in carcinogenesis. J Natl Cancer Inst 62: 1329-39

Slupphaug G., Kavli B., Krokan H.E. (2003) The interacting pathways for prevention and repair of oxidative DNA damage. Mutat Res 531: 231-51

Sung J.S., Demple B. (2006) Roles of base excision repair subpathways in correcting oxidized abasic sites in DNA. Febs J 273: 1620-9

Taanman J.W. (1999) The mitochondrial genome: structure, transcription, translation and replication. Biochim Biophys Acta 1410: 103-23

Valko M., Rhodes C.J., Moncol J., Izakovic M., Mazur M. (2006) Free radicals, metals and antioxidants in oxidative stress-induced cancer. Chem Biol Interact 160: 1-40

van Delft J.H., van Winden M.J., van den Ende A.M., Baan R.A. (1993) Determining N7-alkylguanine adducts by immunochemical methods and HPLC with electrochemical detection: applications in animal studies and in monitoring human exposure to alkylating agents. Environ Health Perspect 99: 25-32

Venter J.C., Adams M.D., Myers E.W., Li P.W., Mural R.J., Sutton G.G., Smith H.O., Yandell M., Evans C.A., Holt R.A., Gocayne J.D., Amanatides P., Ballew R.M., Huson D.H., Wortman J.R., Zhang Q., Kodira C.D., Zheng X.H., Chen L., Skupski M., Subramanian G., Thomas P.D., Zhang J., Gabor Miklos G.L., Nelson C., Broder S., Clark A.G., Nadeau J., McKusick V.A., Zinder N., Levine A.J., Roberts R.J., Simon M., Slayman C., Hunkapiller M., Bolanos R., Delcher A., Dew I., Fasulo D., Flanigan M., Florea L., Halpern A., Hannenhalli S., Kravitz S., Levy S., Mobarry C., Reinert K., Remington K., Abu-Threideh J., Beasley E., Biddick K., Bonazzi V., Brandon R., Cargill M., Chandramouliswaran I., Charlab R., Chaturvedi K., Deng Z., Di Francesco V., Dunn P., Eilbeck K., Evangelista C., Gabrielian A.E., Gan W., Ge W., Gong F., Gu Z., Guan P., Heiman T.J., Higgins M.E., Ji R.R., Ke Z., Ketchum K.A., Lai Z., Lei Y., Li Z., Li J., Liang Y., Lin X., Lu F., Merkulov G.V., Milshina N., Moore H.M., Naik A.K., Narayan V.A., Neelam B., Nusskern D., Rusch D.B., Salzberg S., Shao W., Shue B., Sun J., Wang Z., Wang A., Wang X., Wang J., Wei M., Wides R., Xiao C., Yan C., *et al.* (2001) The sequence of the human genome. Science 291: 1304-51

Wang D., Kreutzer D.A., Essigmann J.M. (1998) Mutagenicity and repair of oxidative DNA damage: insights from studies using defined lesions. Mutat Res 400: 99-115

Wang M., Cheng G., Villalta P.W., Hecht S.S. (2007) Development of liquid chromatography electrospray ionization tandem mass spectrometry methods for analysis of DNA adducts of formaldehyde and their application to rats treated with N-nitrosodimethylamine or 4-(methylnitrosamino)-1-(3-pyridyl)-1-butanone. Chem Res Toxicol 20: 1141-8

Waters T.R., Swann P.F. (2000) Thymine-DNA glycosylase and G to A transition mutations at CpG sites. Mutat Res 462: 137-47

Watson J.D., Crick F.H. (1953) Molecular structure of nucleic acids; a structure for deoxyribose nucleic acid. Nature 171: 737-8

Wellinger R.E., Thoma F. (1996) Taq DNA polymerase blockage at pyrimidine dimers. Nucleic Acids Res 24: 1578-9

Wood R.D. (1996) DNA repair in eukaryotes. Annu Rev Biochem 65: 135-67

Wood R.D. (1997) Nucleotide excision repair in mammalian cells. J Biol Chem 272: 23465-8

Wyatt G.R. (1951) The purine and pyrimidine composition of deoxypentose nucleic acids. Biochem J 48: 584-90

Yakes F.M., Van Houten B. (1997) Mitochondrial DNA damage is more extensive and persists longer than nuclear DNA damage in human cells following oxidative stress. Proc Natl Acad Sci U S A 94: 514-9

You Y.H., Li C., Pfeifer G.P. (1999) Involvement of 5-methylcytosine in sunlight-induced mutagenesis. J Mol Biol 293: 493-503

8.0 Appendix A

Amplified 1kb product (15975-429) of mitochondrial genome

```
1       CTCCACCATT AGCACCCAAA GCTAAGATTC TAATTTAAAC
41      TATTCTCTGT TCTTTCATGG GGAAGCAGAT TTGGGTACCA
81      CCCAAGTATT GACTCACCCA TCAACAACCG CTATGTATTT
121     CGTACATTAC TGCCAGCCAC CATGAATATT GTACGGTACC
161     ATAAATACTT GACCACCTGT AGTACATAAA AACCCAATCC
201     ACATCAAAAC CCCCTCCCCA TGCTTACAAG CAAGTACAGC
241     AATCAACCCT CAACTATCAC ACATCAACTG CAACTCCAAA
281     GCCACCCCTC ACCCACTAGG ATACCAACAA ACCTACCCAC
321     CCTTAACAGT ACATAGTACA TAAAGCCATT TACCGTACAT
361     AGCACATTAC AGTCAAATCC CTTCTCGTCC CCATGGATGA
401     CCCCCCTCAG ATAGGGGTCC CTTGACCACC ATCCTCCGTG
441     AAATCAATAT CCCGCACAAG AGTGCTACTC TCCTCGCTCC
481     GGGCCCATAA CACTTGGGGG TAGCTAAAGT GAACTGTATC
521     CGACATCTGG TTCCTACTTC AGGGTCATAA AGCCTAAATA
561     GCCCACACGT TCCCCTTAAA TAAGACATCA CGATGGATCA
601     CAGGTCTATC ACCCTATTAA CCACTCACGG GAGCTCTCCA
641     TGCATTTGGT ATTTTCGTCT GGGGGGTATG CACGCGATAG
681     CATTGCGAGA CGCTGGAGCC GGAGCACCCT ATGTCGCAGT
721     ATCTGTCTTT GATTCCTGCC TCATCCTATT ATTTATCGCA
761     CCTACGTTCA ATATTACAGG CGAACATACT TACTAAAGTG
801     TGTTAATTAA TTAATGCTTG TAGGACATAA TAATAACAAT
841     TGAATGTCTG CACAGCCACT TTCCACACAG ACATCATAAC
881     AAAAAATTTC CACCAAACCC CCCCTCCCCC GCTTCTGGCC
921     ACAGCACTTA AACACATCTC TGCCAAACCC CAAAAACAAA
961     GAACCCTAAC ACCAGCCTAA CCAGATTTCA AATTTTATCT
1001    TTTGGCGGTA TGCACTTTTA ACAG
```

9.0 Appendix B.

GC-MS Sample Data

Sample: dATP H_2O_2 48 hours							
Species	Retention Time	Area	*m/z* 1	*m/z* 2	*m/z* 3	*m/z* 4	*m/z* 5
Pentanoic Acid	8.695	2.67E+10	145	173			
Trimethyl carbonate	8.991	2.94E+09	147	191	204		
Urea	10.284	5.79E+09	147	189	281		
Trimethyl phosphate	10.907	1.68E+11	298	299	314		
Butanedioic acid	11.332	5.96E+10	147	247	299		
Butanedioic acid	13.717	2.17E+09	73	147	233		
d-erythro-pentonic acid	13.935	9.20E+08	147	219	261		
Silanamine	14.087	1.01E+09	73	306			
Acetic acid	15.032	3.69E+09	73	299	357		
1,3,5-Triazine,2,4,6-oxy]-	15.13	3.29E+09	73	330	345		
Propanoic acid, 3-oxy], (S)-OPO	17.465	1.33E+09	227	299	357		
9H-Purin-6-amine, N,9-	17.983	2.90E+09	264	279			
4,6-diamino-5-formamido-pyrimidine	18.071	2.32E+09	264	280	354		
D-Ribofuranose	18.647	3.56E+08	217	299	315		
D-erythro-2-Pentulose	19.053	6.39E+08	299	315	357		
9H-Purin-6-amine,oxy]-	19.165	1.01E+09	264	352	367		
Sample: dATP H_2O_2 12 hours							
Species	Retention Time	Area	*m/z* 1	*m/z* 2	*m/z* 3	*m/z* 4	*m/z* 5
Pentanoic Acid	8.675	2.88E+09	145	173			
Trimethyl carbonate	8.972	1.30E+08	147	191	204		
Trimethyl phosphate	10.875	9.90E+10	298	299	314		
Butanedioic acid	11.314	9.44E+07	147	247	299		
Acetic acid	15.015	6.88E+07	73	299	357		
Propanoic acid,	17.453	1.36E+08	227	299	357	387	459
Unknown	17.613	4.11E+08	228	242	344	359	

Adenine	17.98	1.89E+10	264	279			
4,6-diamino-5-formamido-pyrimidine	18.054	8.50E+08	264	280	354	369	
Sample: dATP H_2O_2 1 hour							
Species	Retention Time	Area	*m/z* 1	*m/z* 2	*m/z* 3	*m/z* 4	*m/z* 5
Pentanoic Acid	8.674	1.82E+10	145	173			
Trimethyl carbonate	8.976	2.76E+08	147	191	204		
Urea	10.273	1.35E+07	147	189	281	369	
Trimethyl phosphate	10.868	1.42E+11	298	299	314		
Butanedioic acid	11.311	4.74E+07	147	247	299		
Silanol, trimethyl-, pyrophosphate (4:1)	15.878	8.80E+07	147	299	363	451	466
Propanoic acid, 3-[[bis[(trimethylsilyl)oxy]phosphinyl]oxy]-2-[(triSiOSihylsilyl)oxy]-, trimethylsilyl ester, (S)-OPO	17.466	1.61E+07	227	299	357	387	459
Species	17.614	6.68E+07	228	242	344	359	
Adenine 9H-Purin-6-amine, N,9-bis(trimethylsilyl)-	17.994	5.84E+10	264	279			
4,6-diamino-5-formamido-pyrimidine	18.062	8.55E+08	264	280	354	369	
9H-Purin-6-amine, N,9-bis(trimethylsilyl)-8-[(trimethylsilyl)oxy]-	19.157	2.88E+07	264	352	367		
Sample: dGTP H_2O_2 48 hours							
Species	Retention Time	Area	*m/z* 1	*m/z* 2	*m/z* 3	*m/z* 4	*m/z* 5
Pentanoic acid, 4-oxo-, trimethylsilyl ester	8.689	3.15E+10	145	173			
Silanol, trimethyl-, phosphate (3:1) O	10.89	7.97E+10	299	314			
Butanedioic acid, bis(trimethylsilyl) ester	11.319	4.55E+08					
1,3,5-Triazine	15.126	2.43E+09	330	345			
Unknown	18.794	1.46E+08	369/370	385	451	464	
N-Oxide	19.32	9.54E+08	264	280	295		
Unknown	19.389	3.61E+09	299	315	413		
Unknown	20.452	4.48E+08	207	280	355	429	
Guanine	20.518	3.25E+10	352	367			

Sample: dGTP H_2O_2 12 hours							
Species	Retention Time	Area	*m/z* 1	*m/z* 2	*m/z* 3	*m/z* 4	*m/z* 5
Pentanoic acid, 4-oxo-, trimethylsilyl ester	8.691	8.18E+09	145	173			
Silanol, trimethyl-, phosphate (3:1) O	10.869	5.78E+10	299	314			
Guanine	20.518	0.00E+00	352	367			
Sample: dGTP H_2O_2 1hour							
Species	Retention Time	Area	*m/z* 1	*m/z* 2	*m/z* 3	*m/z* 4	*m/z* 5
Pentanoic acid, 4-oxo-, trimethylsilyl ester	8.645	5.91E+09	145	173			
Silanol, trimethyl-, phosphate (3:1) O	10.838	1.42E+11	299	314			
N-Oxide	19.294	5.36E+09	280	295			
Unknown	19.367	1.52E+10	299	315	413		
Unknown	20.422	4.62E+08	280	355	429		
Guanine	20.508	6.18E+10	352	367			
Sample: dCTP H_2O_2 48 hours							
Species	Retention Time	Area	*m/z* 1	*m/z* 2	*m/z* 3	*m/z* 4	*m/z* 5
Acetic acid, [(trimethylsilyl)oxy]-, trimethylsilyl ester O	7.864	6.60E+09	147	177	205		
Pentanoic acid, 4-oxo-, trimethylsilyl ester	8.693	3.85E+10	145	173			
Silanol, trimethyl-, carbonate (2:1)	8.987	3.01E+09	147	191	204		
Silanol, trimethyl-, phosphate (3:1) O	10.876	8.13E+10	299	314			
Parabanic acid, bis-O-(trimethylsilyl)-	13.548	1.09E+09	243	258			
Hydantoin, 5-hydroxy-tris-O-(trimethylsilyl)-	14.019	4.52E+08	189	202	317		
Cytosine	14.107	3.84E+09	240	255			
Pyrimidine, 2,4,5-tris[(trimethylsilyl)oxy]-	14.99	2.54E+08	241	329	344		
1,3,5-Triazine, 2,4,6-tris[(trimethylsilyl)oxy]-	15.13	7.01E+08	330	345			
Unknown	15.179	1.00E+09	291	317	391	406	
Unknown	15.42	1.43E+09	312	326	345		
Cytosine product	16.065	3.25E+08	316	331	332	343	
5-hydroxycytosine	16.119	3.54E+08	328	343			

isodialuric acid	16.895	3.18E+08	329	343	417	432	
Sample: dCTP H_2O_2 12 hours							
Species	Retention Time	Area	*m/z* 1	*m/z* 2	*m/z* 3	*m/z* 4	*m/z* 5
Pentanoic acid, 4-oxo-, trimethylsilyl ester	8.673	7.56E+09	145	173			
Silanol, trimethyl-, carbonate (2:1)	8.97	1.42E+08	147	191	204		
Silanol, trimethyl-, phosphate (3:1) O	10.862	8.38E+10	299	314			
Parabanic acid, bis-O-(trimethylsilyl)-	13.548	9.86E+07	243	258			
Hydantoin, 5-hydroxy-tris-O-(trimethylsilyl)-	14.041	1.50E+09	189	202	317		
Cytosine	14.095	1.08E+10	240	255			
Pyrimidine, 2,4,5-tris[(trimethylsilyl)oxy]-	14.96	4.99E+08	241	329	344		
Unknown	15.394	3.29E+08	312	326	345		
Cytosine product	16.042	2.40E+07	316	331	332	343	
5-hydroxycytosine	16.091	3.08E+08	328	343			
isodialuric acid	16.869	6.78E+07	329	343	417	432	
5-hydroxyuracil	17.598	7.02E+07	326	344	359		
Unknown	17.647	6.12E+07	285	301	447	462	490
Sample: dCTP H_2O_2 1 hour							
Species	Retention Time	Area	*m/z* 1	*m/z* 2	*m/z* 3	*m/z* 4	*m/z* 5
Pentanoic acid, 4-oxo-, trimethylsilyl ester	8.682	8.57E+09	145	173			
Silanol, trimethyl-, carbonate (2:1)	8.984	1.68E+08	147	191	204		
Silanol, trimethyl-, phosphate (3:1) O	10.862	7.61E+10	299	314			
Parabanic acid, bis-O-(trimethylsilyl)-	13.539	6.39E+07	243	258			
Hydantoin, 5-hydroxy-tris-O-(trimethylsilyl)-	14.057	5.36E+09	189	202	317		
Cytosine	14.118	3.73E+10	240	255			
Pyrimidine, 2,4,5-tris[(trimethylsilyl)oxy]-	14.982	5.90E+07	241	329	344		
?	15.375	2.16E+09	312	326	345		
5-hydroxycytosine	16.105	6.12E+09	328	343			
isodialuric acid	16.89	2.31E+07	329	343	417	432	
5-hydroxyuracil	17.619	6.38E+07	326	344	359		
?	17.668	5.60E+07	285	301	447	462	490

Sample: dTTP H_2O_2 48 hours							
Species	Retention Time	Area	*m/z* 1	*m/z* 2	*m/z* 3	*m/z* 4	*m/z* 5
Pentanoic acid, 4-oxo-, trimethylsilyl ester	8.699	1.14E+10	145	173			
Unknown	9.001	3.15E+09	147	191	204		
Silanol, trimethyl-, phosphate (3:1)	10.876	5.00E+10	299	300	314		
Butanedioic acid, bis(trimethylsilyl) ester	11.335	6.66E+08	147	247			
Thymine	12.583	2.87E+10	255	270			
Pyrimidine, 2,4-bis[(trimethylsilyl)oxy]-	13.329	4.54E+09	241	256			
5-hydroxyhydantoin	13.86	4.54E+09	216	331			
Alloxanoic acid, N,N',O,O'-tetrakis(trimethylsilyl)-	13.816	1.08E+09					
Hydantoin, 5-hydroxy-tris-O-(trimethylsilyl)-	14.08	9.29E+08	189	202	317		
5-hydroxyuracil	15.002	5.94E+08	329	344	357		
5-(hydroxymethyl)uracil	15.041	1.55E+09					
thymine glycol	16.809	4.11E+09	259	433	448		
Thymidine, 3'-O-(trimethylsilyl)-, 5'-[bis(trimethylsilyl) phosphSiSi	27.287	9.70E+08	299	323	539		
Sample: dTTP H_2O_2 12 hours							
Species	Retention Time	Area	*m/z* 1	*m/z* 2	*m/z* 3	*m/z* 4	*m/z* 5
Pentanoic acid, 4-oxo-, trimethylsilyl ester	8.67		145	173			
Unknown	8.927	2.53E+08	147	191	204		
Silanol, trimethyl-, phosphate (3:1)	10.858	6.13E+10	299	300	314		
Thymine	12.558	3.39E+10	255	270			
Pyrimidine, 2,4-bis[(trimethylsilyl)oxy]-	13.308	4.41E+07	241	256			
5-hydroxy-5-methylhydantoin	13.829	4.34E+07	216	331			
Pyrimidine, 2,4,5-tris[(trimethylsilyl)oxy]-	14.97	5.70E+07	329	344	357		
thymine glycol	16.787	2.87E+08	259	433	448		
Unknown	17.277	9.85E+09	299	315	397		
Thymidine, 3'-O-(trimethylsilyl)-, 5'-[bis(trimethylsilyl) phosphSiSi	27.277	4.95E+09	299	323	539		

Sample: dTTP H_2O_2 1 hour							
Species	Retention Time	Area	*m/z* 1	*m/z* 2	*m/z* 3	*m/z* 4	*m/z* 5
Pentanoic acid, 4-oxo-, trimethylsilyl ester	8.707	4.74E+09	145	173			
Silanol, trimethyl-, phosphate (3:1)	10.901	3.10E+10	299	300	314		
Butanedioic acid, bis(trimethylsilyl) ester	11.335	3.07E+07	147	247			
Thymine	12.603	2.36E+10	255	270			
5-hydroxy-5-methylhydantoin	13.873	4.17E+07	216	331			
L-Proline, 5-oxo-1-(trimethylsilyl)-, trimethylsilyl ester	14.129	1.70E+08	156	230	258		
Pyrimidine, 2,4,5-tris[(trimethylsilyl)oxy]-	15.018	7.27E+07	329	344	357		
thymine glycol	16.833	7.07E+08	259	433	448		
Unknown	17.33	1.03E+10	299	315	397		
2(1H)-Pyrimidinone, 1-[2-deoxy-3-O-(trimethylsilyl)-.beta.-d-erythro-OS	27.392	3.04E+09	299	323	539		
Sample: dCTP							
Species	Retention Time	Area	*m/z* 1	*m/z* 2	*m/z* 3	*m/z* 4	*m/z* 5
Pentanoic acid, 4-oxo-, trimethylsilyl ester	8.35	6.35E+10	145	173			
Silanol, trimethyl-, phosphate (3:1) O	10.245	2.45E+11	299	314			
Cytosine	13.596	3.90E+10	240	255			
Sample: dTTP							
Species	Retention Time	Area	*m/z* 1	*m/z* 2	*m/z* 3	*m/z* 4	*m/z* 5
Pentanoic acid, 4-oxo-, trimethylsilyl ester	8.355	3.71E+10	145	173			
Silanol, trimethyl-, phosphate (3:1)	10.304	3.08E+11	299	300	314		
Thymine	11.989	7.24E+10	255	270			
Sample: dATP							
Species	Retention Time	Area	*m/z* 1	*m/z* 2	*m/z* 3	*m/z* 4	*m/z* 5
Pentanoic Acid	8.337	5.26E+10	145	173			
Trimethyl phosphate	10.252	2.40E+11	299	314			
Adenine 9H-Purin-6-amine, N,9-bis(trimethylsilyl)-	17.498	5.39E+10	264	279			

Sample: dGTP							
Species	Retention Time	Area	*m/z* 1	*m/z* 2	*m/z* 3	*m/z* 4	*m/z* 5
Pentanoic acid, 4-oxo-, trimethylsilyl ester	8.375	6.68E+10	145	173			
Silanol, trimethyl-, phosphate (3:1) O	10.337	3.36E+11	299	314			
Guanine	20.597	4.27E+10	352	367			
Sample: dCTP DMSO							
Species	Retention Time	Area	*m/z* 1	*m/z* 2	*m/z* 3	*m/z* 4	*m/z* 5
Pentanoic acid, 4-oxo-, trimethylsilyl ester	8.416	1.68E+10	145	173			
Silanol, trimethyl-, phosphate (3:1)	10.611	1.50E+11					
DMSO	13.661	5.20E+10	172	185	263	311	358
DMSO	16.084	7.37E+09	198	323	388		
Sample: dATP DMSO							
Species	Retention Time	Area	*m/z* 1	*m/z* 2	*m/z* 3	*m/z* 4	*m/z* 5
Pentanoic acid, 4-oxo-, trimethylsilyl ester	8.413	4.08E+10	145	173			
Silanol, trimethyl-, phosphate (3:1)	10.497	2.87E+11					
DMSO	13.668	8.54E+10	172	185	263	311	358
DMSO	13.668	2.62E+10	198	323	388		
Sample: dATP Heat/acid Buffer							
Species	Retention Time	Area	*m/z* 1	*m/z* 2	*m/z* 3	*m/z* 4	*m/z* 5
Pentanoic acid, 4-oxo-, trimethylsilyl ester	8.677	1.61E+10	145	173			
Silanol, trimethyl-, phosphate (3:1)	10.883	1.99E+11	299	314			
Silanol, trimethyl-, pyrophosphate (4:1)	15.878	1.97E+09	451	466			
1,2,3-Propanetricarboxylic acid, 2-[(trimethylsilyl)oxy]-	17.611	9.82E+10	347	363	465		
Adenine	1.80E+01	2.70E+10	264	279			
Sample: dCTP							
Species	Retention Time	Area	*m/z* 1	*m/z* 2	*m/z* 3	*m/z* 4	*m/z* 5

Pentanoic acid, 4-oxo-, trimethylsilyl ester	8.435	2.36E+10	145	173			
Silanol, trimethyl-, phosphate (3:1)	10.375	4.64E+10	299	314			
Cytosine	13.616	1.62E+10	240	255			
Sample: dGTP							
Species	Retention Time	Area	*m/z* 1	*m/z* 2	*m/z* 3	*m/z* 4	*m/z* 5
Pentanoic acid, 4-oxo-, trimethylsilyl ester	8.437	2.69E+10	145	173			
Silanol, trimethyl-, phosphate (3:1)	10.375	5.84E+10	299	314			
Guanine	13.616	1.43E+10	352	367			
Sample: dTTP							
Species	Retention Time	Area	*m/z* 1	*m/z* 2	*m/z* 3	*m/z* 4	*m/z* 5
Pentanoic acid, 4-oxo-, trimethylsilyl ester	8.447	3.16E+10	145	173			
Silanol, trimethyl-, phosphate (3:1)	10.375	5.45E+10	299	314			
Thymine	12.163	2.93E+10	255	270			
Sample: dATP							
Species	Retention Time	Area	*m/z* 1	*m/z* 2	*m/z* 3	*m/z* 4	*m/z* 5
Pentanoic acid, 4-oxo-, trimethylsilyl ester	8.45	3.40E+10	145	173			
Silanol, trimethyl-, phosphate (3:1)	10.401	7.48E+10	299	314			
Adenine	17.683	3.59E+10	264	279			
Sample: dNTP H_2O_2 48 hours							
Species	Retention Time	Area	*m/z* 1	*m/z* 2	*m/z* 3	*m/z* 4	*m/z* 5
Pentanoic acid, 4-oxo-, trimethylsilyl ester	8.701	6.64E+09	145	173			
Trimethyl carbonate	8.907	9.36E+08	147	191			
Silanol, trimethyl-, phosphate (3:1)	10.973	2.93E+11	299	314			
2-Butenedioic acid (Z)-, bis(trimethylsilyl) ester	11.236	3.23E+09	147	245			
Butanedioic acid, bis(trimethylsilyl) ester	11.236	1.63E+09	147	247			
1,2-Bis(trimethylsiloxy)cyclohexene	11.377	8.08E+08	147	169	258		
Propanoic acid, 2,3-bis[(trimethylsilyl)oxy]-, trimethylsilyl ester	11.662	3.41E+08	189	292			
2-Butenedioic acid (E)-, bis(trimethylsilyl) ester	11.771	5.70E+08	147	245			

Thymine	12.573	9.72E+09	255	270			
Pyrimidine, 2,4-bis[(trimethylsilyl)oxy]-	13.313	4.92E+08	241	256			
Parabanic acid, bis-O-(trimethylsilyl)-	13.547	2.43E+09	243	258			
Butanedioic acid, [(trimethylsilyl)oxy]-, bis(trimethylsilyl) ester	13.711	1.84E+09	307	319	335		
5-hydroxy-5-methylhydantoin	13.841	4.61E+08	216	331			
D-Erythro-Pentonic acid, 2-deoxy-3,5-bis-O-(trimethylsilyl)-	13.939	3.75E+09	189	219	261		
Hydantoin, 5-hydroxy-tris-O-(trimethylsilyl)-	14.071	4.91E+09	189	202	317		
Cytosine	14.111	2.61E+09	240	255			
Unknown	14.466	3.52E+08	259	359	447	449	
Unknown	14.54	4.59E+08	318	333	333		
Unknown	14.981	5.93E+08	241	256	329	357	424
Acetic acid, [[bis[(trimethylsilyl)oxy]phosphinyl]oxy]-,	15.027	2.35E+09	299	315	328	357	
5-hydroxy-6-hydrocytosine	15.127	4.87E+09	330	345			
Unknown	15.186	2.57E+09	259	317	343	359	374
Silanol, trimethyl-, pyrophosphate (4:1)	15.89	2.59E+09	451	466			
5-hydroxyuracil	16.345	2.76E+09	329	344			
Hydroperoxide/uracil glycol	16.795	4.66E+09	434	448			
5-hydroxyhydantoin	16.936	1.23E+09	316	331			
Thymine Product	17.085	3.08E+09	259	271	286		
5-hydroxycytosine	17.327	8.50E+08	328	343			
3,5-Dioxa-4-phospha-2-silaoctan-8-oic acid, 2,2-dimethyl-4,7-bis[(trimethylsilyl)oxy]-, trimethylsilyl ester, 4-oxide	17.474	1.33E+09	299	357	459		
Adenine	17.998	2.42E+10	264	279			
4,6-diamino-5-formamidopyrimidine	18.065	1.42E+08	354	369			
Adenine (#3-5)	18.778	1.40E+09	280	295			
Unknown	18.947	8.06E+08	342	357	403		
8-hydroxyadenine	19.162	1.44E+09	352	367			
D-Ribofuranose, 1,2,3-tris-O-(trimethylsilyl)-, bis(trimethylsilyl)	19.579	2.50E+09	230	299	315		
erythro-2-Pentulose, 1,3,4-tris-O-(trimethylsilyl)-, 5-[bis(trimethylsilyl) phosphate]	20.37	2.81E+09					
Guanine	20.513	6.81E+09	352	367			

Sample: dNTP UVA							
Species	Retention Time	Area	*m/z* 1	*m/z* 2	*m/z* 3	*m/z* 4	*m/z* 5
Pentanoic acid, 4-oxo-, trimethylsilyl ester	8.748	8.01E+10	145	173			
Trimethyl carbonate	8.993	1.29E+09	147	191			
Silanol, trimethyl-, phosphate (3:1)	10.954	3.17E+11	299	314			
Thymine	12.579	5.36E+10	255	270			
Cytosine	14.145	6.34E+10	240	255			
5-hydroxyuracil	14.979	1.88E+08	329	344			
Unknown (from cytosine)	15.415	8.94E+09	312	326			
Silanol, trimethyl-, pyrophosphate (4:1)	15.884	5.16E+08	451	466			
Unkown	16.82	5.69E+08	249	263	278		
5-hydroxycytosine	16.105	7.31E+08	328	343			
Unkown	17.287	2.83E+10	299	315			
Adenine	18.01	5.05E+10	264	279			
Unknown	19.286	3.10E+09	255	271			
Adenine (#3-5)	19.321	8.30E+08	264	280	295		
Unknown	19.389	1.50E+09	299	315	413		
Purine Product	20.459	1.05E+09	280	295			
Guanine	20.538	5.45E+10	352	367			
Thymidine, 3'-O-(trimethylsilyl)-, 5'-[bis(trimethylsilyl)	27.271	2.97E+09	299	315	317	323	
Sample: dNTP UVB							
Species	Retention Time	Area	*m/z* 1	*m/z* 2	*m/z* 3	*m/z* 4	*m/z* 5
Pentanoic acid, 4-oxo-, trimethylsilyl ester	8.757	7.99E+10	145	173			
Trimethyl carbonate	8.999	8.74E+08	147	191			
Silanol, trimethyl-, phosphate (3:1)	10.919	2.88E+11	299	314			
Thymine	12.579	4.60E+10	255	270			
Cytosine	14.155	6.59E+10	240	255			
5-hydroxyuracil	14.979	9.83E+07	329	344			
Unknown (from cytosine)	15.423	1.15E+10	312	326			
Silanol, trimethyl-, pyrophosphate (4:1)	15.884	4.06E+08	451	466			
Unknown	16.82	1.95E+08	249	263	278		

5-hydroxycytosine	16.105	5.28E+08	328	343			
Unkown	17.293	1.66E+10	299	315	369	397	
Adenine	18.02	5.31E+10	264	279			
Unknown	19.292	1.70E+09	255	271			
Adenine (#3-5)	19.328	2.92E+09	264	280	295		
Unknown	19.394	1.63E+09	299	315	413		
Guanine	20.55	6.17E+10	352	367			
Thymidine, 3'-O-(trimethylsilyl)-, 5'-[bis(trimethylsilyl)	27.271	3.39E+08	299	315	317	323	
Sample: dNTP Heat/acid Buffer							
Species	Retention Time	Area	*m/z* 1	*m/z* 2	*m/z* 3	*m/z* 4	*m/z* 5
Pentanoic acid, 4-oxo-, trimethylsilyl ester	8.697	5.68E+08	145	173			
Trimethyl carbonate	8.996	4.55E+08	147	191			
Silanol, trimethyl-, phosphate (3:1)	10.856	8.18E+09	299	314			
Unknown	11.634	2.17E+09	185	203	230	245	260
Thymine	12.573	7.85E+08	255	270			
Unknown	12.742	2.76E+09	144	234			
Silanamine, 1,1,1-trimethyl-N-[2-[(trimethylsilyl)oxy]-1,1-bis[[(trOSithylsilyl)oxy]methyl]ethyl]-	14.111	2.13E+10	240	255	306		
Unknown	14.377	1.94E+09	103	170	260		
Unknown	14.985	2.32E+09	217	334	422		
Unknown	14.981	4.13E+09	217	234	262		
Adenine	17.988	1.22E+09	264	279			
Guanine	20.521	7.70E+08	352	367			
Sample: Modern Qiagen							
Species	Retention Time	Area	*m/z* 1	*m/z* 2	*m/z* 3	*m/z* 4	*m/z* 5
Pentanoic acid, 4-oxo-, trimethylsilyl ester	8.712	9.79E+07	145	173			
Trimethyl carbonate	8.991	8.74E+08	147	191			
Silanol, trimethyl-, phosphate (3:1)	10.853	1.45E+09	299	314			
Thymine	12.571	2.17E+08	255	270			
Parabanic acid, bis-O-(trimethylsilyl)-	13.586	2.99E+07	243	258			
Silanamine, 1,1,1-trimethyl-N-[2-[(trimethylsilyl)oxy]-1,1-bis[[(trOSithylsilyl)oxy]methyl]ethyl]-	14.087	1.77E+10	306	409			

Adenine	17.996	4.79E+07	264	279			
Unknown	20.432	9.17E+07	341	355			
Guanine	20.517	4.03E+07	352	367			
Sample: Modern Degraded #1							
Species	Retention Time	Area	*m/z* 1	*m/z* 2	*m/z* 3	*m/z* 4	*m/z* 5
Pentanoic acid, 4-oxo-, trimethylsilyl ester	8.713	4.45E+08	145	173			
Silanol, trimethyl-, phosphate (3:1)	10.872	1.67E+09	299	314			
Thymine	12.566	0.00E+00	255	270			
Silanamine, 1,1,1-trimethyl-N-[2-[(trimethylsilyl)oxy]-1,1-bis[[(trOSithylsilyl)oxy]methyl]ethyl]	14.102	2.79E+09	305	306	394	410	
Cytosine	14.111	0.00E+00	240	255			
Adenine	17.998	0.00E+00	264	279			
Guanine	20.513	0.00E+00	352	367			
Sample: Modern Degraded #2							
Species	Retention Time	Area	*m/z* 1	*m/z* 2	*m/z* 3	*m/z* 4	*m/z* 5
Pentanoic acid, 4-oxo-, trimethylsilyl ester	8.713	3.77E+08	145	173			
Trimethyl carbonate	8.992	2.41E+09	147	191			
Silanol, trimethyl-, phosphate (3:1)	10.872	3.69E+09	299	314			
L-Serine, N-(trifluoroacetyl)-O-(trimethylsilyl)-, trimethylsily	11.297	4.05E+08	240	315	330		
Thymine	12.566	1.08E+08	255	270			
Unknown	13.058	4.34E+08	300	328			
Parabanic acid, bis-O-(trimethylsilyl)-	13.558	2.35E+08	243	258			
Silanamine, 1,1,1-trimethyl-N-[2-[(trimethylsilyl)oxy]-1,1-bis[[(trOSithylsilyl)oxy]methyl]ethyl]	14.102	3.89E+10	305	306	394	410	
Adenine	17.998	0.00E+00	264	279			
Guanine	20.513	0.00E+00	352	367			